

Bachelor Degree Project



UNIVERSITY
OF SKÖVDE

MECHANICAL DESIGN OF A COMPLIANT HORSESHOE

Bachelor Degree Project in Mechanical Engineering
C-Level 22,5 ECTS
Spring term 2014

Dionisio Camacho Moreno
Jorge Giner Pérez

Supervisors: Alexander Eklind
M.Sc. Björn Kastenman

Examiner: PhD. Thomas Carlberger

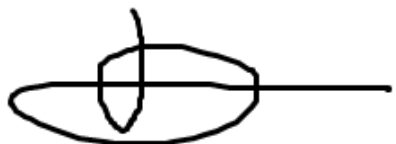
DECLARATION

This Final Year Project is submitted by Dionisio Camacho Moreno and Jorge Giner Pérez to the University of Skövde for the Bachelor Degree in Mechanical Engineering, in the School of Technology and Society.

Date of Submission:

We certify that all the contents in this Final Year Project which is not our own work has been identified and referenced.

Signatures



Dionisio Camacho Moreno



Jorge Giner Pérez

ACKNOWLEDGMENTS

We would like to express our special appreciation and thanks to our project supervisors Alexander Eklind, M.Sc. Björn Kastenman, because without their assistance and dedicated involvement throughout the process, this report would have never been accomplished.

We want to express our gratitude to the University of Skövde for this year in which we have grown both as future engineers as people.

A special thanks to our families because despite the distances have been with us in every moment and thanks for their support and their effort that has made possible that we have been here.

Last but not least, we wish to thank all those people who have accompanied us during this year, to those friends who have already gone; those who still are, those who go, but especially those who will be with us forever. Thanks very much for the unforgettable moments.

ABSTRACT

The principal aim of this research is the design of a more compliant horseshoe which allows the natural expansion and compression of the horse hoof. Three different simulations have been carried out in by using Finite Element Method in order to know the behaviour of the horse hoof when is analysed under the same load conditions. First the hoof will be studied without any horseshoe to obtain the produced displacement by the hoof expansion. Once the displacement of the barefoot hoof is known, an assembly, in which a sample stiff horseshoe is attached to the hoof by nails, will be performed to obtain both the hoof displacement as the horseshoe one. Finally, after three different researches about the current horseshoes, different possible alternative materials and most commons attachment methods, a more flexible horseshoe will be created and analysed. The results obtained in the three simulations will be compared and commented.

TABLE OF CONTENTS

DECLARATION.....	I
ACKNOWLEDGMENTS	II
ABSTRACT.....	III
TABLE OF CONTENTS.....	A
TABLE OF FIGURES.....	C
TABLE OF CHARTS.....	G
1. INTRODUCTION	1
1.1. Background.....	1
1.2. Problem	5
1.3. Purpose and goals	6
1.4. Method.....	6
2. ANALYSIS OF THE HORSE HOOF	9
2.1. Implementation.....	9
2.2. Results	18
3. ANALYSIS OF THE HOOF WITH A REGULAR HORSESHOE	20
3.1. Implementation.....	20
3.2. Results	24
3.2.1. Friction between the hoof and the horseshoe	24
3.2.2. No friction between the hoof and the horseshoe	27
4. DESIGN OF A COMPLIANT HORSESHOE	32
4.1. Comparison of different horseshoes.....	32
4.2. Comparison of different materials	35
4.3. Comparison of different attachments.....	38
4.3.1. Nails attachment	38
4.3.2. Glue-on Shoes	41
4.3.3. Adhesives	43
4.4. Design of the compliant horseshoe	44
4.5. Implementation.....	45
4.6. Results	47
4.6.1. Friction between the hoof and the horseshoe.....	47
4.6.2. No friction between the hoof and the horseshoe.....	52
4.6.3. Attachment with “perfect glue”	55

5. CONCLUSIONS AND DISCUSSIONS	60
5.1. Displacements	60
5.2. Stresses.....	62
5.3. Weights	64
5.4. Costs	65
6. FUTURE RESEARCH.....	66
APPENDIX A	67
APPENDIX B	81
REFERENCES	92

TABLE OF FIGURES

Figure 1. Preparing horses for their new life style (Fleming, 1869)	1
Figure 2. Ancient horseshoe (Fleming, 1869).....	2
Figure 3. Iron hipposandal (SaintJohn, 2008)	2
Figure 4. First horseshoe with nails made by Celts (Fleming, 1869)	3
Figure 5. External and internal view of a horse's hoof (Nassau, 2008)	3
Figure 6. Horseshoes made of different materials (SaintJohn, 2008)	4
Figure 7. Different horseshoes depending on the attachment (Parker, 2010)	4
Figure 8. Therapeutic horseshoes (SaintJohn, 2008)	5
Figure 9. Horseshoe chosen for the analysis (Mustad, 1999).....	7
Figure 10. Real horseshoe used as pattern for the simulation (own source)	9
Figure 11. Details of the real horseshoe used as pattern (own source)	10
Figure 12. Model of the horse hoof (own source).....	11
Figure 13. Different parts of the horse hoof with symmetry (own source).....	11
Figure 14. Dimensions of the 3D model of the horse hoof	12
Figure 15. Model with the mesh (own source).....	12
Figure 16. Model with the boundary conditions (own source)	13
Figure 17. Hoof wall loaded with the 80% of the load (own source)	14
Figure 18. Distribution of forces due to the pressure on the frog (Sandgren, 2007).....	14
Figure 19. Triangle of forces (own source).....	15
Figure 20. Load due to the pressure on the frog and the sole (own source).....	17
Figure 21. The mesh, loads, boundary conditions and materials established in the model (own source).....	17
Figure 22. Fringe diagram of the displacements in all directions (own source)	18
Figure 23. Displacement graph of the outer bottom curve in all directions (own source)	18
Figure 24. Fringe diagram of the displacement in the x- direction (own source)	19
Figure 25. Displacement graph of the outer bottom curve in the x- direction (own source)	19
Figure 26. 3D-model of the regular horseshoe (own source).....	20
Figure 27. Model of the nail (own source).....	21
Figure 28. Model of the horse hoof with a regular horseshoe (own source).....	21
Figure 29. Assembly with the mesh (own source)	21
Figure 30. Assembly with the boundary conditions (own source)	22
Figure 31. Assembly with the loads (own source).....	22
Figure 32. Assembly with the connections set (own source)	23
Figure 33. Cross section of the hoof with a nailed horseshoe (Barefoot-Hoofcare, 2013)	23
Figure 34. The mesh, loads, boundary conditions, materials and connections set (own source).....	24
Figure 35. Fringe diagram of the displacements of the assembly in all directions (own source).....	24
Figure 36. Fringe diagram of the displacements of the horseshoe and nails in all directions (own source).....	25
Figure 37. Horseshoe displacement compared with the hoof displacement in the x- direction (own source).....	25
Figure 38. Horseshoe displacement in the z- direction (own source)	26
Figure 39. Fringe diagram of the Von Mises stress in the hoof (own source)	26

Figure 40. Fringe diagram of the Von Mises stress in the horseshoe (own source).....	27
Figure 41. Fringe diagram of the Von Mises stress in the nails (own source)	27
Figure 42. Fringe diagram of the displacements of the assembly in all directions (own source).....	28
Figure 43. Fringe diagram of the displacements of the horseshoe and nails in all directions (own source).....	28
Figure 44. Horseshoe displacement compared with the hoof displacement in the x- direction (own source).....	29
Figure 45. Horseshoe displacement in the z- direction (own source)	29
Figure 46. Fringe diagram of the Von Mises stress in the hoof (own source)	30
Figure 47. Fringe diagram of the Von Mises stress in the horseshoe (own source).....	30
Figure 48. Fringe diagram of the Von Mises stress in the nails (own source)	31
Figure 49. Steel Horseshoe (Mustad, 1999).....	32
Figure 50. Aluminium Horseshoe (Mustad, 1999).....	33
Figure 51. TruShu-Equine Horseshoe (TruShu-Equine, 2013).....	33
Figure 52. ImprintSport Horseshoe (ImprintSport, 2008).....	34
Figure 53. EponaShoe Horseshoe (EponaShoe, 2010).....	34
Figure 54. Parts of a nail (Windt-im-Wald-Farm, 2007)	39
Figure 55. Different kinds of heads manufactured by Mustad (Independent Farrier Supplies, 2011)	39
Figure 56. Clinched nails in a horse hoof (America's Horse Daily, 2008).....	40
Figure 57. Possible cases of nailing (Stablemade.com, 2009)	40
Figure 58. Some examples of synthetic glue-on horseshoes (Blue Pegasos, 2013).....	41
Figure 59. Glue-on horseshoe with an aluminium core (Horseshoes.com, 1996)	42
Figure 60. Metal glue-on horseshoe (SoundHorse Technologies, 1999)	42
Figure 61. Two-component adhesive (Eki, 2001).....	43
Figure 62. 3D design of the compliant horseshoe with the nails (own source).....	46
Figure 63. Mesh set for the simulation (own source).....	46
Figure 64. Boundary conditions established in the 3D model (own source).....	47
Figure 65. Fringe diagram of the displacements of the design in all directions (own source)....	48
Figure 66. Fringe diagram of the displacements of the horseshoe and nails in all directions (own source).....	48
Figure 67. Horseshoe displacement compared with the hoof displacement in the x- direction (own source).....	49
Figure 68. Horseshoe displacement in the z- direction (own source)	49
Figure 69. Fringe diagram of the Von Mises stress in the hoof (own source)	50
Figure 70. Fringe diagram of the Von Mises stress in the polymer part (own source)	50
Figure 71. Fringe diagram of the Von Mises stress in the metal plates (own source)	51
Figure 72. Fringe diagram of the Von Mises stress in the nails (own source)	51
Figure 73. Fringe diagram of the displacements of the design in all directions (own source)....	52
Figure 74. Fringe diagram of the displacements of the horseshoe and nails in all directions (own source).....	52
Figure 75. Horseshoe displacement compared with the hoof displacement in the x- direction (own source).....	53
Figure 76. Horseshoe displacement in the z- direction (own source)	53
Figure 77. Fringe diagram of the Von Mises stress in the hoof (own source)	54

Figure 78. Fringe diagram of the Von Mises stress in the polymer part (own source)	54
Figure 79. Fringe diagram of the Von Mises stress in the metal plates (own source)	55
Figure 80. Fringe diagram of the Von Mises stress in the nails (own source)	55
Figure 81. Fringe diagram of the displacements of the glued horseshoe in all directions (own source).....	56
Figure 82. Fringe diagram of the displacements of the horseshoe in all directions (own source)	
.....	56
Figure 83. Horseshoe displacement compared with the hoof displacement in the x- direction (own source).....	57
Figure 84. Horseshoe displacement in the z- direction (own source)	57
Figure 85. Fringe diagram of the Von Mises stress in the hoof (own source)	58
Figure 86. Fringe diagram of the Von Mises stress in the polymer part (own source)	58
Figure 87. Fringe diagram of the Von Mises stress in the metal plates (own source)	59
Figure 88. Comparison of the hooves displacements in x- direction (own source)	60
Figure 89. Comparison of the horseshoes displacements in x- direction (own source)	61
Figure 90. Comparison of the horseshoes displacements in z- direction (own source)	61
Figure 91. Volume of the regular horseshoe (own source)	64
Figure 92. Volume of the compliant horseshoe (own source).....	64
Figure 93. Test performed with steel alloy 4340. Displacement in x- direction (own source) ...	67
Figure 94. Test performed with steel alloy 4340. Displacement in z- direction (own source) ...	67
Figure 95. Test performed with gray iron G4000. Displacement in x- direction (own source) ..	68
Figure 96. Test performed with gray iron G4000. Displacement in z- direction (own source) ..	68
Figure 97. Test performed with ductile iron 120-90-02. Displacement in x- direction (own source).....	69
Figure 98. Test performed with ductile iron 120-90-02. Displacement in z- direction (own source).....	69
Figure 99. Test performed with aluminium alloy 7075. Displacement in x- direction (own source).....	70
Figure 100. Test performed with aluminium alloy 7075. Displacement in z- direction (own source).....	70
Figure 101. Test performed with magnesium alloy AZ31B. Displacement in x- direction (own source).....	71
Figure 102. Test performed with magnesium alloy AZ31B. Displacement in z- direction (own source).....	71
Figure 103. Test performed with titanium alloy Ti-6Al-4V. Displacement in x- direction (own source).....	72
Figure 104. Test performed with titanium alloy Ti-6Al-4V. Displacement in z- direction (own source).....	72
Figure 105. Test performed with cooper alloy C17200. Displacement in x- direction (own source).....	73
Figure 106. Test performed with cooper alloy C17200. Displacement in z- direction (own source).....	73
Figure 107. Test performed with PPEK. Displacement in x- direction (own source).....	74
Figure 108. Test performed with PEEK. Displacement in z- direction (own source).....	74
Figure 109. Test performed with LDPE. Displacement in x- direction (own source)	75
Figure 110. Test performed with LDPE. Displacement in z- direction (own source).....	75

Figure 111. Test performed with HDPE. Displacement in x- direction (own source)	76
Figure 112. Test performed with HDPE. Displacement in z- direction (own source)	76
Figure 113. Test performed with PTFE. Displacement in x- direction (own source)	77
Figure 114. Test performed with PTFE. Displacement in z- direction (own source)	77
Figure 115. Test performed with polyurethane thermoplastic. Displacement in x- direction (own source).....	78
Figure 116. Test performed with polyurethane thermoplastic. Displacement in z- direction (own source).....	78
Figure 117. Test performed with rubber. Displacement in x- direction (own source)	79
Figure 118. Test performed with rubber. Displacement in z- direction (own source)	79
Figure 119. Test performed with adiprene LF-950. Displacement in x- direction (own source) 80	
Figure 120. Test performed with adiprene LF-950. Displacement in z- direction (own source) 80	

TABLE OF CHARTS

Table 1. Comparison of metals and metal alloys (Callister & Rethwisch, 2011)	36
Table 2. Comparison of polymers (Callister & Rethwisch, 2011).....	36
Table 3. Comparison of hoof stresses (own source)	63
Table 4. Comparison of horseshoe stresses (own source).....	63
Table 5. Comparison of nail stresses (own source).....	63

1. INTRODUCTION

1.1. Background

Horses, almost since its existence, have been useful to humans, becoming an indispensable part in their daily lives. In the beginning, horses emerge as an accessible source of meat for food and as an important source of leather for making clothes and tents. However, shortly after, historically speaking, horses became a companion, a vehicle, even a very effective weapon in the wars that our ancestors fought in the history of humanity.

According to Butler & Butler (2004), horses began to be tamed about 3000 years B.C. and have been used as a work animal since around 1500 B.C. When horses are used for loading, dragging or riding, everything works fine because horses are strong, agile, intelligent, docile, and obedient; however, this kind of work wears down their hooves.

This is due to the drastic change suffered by horses who used to live free in a meadow but now spend most of the day in a stable or doing hard physical labour (*Figure 1*). Therefore, the new lifestyles of the horse, the composition, the hardness and thus the shape and conformation of the hoof have changed drastically. The first problem that arose was the excessive wear of the hoof, which causes pain and may make the horse lame.



Figure 1. Preparing horses for their new life style (Fleming, 1869)

It is estimated that the Persian and Egyptian civilizations were the creators of the first horseshoes, probably born from the need to protect hooves from the excessive wear that they suffer. The first protections used were made of grass mesh in the form of sandals that were tied to the pastern and the fetlock (*Figure 2*).



Figure 2. Ancient horseshoe (Fleming, 1869)

The next step was to create protections made of wet skin which was placed covering the entire hoof and allowed to dry in order to acquire the shape of the hoof. Later, Genghis Khan, the famous 12th century military leader, perfected this technique to cover the hoof, which offered great abilities to their armies to move faster and more efficiently than their opponents.

Similarly, the Greeks and Romans made sandals, boots and socks to cover the hooves. In fact, the Romans are credited with creating of the hipposandal (*Figure 3*), which is a sandal made of leather with a metal sole.



Figure 3. Iron hipposandal (SaintJohn, 2008)

It is very difficult to determine the origin of the metal horseshoe with nails. Nonetheless, several researchers suggest that horseshoes with nails were first used in the area of Gaul, Britain and Germania. According to Nassau (2008), the Celtic civilization is assumed to be the first to use horseshoes with nails around the sixth century BC. What is certain is that when Julius Caesar conquered Gaul in 52 BC they use several kinds of horseshoes and nails in that area. The most common nails were denominated in French “clef de violon” and they were made of iron with a flat head that served to attach the horseshoe as can be seen in *Figure 4*.



Figure 4. First horseshoe with nails made by Celts (Fleming, 1869)

Already, around 400 B.C., the Greek Xenophon spoke about the importance of the frog in the pressure of the hoof and the hardness of the wall (*Figure 5*). Hence, it has been clear since antiquity that a good shoe is critical to horse welfare and the development of the work that horses do. Throughout history, the discovering and development of new materials such as steel, aluminium, plastics and different alloys have facilitated the creation of a wide multitude of horseshoes designed in order to try to solve different problems of the hoof. Nevertheless, although the techniques and materials have changed, there are currently no horseshoes that adapt satisfactorily to the horse's hoof.

According to Colles (2009), a horse's hoof is made of keratin, which grows constantly and allows the hoof to have a certain expansion stability in order to support the equine weight and distribute the impact forces. The hoof has two different structures, a sensitive tissue and an insensitive one. In the sensitive one, there are a great amount of nerves and blood vessels which provides blood to the hoof and thereby also nutrients for its growth and defence mechanisms in case of inflammation or infection. The insensitive tissue is a zone where there is not innervation or blood supply and this is where horseshoes can be attached with nails without damaging the hoof.

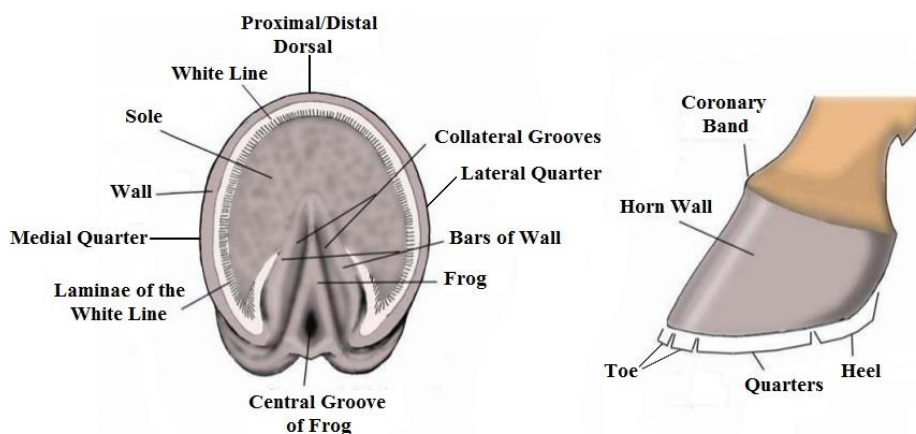


Figure 5. External and internal view of a horse's hoof (Nassau, 2008)

One of the main internal structures of the hoof is the frog which provides correct blood circulation through the hoof and the leg. The frog is the most elastic part of the outer hoof and usually it is the first part that touches the ground. When the hoof is raised, the frog and the flexible inner structures of the hoof come back to their normal position and when the hoof rests on the ground, the blood is forced to circulate to the veins which transport the blood to the horse leg. Thereby, it can be said that the frog works as a pressure pump.

Nowadays, there is a wide variety of horseshoes that can be classified according to several criteria. On the one hand, it is possible to find many horseshoes made with different materials such as iron (see A in **Figure 6**), steel (see B in **Figure 6**), aluminium (see C in **Figure 6**), some kind of polymer (see D in **Figure 6**) or a combination of them or other materials.



Figure 6. Horseshoes made of different materials (SaintJohn, 2008)

On the other hand, depending on how the horseshoe is attached to the hoof, there are horseshoes to be attached with nails (see A in **Figure 7**), with adhesive (see B and C in **Figure 7**) or horseshoes similar to a normal shoe which are usually fasten with Velcro (see D in **Figure 7**), brooches (see E in **Figure 7**) or laces (see F in **Figure 7**).

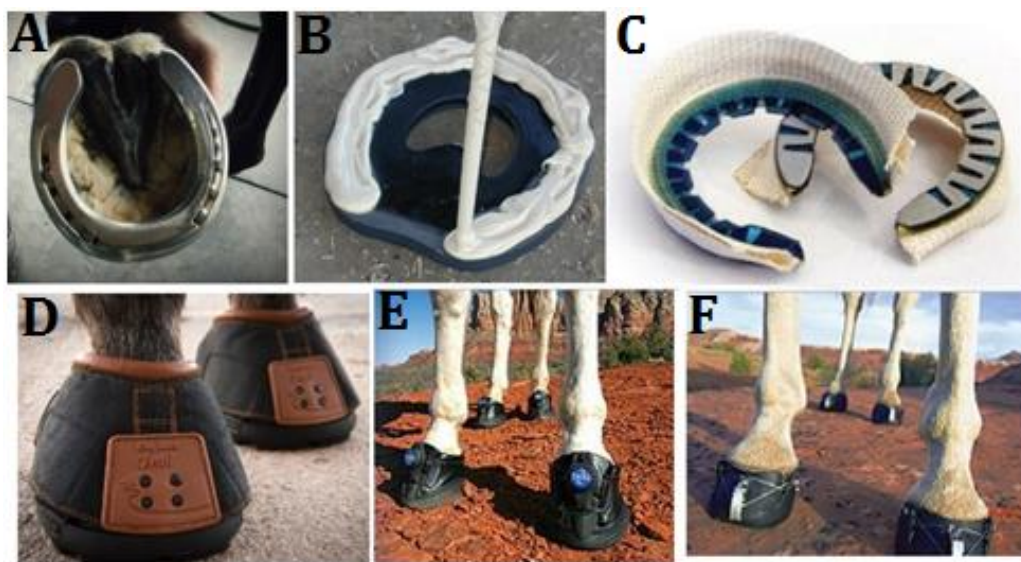


Figure 7. Different horseshoes depending on the attachment (Parker, 2010)

There are also different kinds of horseshoes according to the activity carried out by the horse. For example, many horseshoes used for running are often made of aluminium to reduce the weight of the shoe and have some kind of grip in order to do more efficient the footstep. Consequently, the horse is well attached to the ground at the beginning and during the race. Another example is the polo horseshoes which are made with an iron profile to provide the horse a good traction on grass and with a caulk of about 15 millimetres in length so that the horse can make quick turns without damaging their joints. Furthermore, there are special horseshoes whose aim is the correction and treatment of different diseases related to the horse's hoof. Some of these horseshoes are shown in *Figure 8*.



Figure 8. Therapeutic horseshoes (SaintJohn, 2008)

Most people and enterprises related with the field of horses are interested in finding a perfect horseshoe with the aim of improving the welfare of the horse and its performance, which means health and money. A perfect horseshoe should be compliant, lightweight, balanced, impact absorbing, wear resistant, anti-slip, cheap and suitable to be attached to the hoof without nails.

1.2. Problem

Horse hooves are submitted to great efforts due to the heavy weight of horses, their strength and their ability to move fast. When a horseshoe is attached to the hoof all those efforts are carried to the shoe. A barefoot horse hoof can be displaced around 8 mm each side (García, 2013) in the rear part. The expansion and compression of the hoof is known as hoof mechanism and its main function is to pump blood along the hoof and the leg. The use of a common horseshoe complicates the good working of the hoof mechanism due to the stiffness of the shoe.

Shoeing stiff horseshoes can be harmful to horses because the hoof mechanism is impeded due to the insufficient flexibility of the material, which cannot follow the movement of the hoof. A non-correct blood flow can damage the hoof and therefore the horse health would be affected (Hinterhofer et al. 2006, Roepstorff et al. 1999 and 2001). In addition, knowing that the most common attachment method is the fastened by nails and according to Nassau (2008), the last nail should not be behind of the branch middle length of the hoof to allow the hoof mechanism to work with less difficulty. So, a more compliant horseshoe shall be designed to avoid these problems.

1.3. Purpose and goals

The main goal of this project is to design a compliant horseshoe which allows a compression and expansion of the hoof to obtain a correct blood flow. Thereby, the correct hoof mechanism favours the blood circulation as well as the hoof growth. Taking into account the horse health it is necessary that the horseshoe can absorb the impact caused by the horse footstep. This will help to prevent the impact goes up through its leg damaging ligaments and tendons.

Although the purpose of this project is to design a compliant horseshoe, according to the background there are also other important goals that will be taken into account as far as possible with the aim to obtain a perfect horseshoe. These goals are: reducing the weight of the horseshoe; reducing the impact due to footstep by using, for example, an elastic pad; setting a contact surface enough hard to avoid the wear with the ground; establishing an adequate friction in the contact surface to provide a good grip; reducing the number of nails to attach the horseshoe or not to use nails and reducing costs as far as possible.

1.4. Method

To create a new horseshoe design it is important to know and understand how the hoof mechanism works. This mechanism makes the correct blood pumping possible along the horse limb due to the expansion and compression of the hoof.

A 3D-model of the horse hoof will be created to know how the hoof is deformed. The forces suffered by the horse will be simulated in the 3D model. Thereby, the deformation of the hoof will be determinate in this study that will be carried out using the software *PTC Creo*.

Once the hoof displacement has been obtained, the next step will be simulating the hoof with a regular horseshoe. The regular horseshoe chosen for the analysis is a Mustad horseshoe, whose features are shown in *Figure 9*.



Figure 9. Horseshoe chosen for the analysis (Mustad, 1999)

The nails will attach the horseshoe to the hoof. These nails will be simulated in their original form, without any curved deformation, since that is hard to know the curve that the nails follow exactly in the inner of the horn wall. The aim of the nails is to transfer the movement of the hoof to the horseshoe and compare it with the displacement of the barefoot hoof. Obtaining these results, an initial idea can be taken for the future design of the compliant horseshoe. An analysis about the stress, which the hoof and the nails suffer, will be performed. These results will be taken into account for the creation of the new shoe design, trying to decrease the stress of the new model as far as possible.

When the hoof deformations and the behaviour of the sample horseshoe are known, some studies about shapes, materials and attachment methods will be carried out. In the shape study some current horseshoes will be compared and studied in order to obtain a better knowledge about which shapes make the horseshoe more compliant and allow a better flexion.

For the study of the materials, the most common horseshoe materials will be analysed in order to obtain the behaviour of them when they are submitted to the loads applied in the hoof. This study will be performed using the software *PTC Creo*. One feasible way to carry out the experiment is to use the sample horseshoe analysed before changing the materials properties. In this way, it is possible to know how the different materials are

deformed without changing the applied load or the shape, which means to study different materials without changing any condition.

In the attachment method study, it will be studied the different attachment methods to fasten horseshoes. This study will be a theoretical study due to the limitations of the software, which is not able to simulate the attachment by adhesives. These methods will be compared and their advantages and disadvantages will be taking into account to choose one of these fastening methods.

After performing the previous studies about the hoof, the horseshoe, the shapes, the materials and the attachment methods; the design of the horseshoe can be carried out. The design will be created in *PTC Creo* in order to perform the analysis under the same conditions that displays the sample horseshoe. Comparing the obtained results, it will be possible to know how flexible the new design is. Although the main goal of this project is the design of a compliant horseshoe, the possibility of creating a more shock-absorbing horseshoe will be taken into account.

Finally, an economic study will be performed in order to calculate an estimate cost of the materials for the designed horseshoe. However, it must be highlight that the main goal of this project is the design of a compliant horseshoe.

2. ANALYSIS OF THE HORSE HOOF

A simulation of the barefoot hoof will be carried out in this section. The dimensions of the different hoof parts and their Young's modulus will be explained. Furthermore, the mesh, loads and boundary conditions set in the 3D model will be described. This simulation will be performed using the software *PTC Creo* with the aim to know the maximum displacement of the hoof.

2.1. Implementation

The frog is the first part that touches the ground when a horse puts down its hoof. So, the main deformation of the horse hoof is due to the reaction force transmitted by the frog to the rest of the hoof. In this way, each side of the hoof can be displaced around 8 mm (García, 2013).

The first step to design a compliant horseshoe is to understand how the hoof is deformed. For this reason, the horse's hoof will be simulated with the aim to obtain the displacement of the horn wall, which should be the same as the displacement of the compliant horseshoe.

As is described below, the model of the horse hoof will be carried out using the real horseshoe shown in *Figure 10* as pattern. This horseshoe, which is the same as the one described in the method part of the project, is for the hind limbs of the horse.



Figure 10. Real horseshoe used as pattern for the simulation (own source)

Some details of the above horseshoe are shown in *Figure 11*. In these pictures can be seen how the movement of the hoof has caused the horseshoe wear.



Figure 11. Details of the real horseshoe used as pattern (own source)

At time of selecting the most unfavourable case of the horse footstep, it is assumed that when the horse is running, galloping in this case, it is possible that the horse can stand over one of its leg. So it is important to consider that one hoof could support the whole weight of the horse. The obtained stress concentrations in this case will be the maximum values which the horseshoe, the nails and the hoof will support.

To do the simulation, some previous approximations have been done. A horse with a mass of 650 kg has been chosen, which results in a weight of 6370 N by multiplying the mass by the gravity acceleration. However, the hoof has to support an extra force due to the force exerted by the horse when it steps; so that a factor of 2.4 (Witte, et al., 2004) has been assumed to amplify the ground reaction force.

Figure 12 shows the hoof which has been modelled by assembling four different parts. Each part has a specific Young's modulus: the dorsal part has a Young's modulus equal to 1004 MPa (Douglas, et al., 1996), the quarter part has a Young's modulus equal to 657 MPa (Douglas, et al., 1996), the sole has been simulated with a Young's modulus equal to 230 MPa (Hinterhofer, et al., 1998) and the frog has been modelled with a Young's modulus equal to 9.9 MPa (Hinterhofer, et al., 1998). Furthermore, all the parts have been simulated by establishing a Poisson coefficient equal to 0.3 (Salo, et al., 2010).

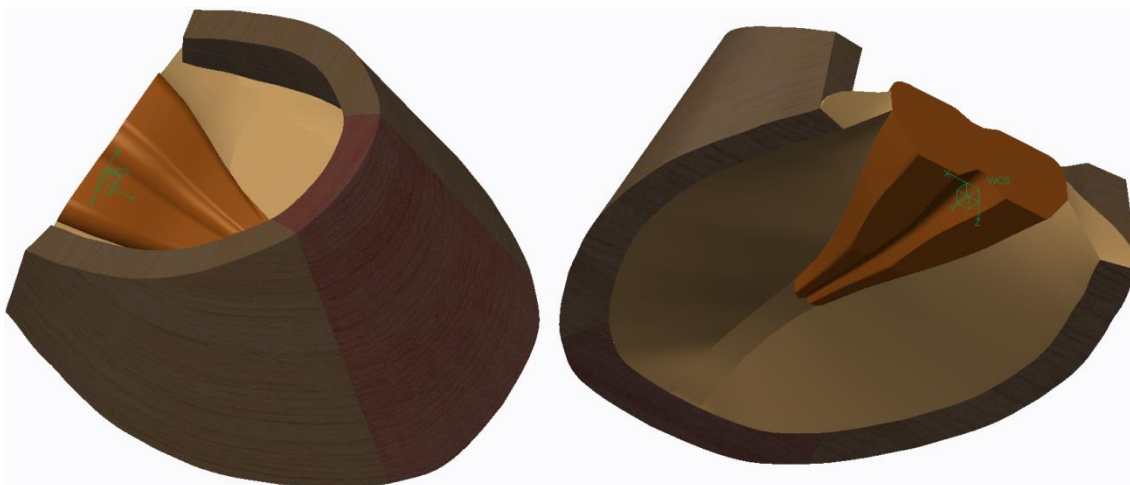


Figure 12. Model of the horse hoof (own source)

The name of each part of the hoof that has been modelled is shown in *Figure 13*. As can be seen, the hoof has been considered symmetric respect to the plane $x=0$.

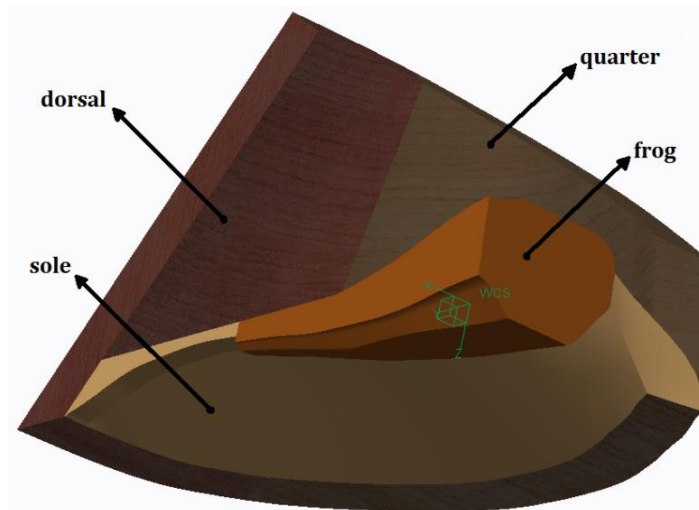


Figure 13. Different parts of the horse hoof with symmetry (own source)

The 3D model of the horse hoof has been created by using different measures. According to Hinterhofer, et al., (2001), the dorsal wall angle is 50° , the lateral wall angle of the quarter is 80° and the sole has to be concave. Moreover, according to Stachurska, et al., (2008), the toe length is 85.8 mm, the hoof width is 124.5 mm, the hoof solar length is 125.6 mm, the heel buttress distance is 74.5 mm, the toe thickness is 11.9 mm and the heel length is 45.3 mm. The sole curvature has been estimated by means of a MicroScribe and taking points of the outer curve of the sample horseshoe. Once the points were obtained, they were introduced into the software to form the sole curvature. The main dimensions used for the creation of the model are shown in *Figure 14*.

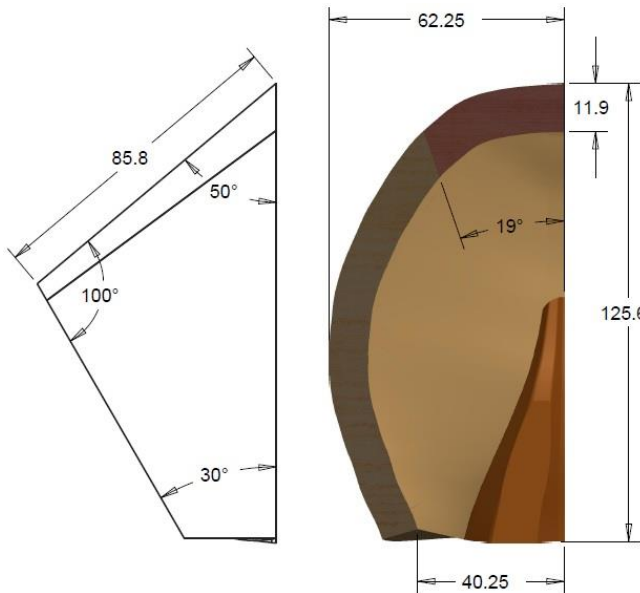


Figure 14. Dimensions of the 3D model of the horse hoof

To obtain more accurate results in the simulation of the hoof, a mesh with a Maximum Element Size of 7.5 mm has been created by using the tool AutoGEM in *PTC Creo* software. The created mesh is shown in *Figure 15*.

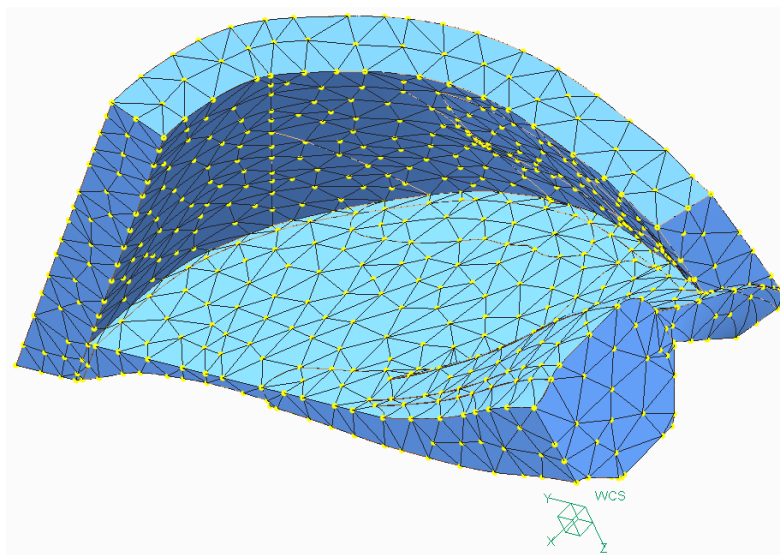


Figure 15. Model with the mesh (own source)

The boundary conditions that have been established are shown in *Figure 16*. On one hand, in the symmetry plane ($x = 0$), the design has been constrained in the x-direction. On the other hand, in the bottom plane ($z = 0$), the parts in contact with the ground have been constrained in the z- direction. Moreover, the edge of the dorsal part coincident with the y- axis has been constrained in the y- direction due to the model has to be constrained in all directions and the bottom dorsal part of the hoof is the more rigid part.

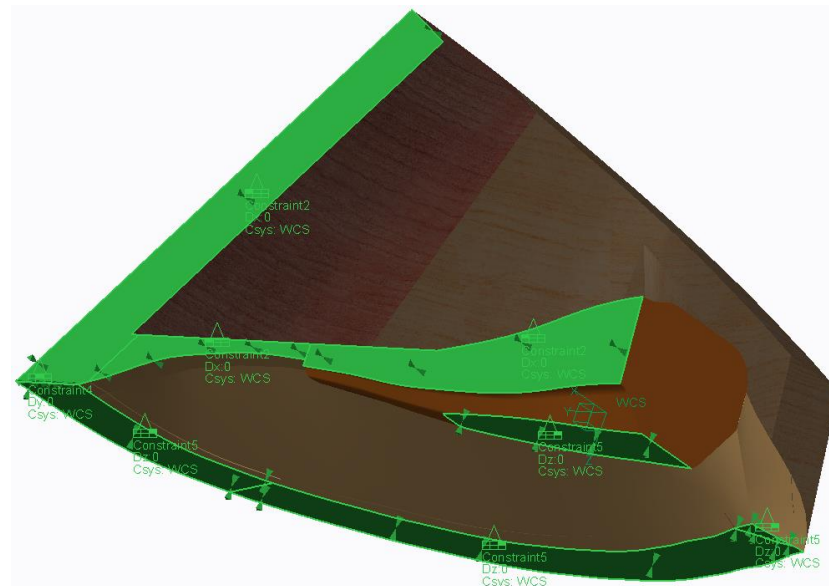


Figure 16. Model with the boundary conditions (own source)

The first thing to do before establishment the loads on the model is to determine the maximum peak of force that is supported by the horse hoof. According to Witte, et al., (2004), the maximum force supported by the hoof may reach 2.4 times the weight of the horse. This force, given by *Equation 1*, occurs when the horse gallops.

$$F = m \cdot g \cdot 2,4 = 650 \cdot 9,82 \cdot 2,4 = 15.32 \text{ [kN]} \quad (1)$$

As can be seen in *Equation 2*, since the hoof is analysed by applying symmetry in the plane $x = 0$, the above force has been divided by two.

$$F_s = \frac{F}{2} = 7.66 \text{ [kN]} \quad (2)$$

According to Hinterhofer, et al., (2001), the inner wall of the hoof has been loaded with the eighty per cent of the total load set in the model (F_s). The value of that load has been calculated in *Equation 3*.

$$F_{HW} = 0,8F_s = 6.13 \text{ [kN]} \quad (3)$$

As can be seen in *Figure 17*, the load has been established in the model as a vertical force distributed on all the inner surface of the hoof wall. This load should be parallel to the inner hoof wall surface, but due to the hoof geometry and the limitations of the software it has been decided approximate the load as a vertical one.

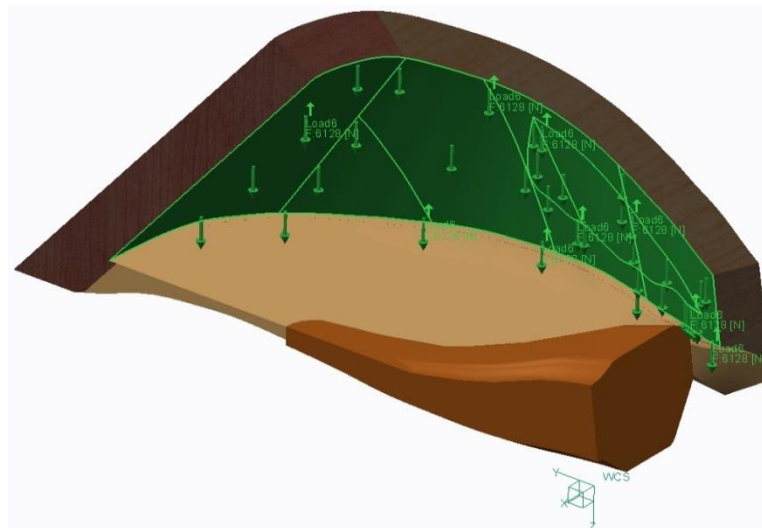


Figure 17. Hoof wall loaded with the 80% of the load (own source)

According to Hinterhofer, et al., (2001), the rest of the load (20%) is supported by the sole and the frog. Nevertheless, the frog is the part that supports the most of this force due to the anatomy of the hoof and because of being the first part of the hoof that makes contact with the ground. The load applied on the frog and the sole has been calculated in *Equation 4*.

$$F_{SF} = 0,2F_s = 1.53 \text{ [kN]} \quad (4)$$

The loads applied on the frog are transmitted by means of the digital cushion and the lateral cartilages to the horn wall. This pressure on the inner horn wall is the main cause of the hoof expansion. In *Figure 18*, it can be seen the transmitted forces as well as the different parts of the hoof which are involved in the transmission of such forces.

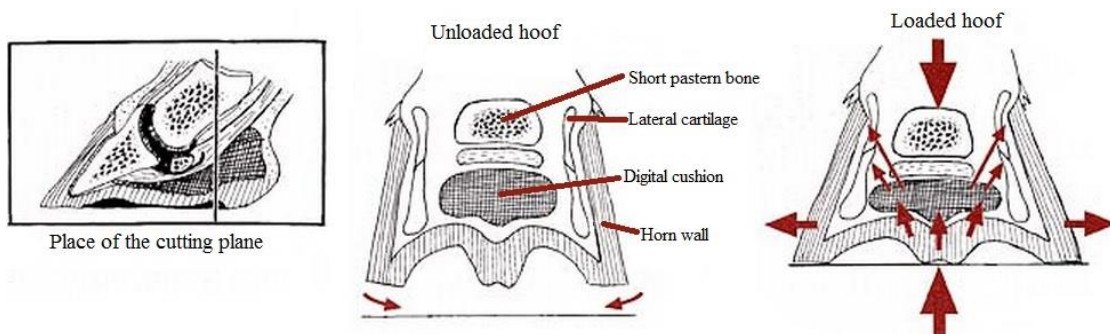


Figure 18. Distribution of forces due to the pressure on the frog (Sandgren, 2007)

Due to the anatomy and geometry of the frog, the load transmitted to the horn wall can be estimated as a triangular load distribution. In this way, as shown in *Figure 19*, a triangle of forces has been sketched keeping the proportion of the frog to calculate the pressure on the horn wall.

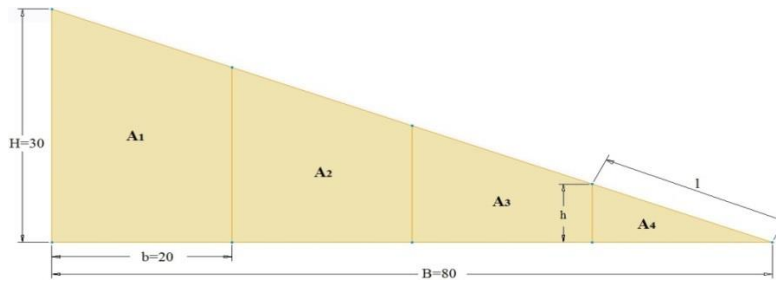


Figure 19. Triangle of forces (own source)

As can be seen in the figure above, the load will be distributed in four different areas: A_1 , A_2 , A_3 and A_4 . Thereby, the total load F_{SF} given by *Equation 5* will be divided in four different forces.

$$F_{SF} = F_1 + F_2 + F_3 + F_4 \quad (5)$$

Each load is related to one area by *Equation 6*.

$$\frac{A_i}{A_T} = \frac{F_i}{F_{SF}} \rightarrow F_i = F_{SF} \frac{A_i}{A_T} \quad (6)$$

The total area of the triangle and the area of each one of its elements have to be determined before to calculate the forces F_1 , F_2 , F_3 and F_4 . The total area of the triangle is given by *Equation 7*.

$$A_T = \frac{BH}{2} = 1200 \text{ [mm}^2\text{]} \quad (7)$$

Before obtaining the value of the area A_4 , it is necessary to calculate the hypotenuse and height of the smaller triangle. The hypotenuse l is given by *Equation 8* and the height h is given by *Equation 9*.

$$l = \frac{\sqrt{B^2 + H^2}}{4} = 21.36 \text{ [mm]} \quad (8)$$

$$h = \sqrt{l^2 - b^2} = 7.5 \text{ [mm]} \quad (9)$$

The different areas of the triangle have been calculated in *Equation 10*, *11*, *12* and *13*.

$$A_4 = \frac{bh}{2} = 75 \text{ [mm}^2\text{]} \quad (10)$$

$$A_3 = A_4 + bh = 225 \text{ [mm}^2\text{]} \quad (11)$$

$$A_2 = A_4 + 2bh = 375 \text{ [mm}^2\text{]} \quad (12)$$

$$A_1 = A_4 + 3bh = 525 \text{ [mm}^2\text{]} \quad (13)$$

Considering the total load F_{SF} , the total area of the triangle A_T and the different subareas calculated above, it is possible to obtain the forces corresponding to each area by using the *Equation 6*. The values of these forces have been determined in *Equation 14, 15, 16 and 17*.

$$F_1 = F_{SF} \frac{A_1}{A_T} = 0.67 \text{ [kN]} \quad (14)$$

$$F_2 = F_{SF} \frac{A_2}{A_T} = 0.48 \text{ [kN]} \quad (15)$$

$$F_3 = F_{SF} \frac{A_3}{A_T} = 0.29 \text{ [kN]} \quad (16)$$

$$F_4 = F_{SF} \frac{A_4}{A_T} = 95.75 \text{ [N]} \quad (17)$$

Finally, as has been explained above, the forces are transmitted by means of the digital cushion and the lateral cartilages to the horn wall. Thereby, these forces have been set in the model by applying four different pressures on four different surfaces of the inner hoof wall. Each one of these surfaces has been measured directly in *PTC Creo* and their values are: $S_1 = 569.99 \text{ mm}^2$, $S_2 = 913.26 \text{ mm}^2$, $S_3 = 1217.20 \text{ mm}^2$ and $S_4 = 490.14 \text{ mm}^2$. The values of the pressures have been calculated in *Equation 18, 19, 20 and 21*.

$$P_1 = \frac{F_1}{S_1} = 1.18 \text{ [MPa]} \quad (18)$$

$$P_2 = \frac{F_2}{S_2} = 0.52 \text{ [MPa]} \quad (19)$$

$$P_3 = \frac{F_3}{S_3} = 0.24 \text{ [MPa]} \quad (20)$$

$$P_4 = \frac{F_4}{S_4} = 0.20 \text{ [MPa]} \quad (21)$$

The different pressures applied in their corresponding surfaces are shown in *Figure 20*. The highest pressure has been applied in the part of the horn wall where the frog is bigger and the lowest pressure in the part where the frog is smaller. In this way, the pressure P_1 has been set in the surface shown in the upper left picture, the pressure P_2 has been set in the surface shown in the upper right picture, P_3 has been set in the

surface shown in the bottom left picture and P_4 has been set in the surface shown in the bottom right picture.

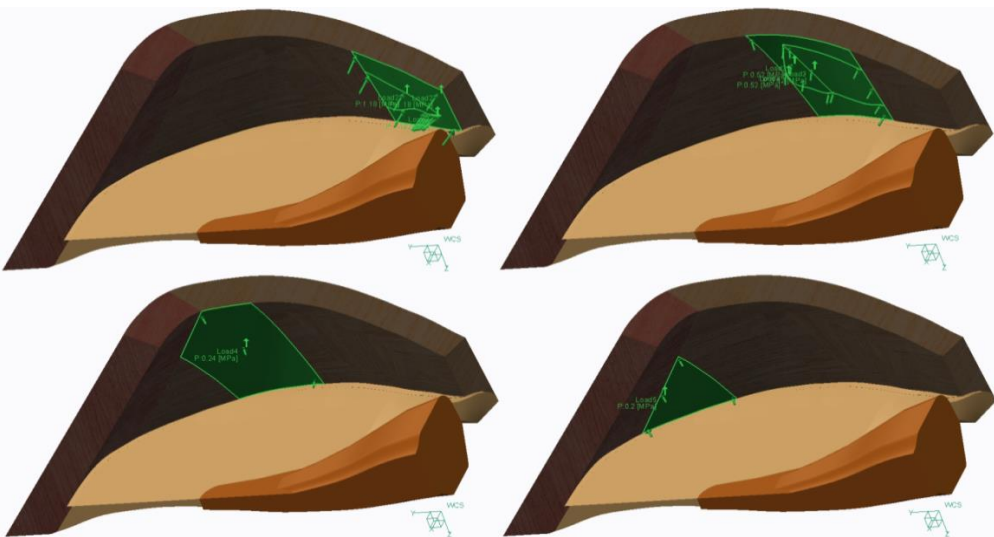


Figure 20. Load due to the pressure on the frog and the sole (own source)

The mesh, loads, boundary conditions and materials that have been established in the 3D model to enable the simulation of the part are represented in *Figure 21*.

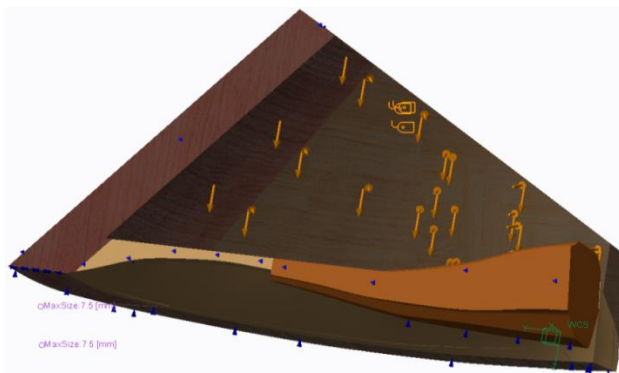


Figure 21. The mesh, loads, boundary conditions and materials established in the model (own source)

It should be noted that any kind of friction has been set in the implementation of the hoof. This is because any displacements have not been obtained when a coefficient of friction has been established between the hoof and the ground. The reason is that the command “Infinite friction” has to be selected in the software before establishing a coefficient of friction. So, the results obtained will be greater than if friction would have been set. However, this will be not a problem because a well done design takes into account the worst conditions and, in this case, the worst conditions are the maximum displacement.

2.2. Results

The results of the simulation are shown in *Figure 22*, the displacements in all directions have been represented in a fringe diagram with the deformed model. These diagrams have been compared with the original model where there are no applied loads. The transparent overlay of the model has a deformation scale of 7.5 %. It can be observed that the maximum displacement is given in the rear part of the hoof.

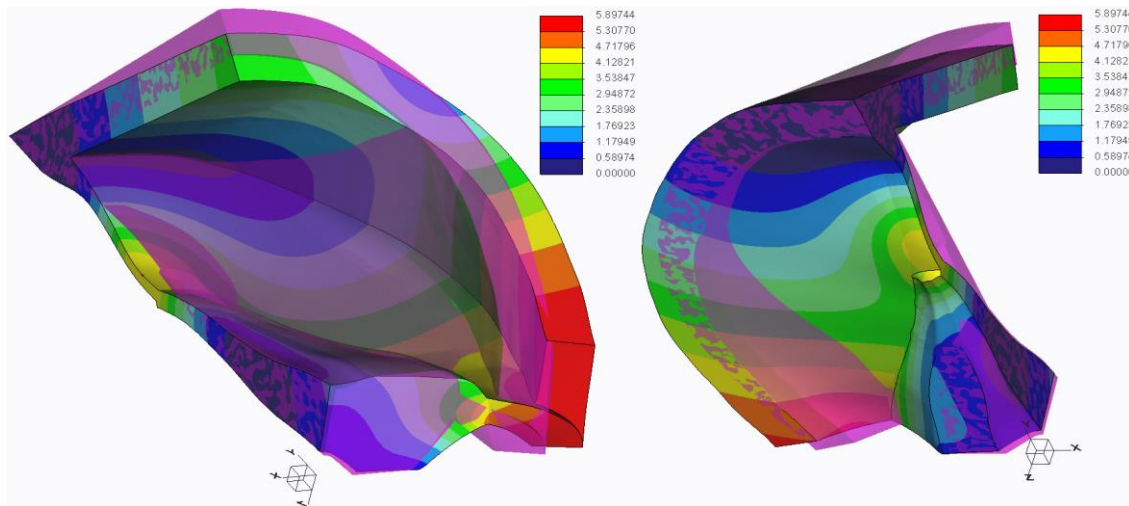


Figure 22. Fringe diagram of the displacements in all directions (own source)

The outer bottom curve of the hoof has been selected to show the displacements in all directions. As can be seen in the graph in *Figure 23*, the maximum displacement obtained is 5.50 mm.

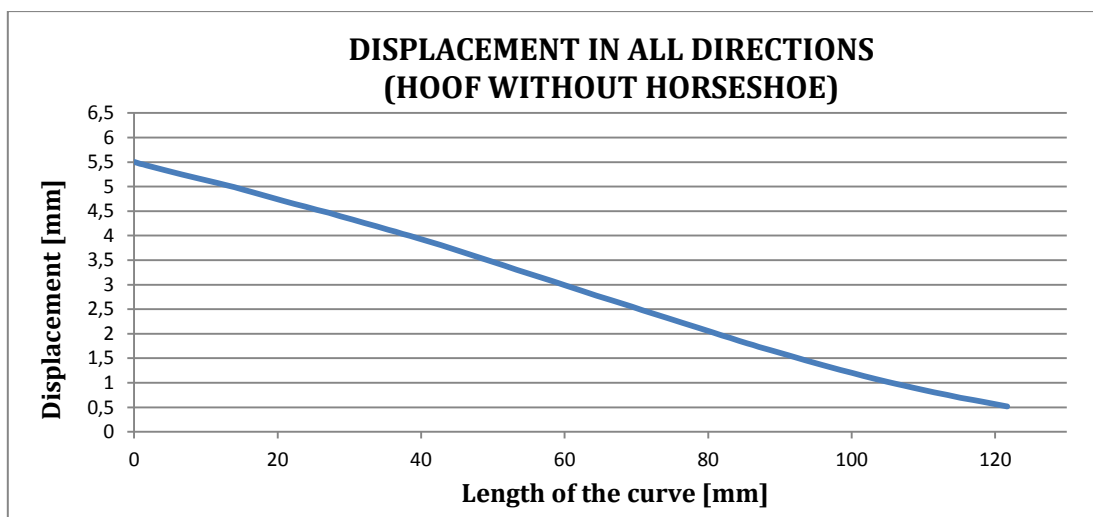


Figure 23. Displacement graph of the outer bottom curve in all directions (own source)

As shown in *Figure 24*, the displacements in x- direction have been represented in a fringe diagram with the deformed model. A transparent overlay unloaded model is shown in order to compare the behaviour of the unloaded and loaded hoof.

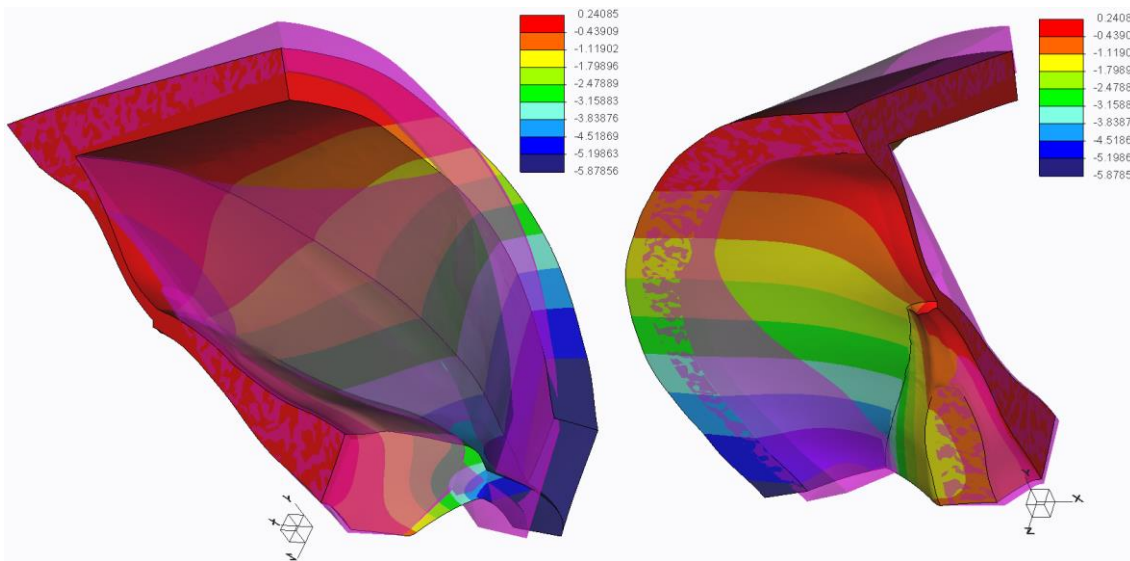


Figure 24. Fringe diagram of the displacement in the x- direction (own source)

The outer bottom curve of the hoof has been selected again to show the displacements in x- direction. As can be seen in the graph in *Figure 25*, the maximum displacement obtained is 5.45 mm, so this proves that the main deformation of the hoof takes place in the x- direction.

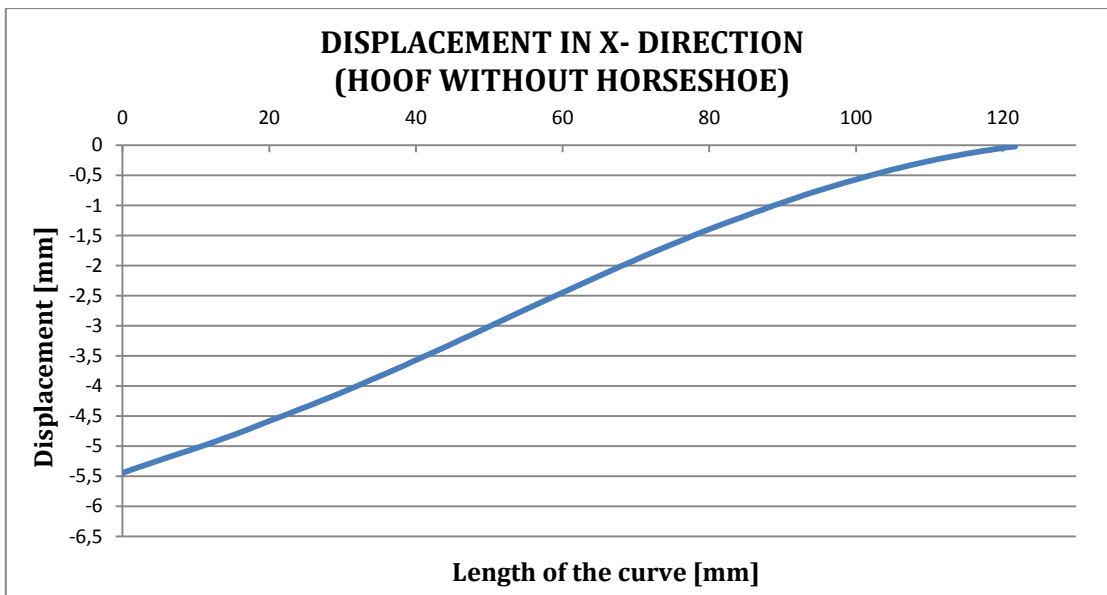


Figure 25. Displacement graph of the outer bottom curve in the x- direction (own source)

The obtained results show the maximum displacement of the hoof along x- direction, it has not been able to reach the displacement given by Garcia (2013) which is 8 mm, however, the obtained value is acceptable and the curve described by the hoof model is quite similar to a real one, being maximum in the rear part and decreasing while it is approximating to the toe.

3. ANALYSIS OF THE HOOF WITH A REGULAR HORSESHOE

In this study, a regular horseshoe will be attached by nails to the previously analysed hoof in order to evaluate the behaviour both the hoof as the horseshoe. The applied loads of the hoof will be the same than the prior section.

3.1. Implementation

Figure 26 shows the model of the regular horseshoe which is going to be attached to the hoof model. The model taken for the design is a Mustad LiBero horseshoe which has been shown previously. As in the simulation there is not any external force or an irregular ground which can displace the horseshoe from the hoof, the two side clips have been removed of the original design due to their function is to help to keep the horseshoe in its place. The material properties taken for the horseshoe have been taken from PTC Creo Database. The chosen material is steel which has a density of 7.83 g/cm^3 , a Poisson's Ratio of 0.27 and a value of Young's Modulus of 200 GPa.



Figure 26. 3D-model of the regular horseshoe (own source)

A nail model has been created to attach the horseshoe to the hoof in the simulation. The chosen nail material is the same selected steel for the regular horseshoe. The head type of the nail is known as City. A 3D model of the nail is represented in *Figure 27*.



Figure 27. Model of the nail (own source)

In *Figure 28*, as it has made before, the model of the horse hoof assembled with the regular horseshoe has been simulated by using the symmetry in the plane $x = 0$.

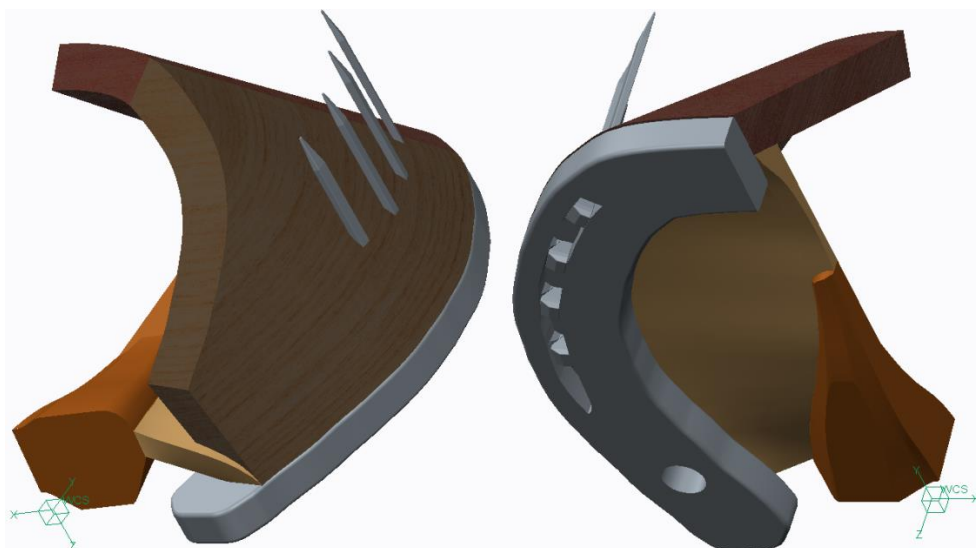


Figure 28. Model of the horse hoof with a regular horseshoe (own source)

In order to obtain more accurate results a mesh of the whole assembly has been created. The selected Maximum Element Size for the assembly is 7.5 mm. The mesh is shown in *Figure 29*.

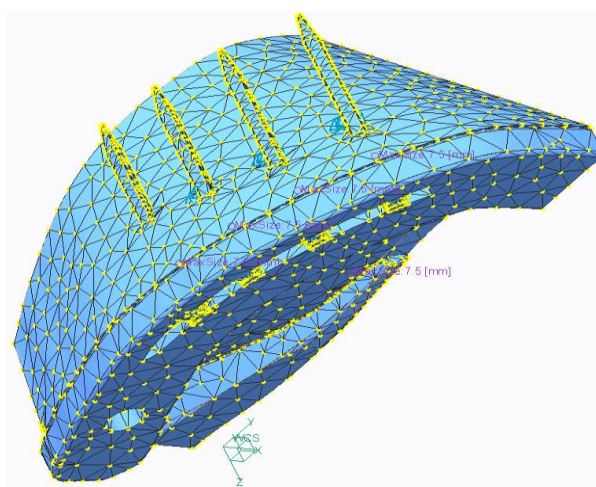


Figure 29. Assembly with the mesh (own source)

The boundary conditions that have been established are shown in *Figure 30*. On one hand, in the symmetry plane ($x = 0$), the assembly has been constrained in the x- direction. On the other hand, the parts in contact with the ground have been constrained in the z- direction. Moreover, the edge of the dorsal part coincident with the y- axis has been constrained in the y- direction.

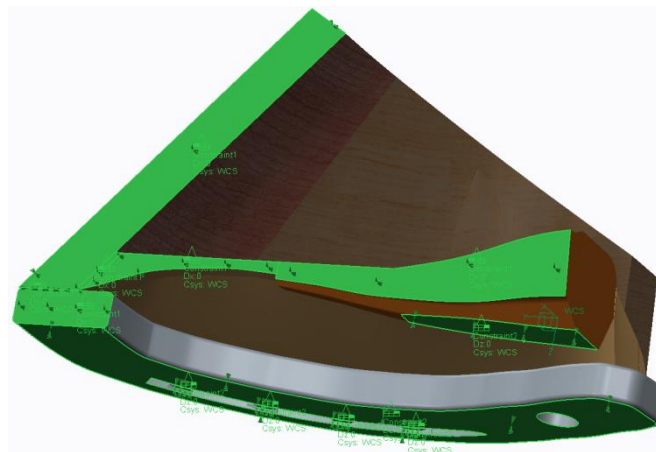


Figure 30. Assembly with the boundary conditions (own source)

In order to make the analysis under the same conditions, the loads set in this assembly have been the same that the loads set in the model of the hoof described in the section above. The assembly with the loads is shown in *Figure 31*.

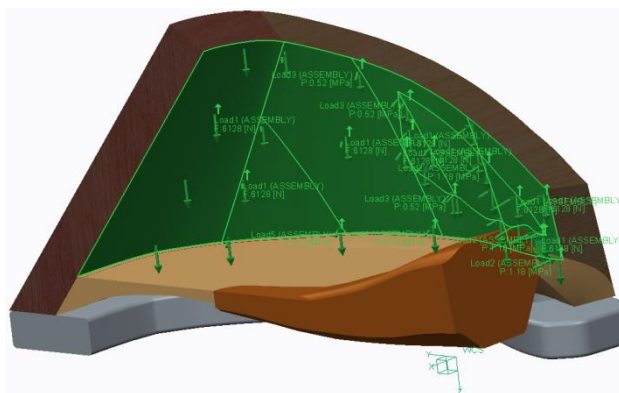


Figure 31. Assembly with the loads (own source)

Figure 32 shows the connections between the horseshoe, the nails and the hoof. These links have been simulated by setting different coefficients of friction, although the results obtained have always been the same. This is because the command “Infinite friction” has to be selected in the software before establishing a coefficient of friction. Because of this, *PTC Creo* analyses all the simulations as if infinite friction between the different surfaces would have been established.

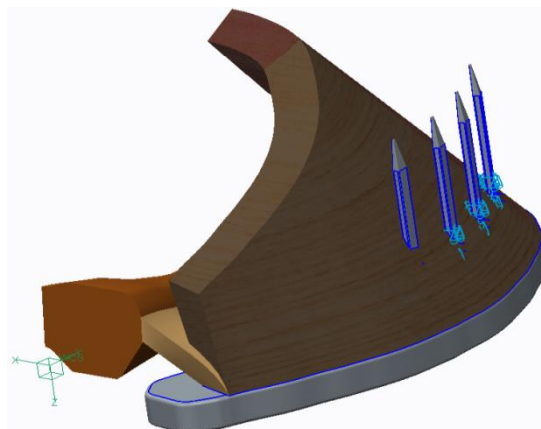


Figure 32. Assembly with the connections set (own source)

For this reason, two different simulations have been performed. One of the simulations has been done by establishing infinite friction between the horseshoe and the hoof. The other analysis has been done by simulating the model without friction between them. Thereby, the real deformation of the horseshoe and the hoof will be between the results obtained in both simulations.

Moreover, the connections between the nails and the hoof have always been set with infinite friction for several reasons. The first reason is because the coefficient of friction between these parts is unknown and, as it has been explained above, if the coefficient were known or estimated the software would perform the simulation with infinite friction. On the other hand, if a contact interface between the hoof wall and the nails is set without infinite friction, it will mean that the nails can be displace along the hoof wall. As can be seen in *Figure 33*, the other reason is because the nails are attached to the hoof in a way that makes almost impossible to have any relative displacement between the hoof wall and the nails.



Figure 33. Cross section of the hoof with a nailed horseshoe (Barefoot-Hoofcare, 2013)

The mesh, loads, boundary conditions, materials and connections that have been established in the 3D model to enable the simulation of the assembly are represented in *Figure 34*.

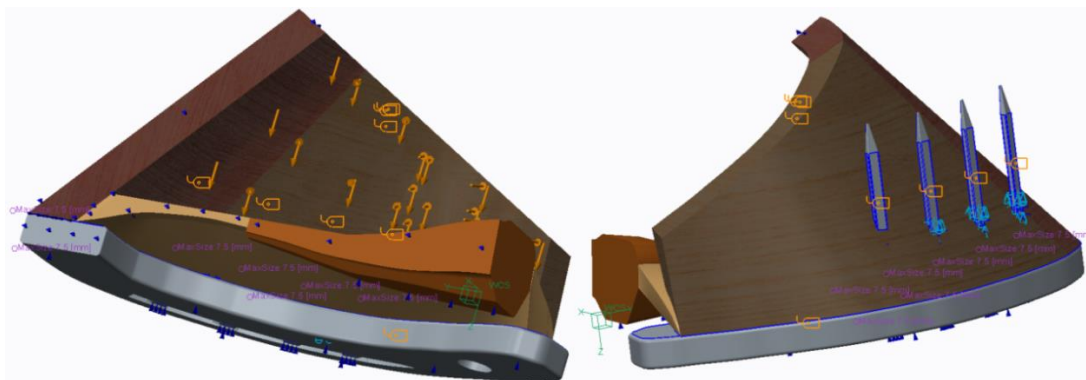


Figure 34. The mesh, loads, boundary conditions, materials and connections set (own source)

3.2. Results

In this section, the results of the horseshoe-hoof assembly will be shown. The assembly will be analysed twice. In the first analysis, the friction between the hoof and the horseshoe will be considered. On the other hand, in the second test, such friction will be removed in order to observe the maximum displacement of the hoof.

3.2.1. Friction between the hoof and the horseshoe

As can be seen in *Figure 35*, the displacements in all directions have been represented in a fringe diagram with the deformed assembly. The value of the deformation scale is 7.5%. A transparent overlay of an unloaded model is added to compare the displacement caused by the forces applied on the hoof.

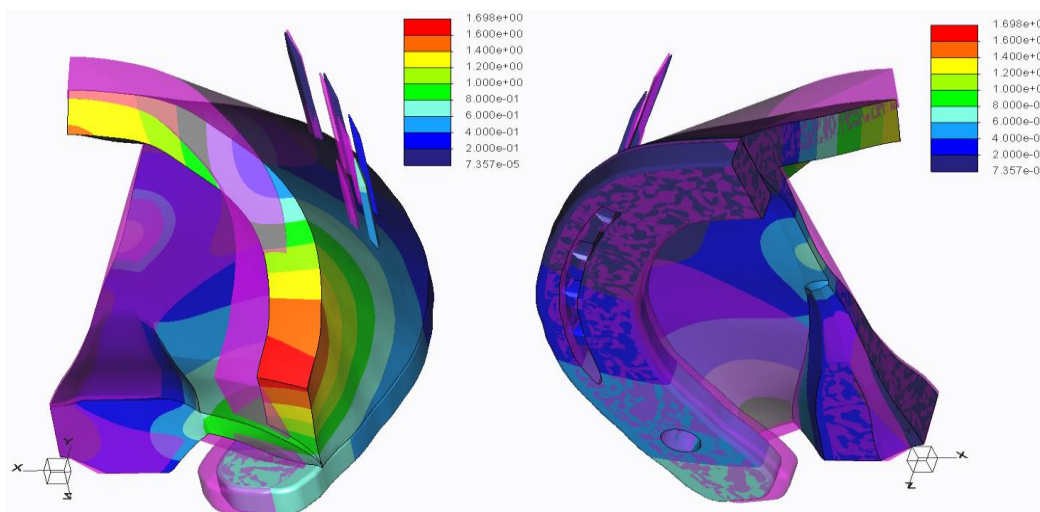


Figure 35. Fringe diagram of the displacements of the assembly in all directions (own source)

In *Figure 36*, the hoof has been removed from the fringe diagram to have a better view of the displacement suffered by the horseshoe and the nails in all directions. It can be observed that the maximum displacement goes from the rear part decreasing until the toe, where the displacement tends to zero.

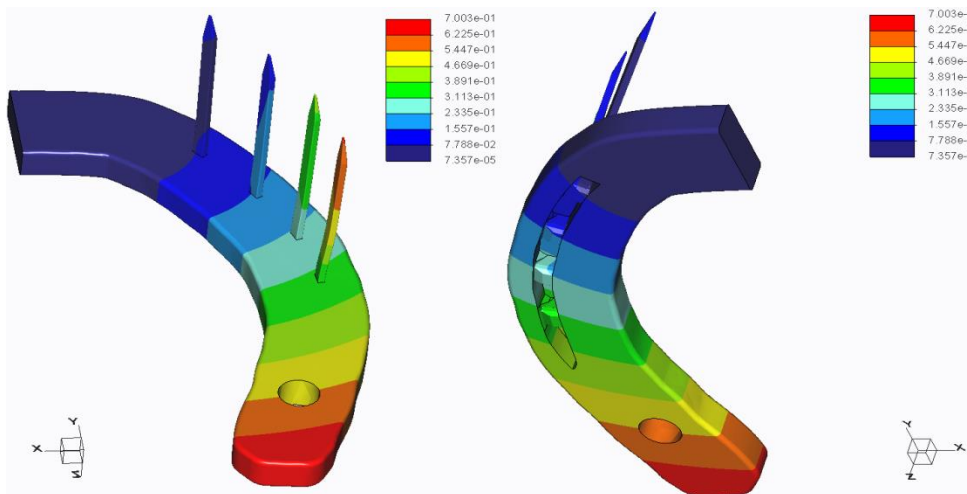


Figure 36. Fringe diagram of the displacements of the horseshoe and nails in all directions (own source)

Since the main deformation of the hoof takes place in the x- direction, the outer bottom curve of the hoof has been selected to show the displacements in the x- direction. As can be seen in the graph in *Figure 37*, the displacement of the hoof has been compared with the displacement of the outer upper curve of the horseshoe. The maximum displacement of the hoof is equal to 0.65 mm and the maximum displacement of the horseshoe is equal to 0.64 mm. The reason of that these obtained values have been practically equal is because the simulation has been carried out by setting infinite friction.

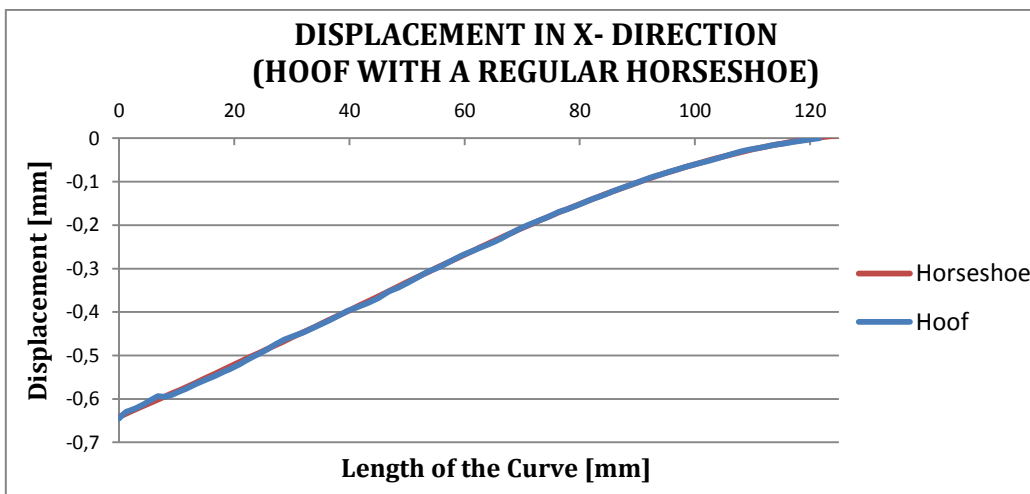


Figure 37. Horseshoe displacement compared with the hoof displacement in the x- direction (own source)

In *Figure 38* has been represented a graph with the displacement in the z- direction of the outer upper curve of the horseshoe. This representation has been chosen as a parameter to quantify the impact absorption capacity of a regular horseshoe. As can be seen in the graph, the maximum compression of the horseshoe is equal to $6.92 \cdot 10^{-4}$ mm, so this horseshoe is not able to absorb impacts.

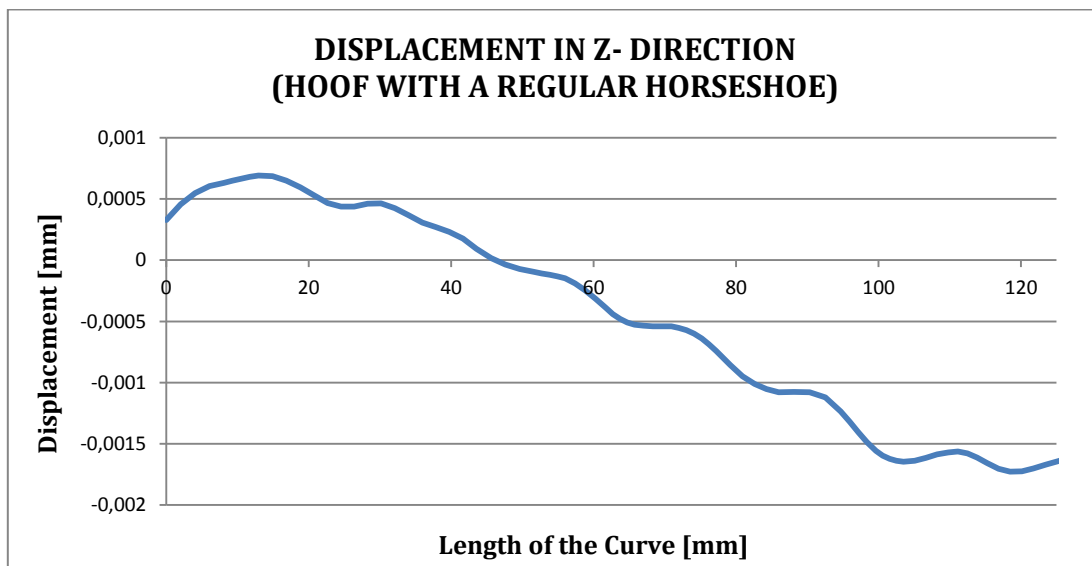


Figure 38. Horseshoe displacement in the z- direction (own source)

Since the ductility of the horseshoe, the nails and the hoof, the Von Mises stress has been chosen to show the distribution of stresses in the assembly. The Von Mises stress is given by *Equation 22* (Romero, et al., 2002), where σ_1 , σ_2 and σ_3 are the principal stresses.

$$\sigma_{VM} = \sqrt{\frac{1}{2}[(\sigma_1 - \sigma_2)^2 + (\sigma_1 - \sigma_3)^2 + (\sigma_2 - \sigma_3)^2]} \quad (22)$$

Figure 39 shows a fringe diagram of the Von Mises stress in the hoof. As can be seen in the right picture of the figure, the maximum stress is about 108 MPa and it is located in one nail hole.

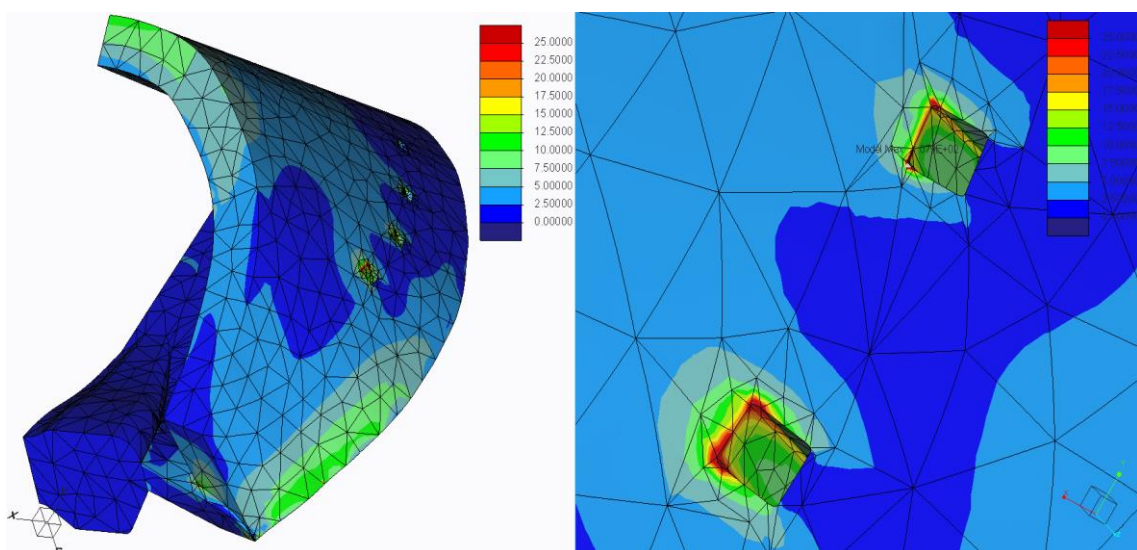


Figure 39. Fringe diagram of the Von Mises stress in the hoof (own source)

Figure 40 shows a fringe diagram of the Von Mises stress in the horseshoe. As can be seen in the right picture of the figure, the maximum stress is about 1417 MPa and it is also located in one nail hole.

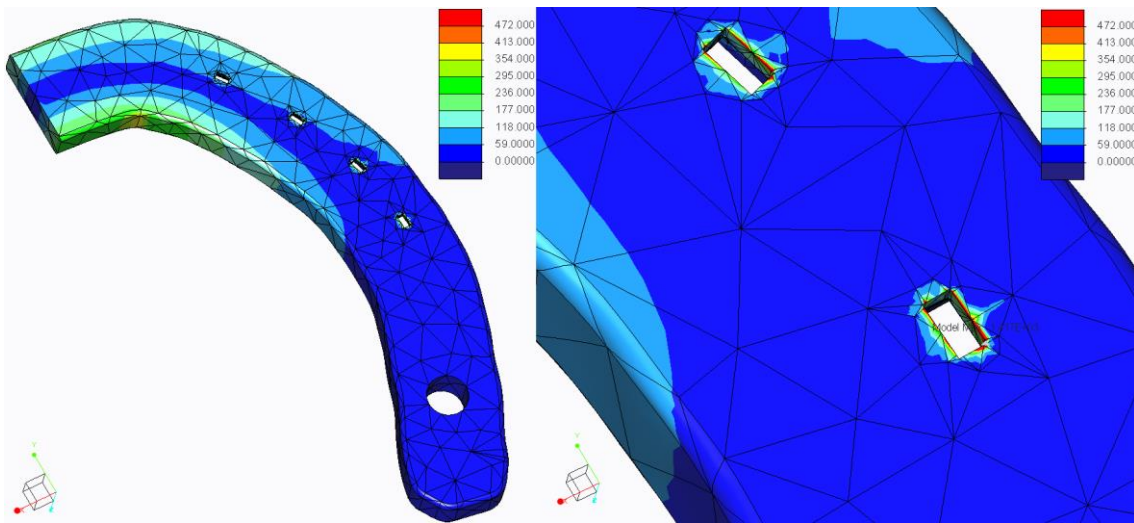


Figure 40. Fringe diagram of the Von Mises stress in the horseshoe (own source)

Figure 41 shows a fringe diagram of the Von Mises stress in the nails. As can be seen in the right picture of the figure, the maximum stress is about 1375 MPa and it is located at the bottom of one nail.

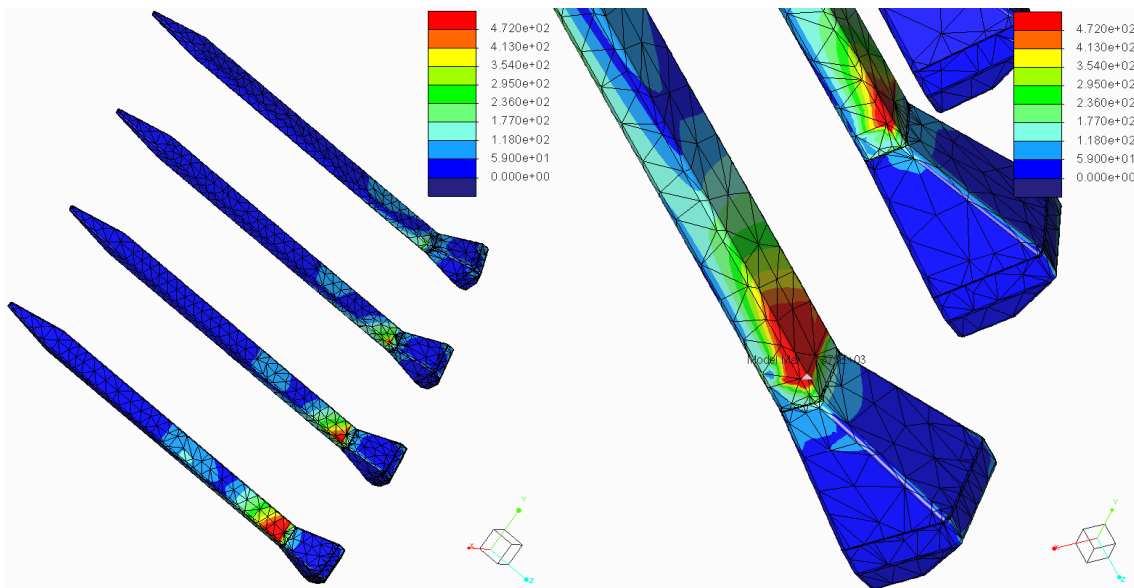


Figure 41. Fringe diagram of the Von Mises stress in the nails (own source)

3.2.2. No friction between the hoof and the horseshoe

As can be seen in *Figure 42*, the displacements in all directions have been represented in a fringe diagram with the deformed assembly. These diagrams have been compared with a transparent overlay where there are not any applied loads.

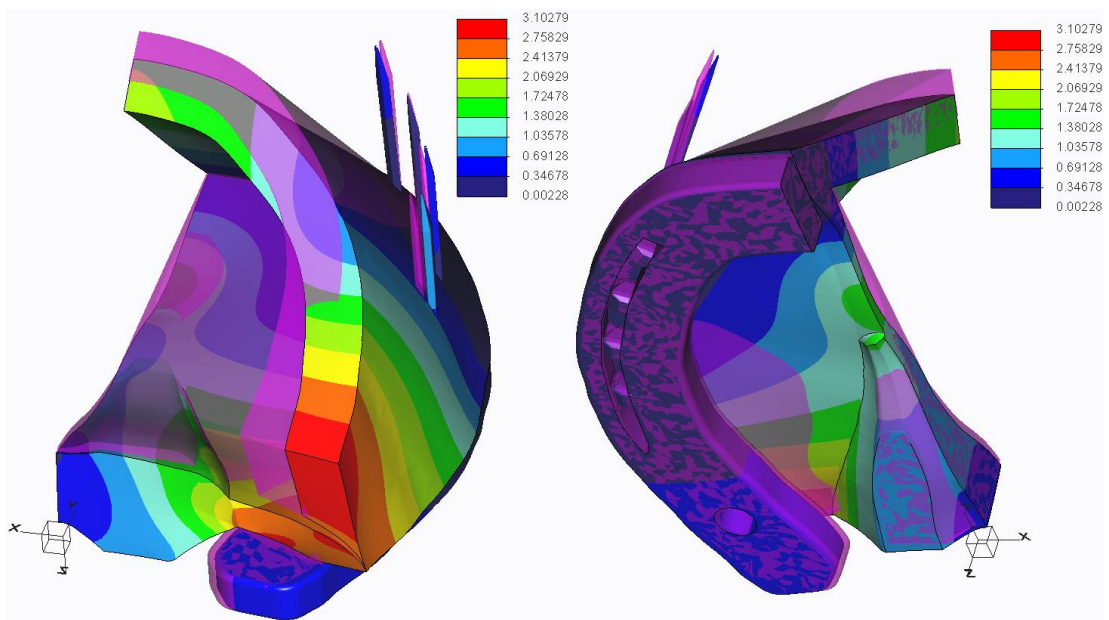


Figure 42. Fringe diagram of the displacements of the assembly in all directions (own source)

The displacements in all directions are represented in a fringe diagram with the deformed model of the horseshoe with the nails. This diagram is shown in *Figure 43*.

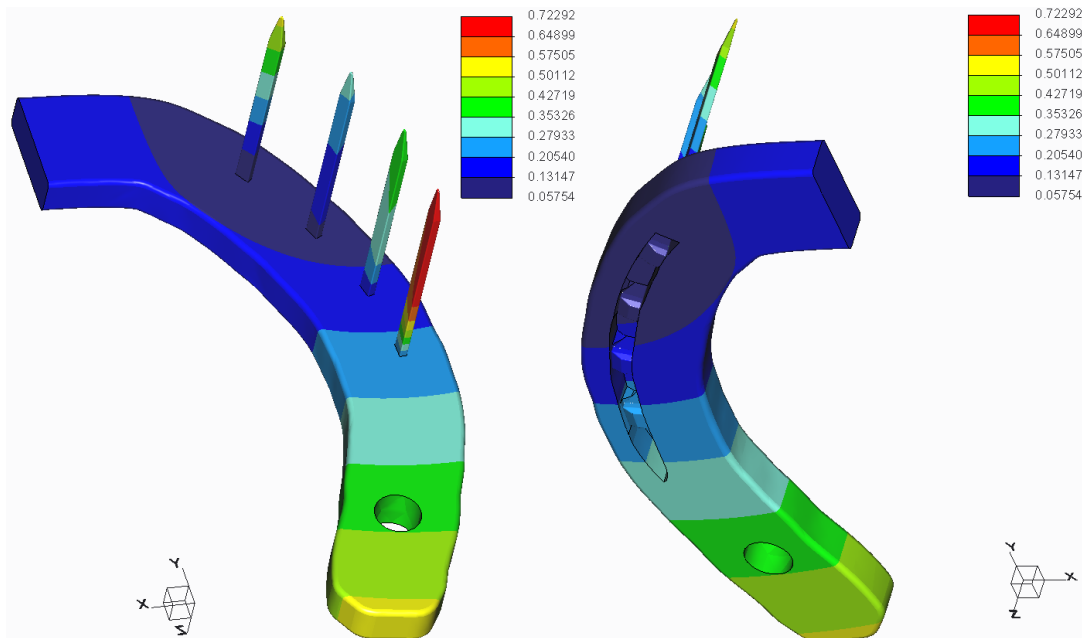


Figure 43. Fringe diagram of the displacements of the horseshoe and nails in all directions (own source)

Since the main deformation of the hoof takes place in the x- direction, the outer bottom curve of the hoof has been selected again to show the displacements in the x- direction. As can be seen in the graph in *Figure 44*, the displacement of the hoof has been compared with the displacement of the outer upper curve of the horseshoe. The maximum displacement of the hoof is equal to 2.73 mm and the maximum displacement of the horseshoe is equal to 0.48 mm. The difference between these values is due to the

simulation has been done by setting a connection between the horseshoe and the hoof without friction. So, as is logical, the displacement of the hoof is larger than the displacement of the horseshoe.

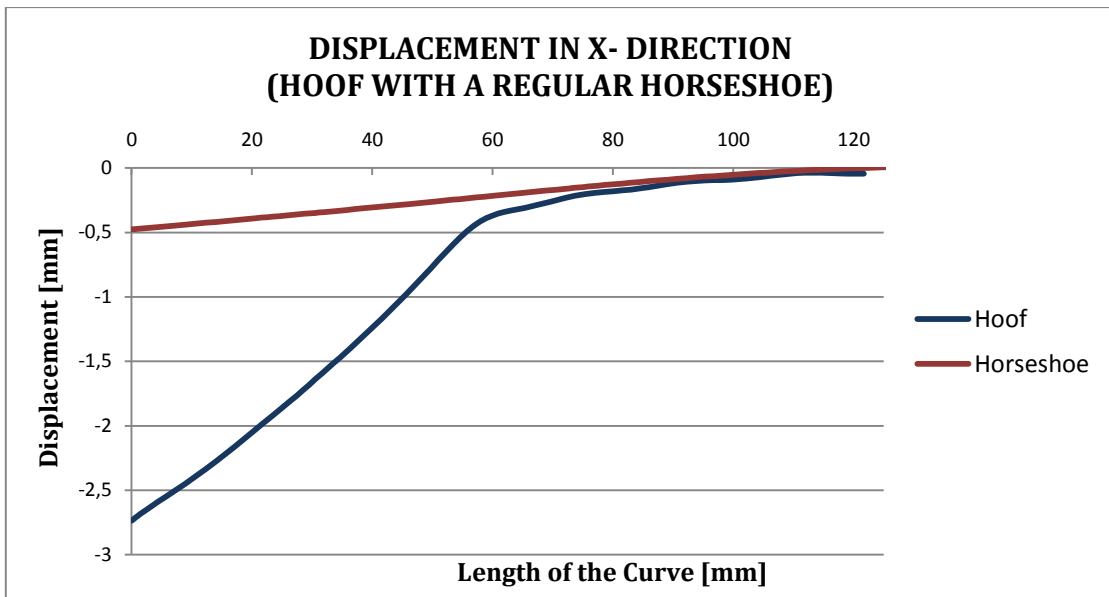


Figure 44. Horseshoe displacement compared with the hoof displacement in the x- direction (own source)

In *Figure 45* has been represented a graph with the displacement in the z- direction of the outer upper curve of the horseshoe. As described above, this representation has been chosen as a parameter to quantify the impact absorption capacity of a regular horseshoe. As can be seen in the graph, the maximum compression of the horseshoe is equal to $2.81 \cdot 10^{-4}$ mm, so this horseshoe is not able to absorb impacts.

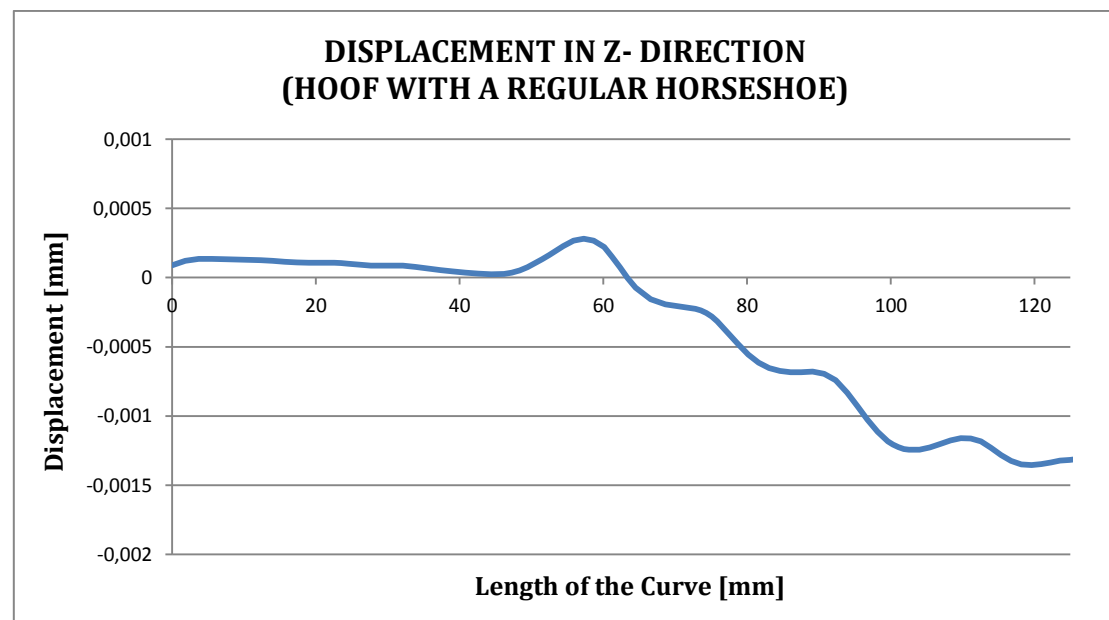


Figure 45. Horseshoe displacement in the z- direction (own source)

Figure 46 shows a fringe diagram of the Von Mises stress in the hoof. As can be seen in the right picture of the figure, the maximum stress is about 263 MPa and it is located in one nail hole.

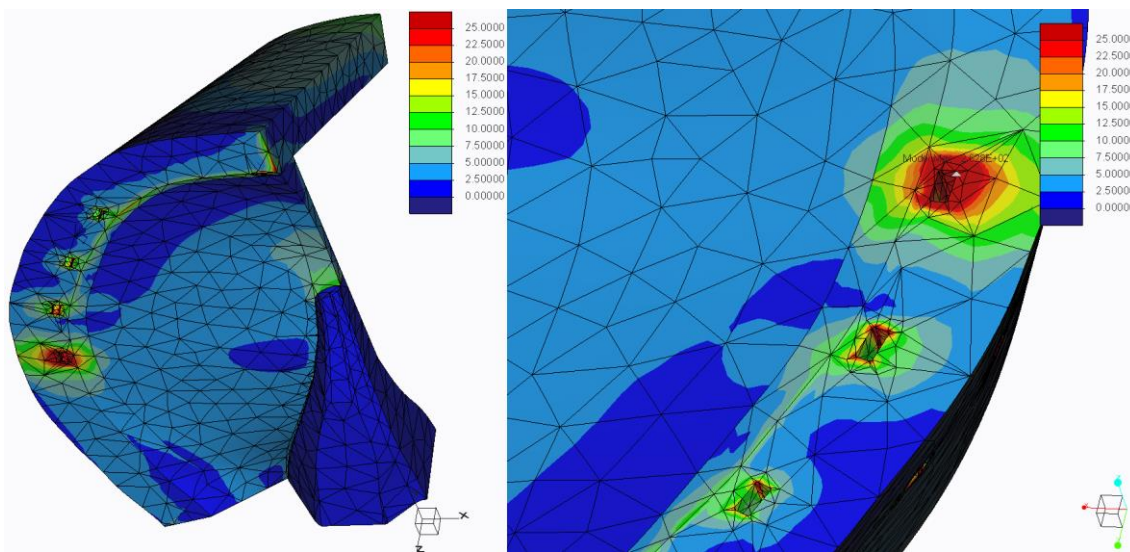


Figure 46. Fringe diagram of the Von Mises stress in the hoof (own source)

Figure 47 shows a fringe diagram of the Von Mises stress in the horseshoe. As can be seen in the right picture of the figure, the maximum stress is about 5825 MPa and it is also located in one nail hole. This high stress is due to the corners of the nail holes have not been rounded in the regular horseshoe. However, the stress in the most of the horseshoe is between 0 and 413 MPa. So, this is a proof that the corners of the holes have to be rounded to avoid any kind of failure.

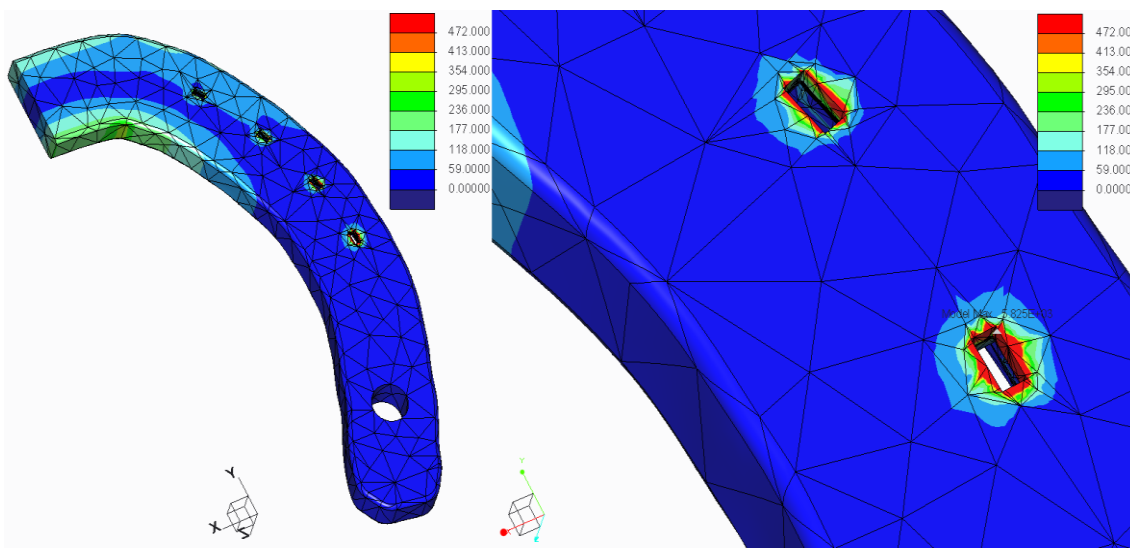


Figure 47. Fringe diagram of the Von Mises stress in the horseshoe (own source)

The fringe diagram of the Von Mises stress in the nails is shown in *Figure 48*. As can be seen in the right picture of the figure, the maximum stress is about 5774 MPa and it is located at the bottom of one nail.

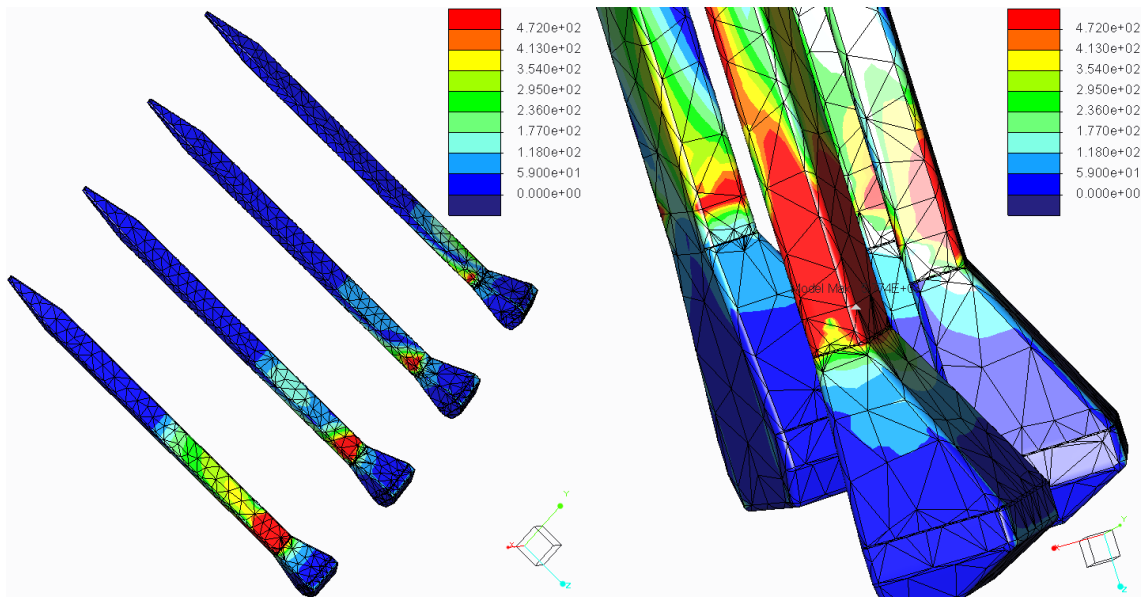


Figure 48. Fringe diagram of the Von Mises stress in the nails (own source)

The high obtained value is due that the corner of the horseshoe which is in contact with the nail is not rounded, the software fails when it treat to round the edges, making impossible the mesh creation. It has been tried to solve this issue without any satisfactory result. If the stress concentration in this tiny region of the nail will be consider as an abnormal peak of stress, the stress value in the nail would be from 0 to 472 MPa.

4. DESIGN OF A COMPLIANT HORSESHOE

After the simulations and analyses performed, the next step will be the design of the compliant horseshoe. To do that, several studies will be done by comparing some current horseshoes, different materials and some attachment methods.

4.1. Comparison of different horseshoes

Different horseshoes have been compared with the aim of obtaining the most relevant features and advantages of each one. The horseshoes chosen for the comparison have been two common horseshoes, one made of steel and other made of aluminium, and three modern shoes.

Figure 49 shows a steel horseshoe of the brand “Mustad”. This shoe is for the hind limb and is used for sport. It is attached to the hoof by nailing and has a thickness of 8.3 mm. The two side clips allow a better attachment to the hoof. This horseshoe is not flexible obviously due to the stiffness of the steel



Figure 49. Steel Horseshoe (Mustad, 1999)

Another horseshoe of the same brand is the one shown in *Figure 50*. This horseshoe is made of aluminium and is very light, against the horseshoe above. It has a thickness of 8 mm and is also attached to the hoof by nailing. Since this shoe is used for racing it has a toe grip of 3 mm to provide to the horse a better traction. The shoe represented in the figure is a hind limb shoe.



Figure 50. Aluminium Horseshoe (Mustad, 1999)

The horseshoe represented in *Figure 51* is composed by three different pieces made of steel or aluminium and assembled between them by polyurethane. This horseshoe, made by the brand Tru-Shu Equine, is special for its flexibility obtained due to the two urethane “hinges”. The shoe can be attached to the hoof by nailing and/or glue depending on the conditions and needs required by the horse. Furthermore, this horseshoe also has a toe grip to provide to the hoof traction.



Figure 51. TruShu-Equine Horseshoe (TruShu-Equine, 2013)

The fourth horseshoe, shown in *Figure 52*, is a modern horseshoe made by the brand “ImprintSport”. The main features of the shoe are described in the figure. The whole horseshoe is made of polymer with the aim of getting flexibility. Unlike the models above described, this horseshoe has a central part under the frog whose function is maximise the ground bearing surface and facilitate the natural movement of the hoof. This design used for sport is attached to hoof only by glue.



Figure 52. ImprintSport Horseshoe (ImprintSport, 2008)

The following horseshoe has been design by the brand “EponaShoe” by utilizing composite polymers. As can be seen in *Figure 53*, it also has a part for the frog to provide a correct blood circulation along the horse leg. The shoe is hard and stiff where the nails are attached and soft under the sole and frog. It is used for sport and it is really good to walk in asphalt. Moreover, it is possible to attach some grips to the horseshoe with the aim of providing to the horse a better traction.



Figure 53. EponaShoe Horseshoe (EponaShoe, 2010)

By comparing and analysing these horseshoes it is possible to come to several conclusions about some features that a good horseshoe should have. Since horseshoes are exposed to a high wear, the material of the shoe in contact with the ground should be one with a great hardness to avoid the wear as far as possible. Polymers can be adapted to the movement of the hoof easily, but their wear resistant is very low. This problem could be solved with a design similar to the Tru-Shu Equine horseshoe, which uses the hardness and stiffness of the metals and the flexibility of the polymer to make a wear resistant and flexible shoe. Since polymers allow absorbing the shock too, the new design should have a polymer layer to reduce the impacts suffered by the hoof.

The hoof mechanism works correctly with the barefoot hoof. This is mainly due to two reasons: the hoof has not any abnormal restrictions and all the hoof wall and frog make contact with the ground. Thereby, it should be interesting to include in the design of the compliant horseshoe a part under the frog to provide to the hoof the correct support surface, which will facilitate the hoof movement.

4.2. Comparison of different materials

The main features (compliant, lightweight, impact absorbing and wear resistant) of a perfect horseshoe are largely dependent on the different materials chosen and their properties. For this reason, the regular horseshoe above has been simulated by setting different materials to determine which material or materials are the most appropriate for the compliant horseshoe.

In Table 1 some features as Young's Modulus, Poisson's Ratio, Density, Yield Strength, Ultimate Tensile Strength and Brinell Hardness of some metal and metal alloys are shown. The chosen metals are the most common materials used in the horseshoes manufacturing. In *Table 2* is shown some polymers properties. Polymers are more and more used in the field of horseshoes. Polymer horseshoes have the advantage of being quite lightweight and have a low value of Young's Modulus which implies it is extremely flexible and allow the natural expansion and compression of the horse hoof.

For this reason, this kind of material is taking into account in the design of the compliant horseshoe. However, the hardness of the polymers is relatively low comparing with other materials. Its value is approximately around 5 and 30 in the Brinell Scale.

METALS AND METAL ALLOYS						
Material	Young's Modulus [GPa]	Poisson's Ratio	Density [g/cm³]	Yield Strength [MPa]	Ultimate Stress [MPa]	Hardness [Brinell]
Steel Alloy 4340	207	0.30	7.85	472–1620	745–1760	217
Gray Iron G4000	66–97	0.26	7.30	—	276	217–269
Ductile Iron 120-90-02	164	0.28	7.10	621	827	331
Aluminium Alloy 7075	71	0.33	2.80	103–505	228–572	150
Magnesium Alloy AZ31B	45	0.35	1.77	220	290	46–73
Titanium Alloy Ti-6Al-4V	114	0.34	4.43	830–1103	900–1172	334
Copper Alloy C17200	128	0.30	8.25	195–1205	415–1310	100–363

Table 1. Comparison of metals and metal alloys (Callister & Rethwisch, 2011)

POLYMERS					
Material	Young's Modulus [GPa]	Poisson's Ratio	Density [g/cm³]	Yield Strength [MPa]	Ultimate Stress [MPa]
Polyetheretherketone (PEEK)	1.10	0.40	1.31	91	70.3–103
Polyethylene (LDPE)	0.172–0.282	0.33–0.40	0.925	9.0–14.5	8.3–31.4
Polyethylene (HDPE)	1.08	0.46	0.959	26.2–33.1	22.1–31.0
Polytetrafluoroethylene (PTFE)	0.40–0.55	0.46	2.17	13.8–15.2	20.7–34.5
Polyurethane Thermoplastic	0.025	0.25	1.12	7.6	33
Rubber	0.00235	0.475	1.13	7	20
Adiprene LF-950	0.0152	0.46	1.2	-	350

Table 2. Comparison of polymers (Callister & Rethwisch, 2011)

All these materials have been analysed by PTC Creo software. The analysis which was done previously with the sample horseshoe is going to be the method to compare the chosen materials. One study of each material has been carried out by using the same assembly hoof-horseshoe, the same applied loads, the same constrains and any other feature. Results are shown in *Appendix A*.

After have performed all the simulations of the different materials seen in the tables above under the same loads conditions, the obtained results are going to be arranged from highest to lowest displacement in x- direction and z- direction successively.

Order by highest to lowest displacement in x- direction:

Rubber > PTFE = LDPE > PEEK > HDPE > Polyurethane Thermoplastic > Adiprene LF-950

Order by highest to lowest displacement in z- direction:

Rubber > Adiprene LF-950 > Polyurethane Thermoplastic > LDPE > PTFE > HDPE > PEEK

As can be checked, rubber is the material which has the bigger deformation in both directions; in addition, the value of the displacement in x- direction is the closest to the obtained in the barefoot hoof. In the results, rubber has a bigger displacement than the hoof. The reason of this is due that the deformation of the horseshoe when the load is applied displaces the outer side of the horseshoe, moving the reference line taken to measure the displacement. In addition, rubber has the value of the bigger displacement in z- direction too, that implies rubber is the best impact absorber of the tested materials. Rubber is being used in the manufacturing of some synthetic horseshoes, usually is combined with other polymers as Polyurethane but the search of this compound has been complicated due to the lack of knowledge of the proportions of each material and consequently, the search of the properties of the compound.

On the other hand, as was expected metals are stiffer so the obtained displacement is quite smaller than the reached with the polymers. However, the purpose of the metals is to achieve wear resistance. Next, the different metals will be arranged from highest to lowest according to their displacement in x- direction and according their hardness.

Order by highest to lowest displacement in x- direction:

Magnesium Alloy AZ31B > Aluminium Alloy 7075 > Gray Iron G4000 > Titanium Alloy Ti-6Al-4V > Copper Alloy C17200 > Ductile Iron 120-90-02 > Steel Alloy 4340

Order by highest to lowest according the hardness:

Titanium Alloy Ti-6Al-4V > Ductile Iron 120-90-02 > Gray Iron G4000 > Copper Alloy C17200 > Steel Alloy 4340 > Aluminium Alloy 7075 > Magnesium Alloy AZ31B

The hardest metal, as have been seen, is Titanium Alloy Ti-6Al-4V and besides it is one of the metals with more displacement in x- direction. Nevertheless, the main property of the Titanium is its density, being almost the half of the rest of the tested metals. This property it is very important at time of design a horseshoe due to that the more lightweight horseshoe the better for the horse.

4.3. Comparison of different attachments

In this section the attachment methods are going to be studied and compared. This study will be theoretical due to the limitations of the software to simulate the different fastening methods, such as adhesives. The most common ways of attaching horseshoes will be studied in this section. These methods are nail attachment and glue-on horseshoes. Last, different functions and features of the adhesives will be exposed.

4.3.1. Nails attachment

There are various methods to attach the horseshoe to the hoof. However, the most common fastening still is nailing.

First horseshoe nails were made of iron. According to Nassau (2008) these nails were found around 500 B.C. by the Celts in Britain. In the XVIII Century, horseshoe nails were hand-made by nailers journeyman. From the Industrial Revolution, nails were produced in a variety of machinery as, for example, rolling mills. Normally, machines, which were used to manufacture of nails, used heated metals, as steel or iron, in their production process. The progress of studies carried out about steel industry in the late 1800's allowed the manufacture of horseshoe nails through cold forging, that is, without the necessity of heating the base materials. Nowadays, the most common processes used to the nails manufacturing are rolling process (Vector, Izumi, Capewell), forging process (Liberty, Mustad, Equiclav) and stamping process (Australian Nails).

These nails penetrate into the white line, placed in the hoof wall, and their function is to attach the horseshoe to the hoof allowing horses to perform their activities.

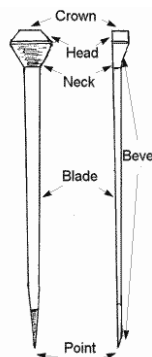


Figure 54. Parts of a nail (Windt-im-Wald-Farm, 2007)

According to Nassau (2008) and Breningstall (1998), a nail can be divided into the parts shown in *Figure 54*. The crown or top is the part which is hammered to penetrate the nail into the hoof and it is perpendicular to the blade. The head, which should fit in perfectly into the nail groove, sometimes the head of the nail stands out slightly of the horseshoe, but the rest of the nail have to be well-introduced and in contact with the shoe; there are different kinds of head as can be seen in *Figure 55*.



Figure 55. Different kinds of heads manufactured by Mustad (Independent Farrier Supplies, 2011)

The neck is the part of the nail which has to fit in the nail groove; therefore, it should have the same shape that the groove. The blade or shank is the long part of the nail which is thinner in comparison with the head and the neck to reduce the contact of the wall as much as possible during the shoeing. The blade has a flat and a bevel side with smoothed edges. The edges are smoothed in order to avoid that the hoof wall can be broken when the nail is driven into the hoof; the blade is straight until the end, and has to leave accurately by the hole placed in the upper side of the horseshoe without any looseness. Finally, the bevel point allows the nail can turn outward and exit when it is being introduced into the wall, to be bent and clinched.

Horseshoes nails should be introduced vertically in the white line taking care of not drive it into the sensitive parts of the hoof. First, the nail enters straight into the wall and due to its bevel shape, it curve outward of the wall. As Roland Perrin says,

"This is caused by two forces: a straight force which follows the nail's axis when the nail is driven into the hoof and a curved

force arising from the hoof wall's resistance against the beveled point. These two forces determine how the nail is driven into the hoof"

(Perrin, 2010)

When the nail exits the wall should be wrung and clinched to form a square shape surface at the outer side of the hoof wall as it can be seen in *Figure 56*.



Figure 56. Clinched nails in a horse hoof (America's Horse Daily, 2008)

It is important that nails are driven correctly through the hoof wall due to a wrong nailing can cause injuries in the internal organs of the hoof, as can be called "hot nail". *Figure 57* shows three different possible cases of nailing a shoe.

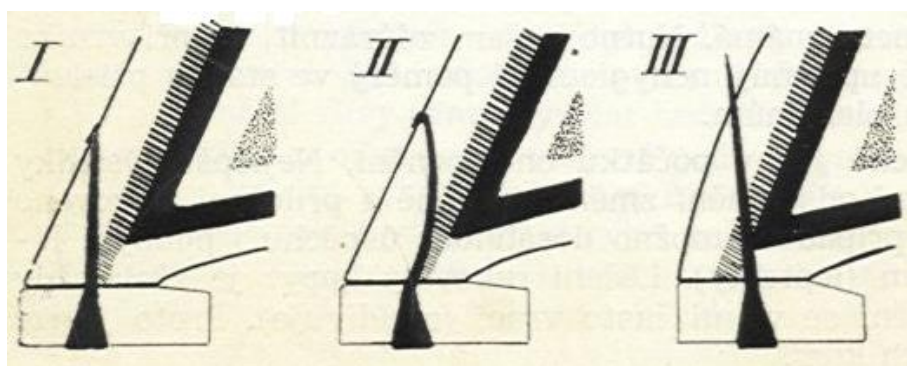


Figure 57. Possible cases of nailing (Stablemade.com, 2009)

In case I, it can be seen the properly way of the nail penetration along the white line until the hoof wall, it shows also the lamina, which is a hoof wall tissue that separates the sensitive part of the hoof from the insensitive or one. In case II, it can be observed the so-called "indirect hot nail" or "nail blind"; it is produced when the nail is pressing

against the sensitive part. This kind of improper nailing does not affect to horses immediately and sometimes does not produce any limp, but when the nail is in contact with the sensitive part, this part will be inflamed and in some cases it will be also infected. Finally, in case III is shown the "direct hot nail", also known as "nail prick", This occurs when the nail is accidentally penetrated into the sensitive part of the horse hoof, in this case the produced damage is quite serious and due to this type of injuries can cause infections the horse can have some complications and it should to be treated as soon as possible.

Other cases of a wrong nailing can cause that the wall can suffer breaks, cracks, chips, etc. On the other hand, nails can damage the internal hoof structure and it could cause the drop of the shoe. But even taking into account these problems, nails are still the most widely used method for attaching horseshoes.

4.3.2. Glue-on Shoes

Other type of attachment method is the join of a horseshoe with the glue in one piece, these kinds of horseshoes, which are called Glue-on horseshoes, are mainly used in the treatment of many horse diseases. In last years both design and materials are been improved in order to create stronger glues. Nowadays, glue-on horseshoes are a feasible choice for horse in any activities. Looking the current glue-on horseshoes, it is possible to differentiate three main types: synthetic glue-on shoes, aluminum core shoes and metal horseshoes.



Figure 58. Some examples of synthetic glue-on horseshoes (Blue Pegasos, 2013)

Acrylic polymers, polyurethane or polyethylene are the main materials of synthetic glue-on horseshoes (*Figure 58*). These shoes are light, can absorb the impact adequately and permit the natural hoof expansion. At time to use these shoes it is necessary to carry out some previous works in the horse hoof as they can be the clean and degrease. When the shoe is going to be glued on, it is important that the surface, which will be joined, do not have any abscess or damp area, as pay attention that the glue is not in contact with any sensitive part of the hoof. The adhesive is applied in the outer band of the shoe perimeter, after that, the shoe is carefully attached to the hoof in the correct position until the adhesive is set in a few minutes.



Figure 59. Glue-on horseshoe with an aluminium core (Horseshoes.com, 1996)

Glue-on horseshoes with a core of aluminum, *Figure 59*, are manufactured by covering with polyurethane an aluminum horseshoe. The polyurethane is a good shock absorber and the aluminum provides stiffness. It is common that these horseshoes have clips or tabs in order to glue the shoes to the hoof wall. It is possible to nail-on the shoe too.



Figure 60. Metal glue-on horseshoe (SoundHorse Technologies, 1999)

The third kind of glue-on horseshoe is a metal one (*Figure 60*), which is commonly used in broken hooves. It is used to help the horse to make its normal activity without the use of nail attachment until the hoof wall has recovered and grown.

4.3.3. Adhesives

Since the last century, many adhesives have been used as additional attachment methods. Nevertheless, urethanes and acrylics are the most common glues materials used nowadays. These materials, first used in industry, became in the late 80's in the first which were used in horse field. Both materials have been accepted from the farrier industry but they are not quite close to replace the nail attachment in a near future. The join by adhesives tends to use for shoeing or repairing the hoof and its use can be more difficult than the nails attachment. The use of adhesives can be beneficial to the horse and its hoof due to glues keep the hoof intact not penetrating the nails on it and in addition, some glues help to get a better shocks absorbing, although the use of adhesives can interfere in the correct moisture of the nail and increase the cost of the shoeing.

On one hand, urethanes are a chemical compound used both to set the horseshoe to the hoof as to cure the damaged hoof. This chemical compound has as property its fast set time, which is around 30 to 60 seconds. The most common use of the urethane is for direct attachment of steel or aluminium horseshoes, for hoof reparation and for the creation of protector pads for the sole and the frog. In *Figure 61* can be seen a two-component adhesive being used with the aim of attaching a horseshoe.



Figure 61. Two-component adhesive (Eki, 2001)

On the other hand, there are a great amount of different types of acrylics; however, in shoeing field, the most of the farriers agrees that the most used acrylic is a modified one, especially, the epoxy-methylmethacrylate. These kinds of acrylics have as advantage the slower set time comparing with urethanes. This set time is around 2 or 3

minutes, that means the farrier has enough time to work in the horseshoe attachment. The cure time is slower than urethanes too, being about 6 to 8 minutes the time to reach the optimal strength. This compound is used both in glue-on horseshoes attachment and in hoof reparation.

In conclusion, the nail attachment still is the most common fastening method even knowing that is the more harmful method for the horse and its hoof. Nailing is able to cause serious harm to the hoof as damage the internal structure of the wall, a wrong placed nail can produce lameness or some hoof infections. The progress in the field of adhesives has allowed glues to take importance although the use of this method can affect to the horse impeding the correct moisture of the hoof. This implies that the hoof will grow drier than normal which can cause the chip of the hoof wall. In addition, new adhesives serve as attachment method, hoof repairing and impact absorbing.

4.4. Design of the compliant horseshoe

Once the hoof displacement and its behaviour with the sample horseshoe are known, and also the comparison between different materials, current horseshoes and attachment methods; it is possible to begin with the design development.

According to Nassau (2008) a horseshoe has an upper side which is in contact with the hoof wall and a bottom side which rest in the ground. The upper side had to be totally flat and it should be wide enough to support the hoof wall, the white line and some small parts of the sole. It has an outer and an inner edge. The groove, where the nail holes are located, is place in the bottom side of the shoe and the deep of the groove should be two thirds of the horseshoe thickness. The nail hole grooves of the front shoe are placed both sides of the horseshoe vertex at an approximate distance between them of one and a half or two times the shoe width. Last nail hole should not be behind of the middle of the front horseshoe length to allow that the hoof mechanism can work with the less possible difficulty, however, in the hind horseshoe the last nail hole can be further back. Although if the horseshoe is enough flexible the place of the nail holes can vary. In the heels the edge of the hoof wall has to be completely supported to help the hoof mechanism work. The horseshoe branches should be larger than the hoof due to the hoof is expanded backward and sideways. Front shoes usually have rocker shape; this shape allows that the hoof can take off the ground more easily.

The chosen material for the design is rubber. This material has been chosen due to its flexibility, which allows as far as possible the natural displacement of the hoof wall. Also, by seeing the obtained results, the chosen material for the main body of the horseshoe is a good impact absorber. However, owing its low hardness and therefore its low wear resistance, it has been decided the establishment of three metal parts which will be in contact with the ground. After the different materials comparison, the chosen metal for the plates has been Titanium Alloy Ti-6Al-4V due to its great hardness and its lightweight.

In the simulation of the barefoot hoof has been possible to estimate the curve which the hoof wall follows, for this reason, a reduction of the horseshoe width has been done in five points of the inner side of the shoe, each one between two metal plates.

Knowing the importance of the frog and its necessity of being in contact with the ground, a frog pad has been added to the horseshoe. The aim of this pad is to help the compression of the frog, to not impede the hoof mechanism. This pad has a groove in the middle to allow a bigger displacement of the shoe.

The horseshoe has been developed for adhesive fastening, nails attachment or a combination of them. On the one hand, taking into account that the software cannot simulate the behaviour of the different glues, a simulation is carried out by setting infinite friction between the hoof and the shoe. The purpose of this simulation is to obtain approximate results when the attachment is done with “perfect glue”, i.e. a fastening in which the contact between the surfaces cannot allow any displacement.

On the other hand, in the nails attachment simulation, four nail holes have been distributed, being coincident with the metal parts. The design of the horseshoe is fully described in *Appendix B*, where the geometry dimensions and details are also explained.

4.5. Implementation

The 3D model of the compliant horseshoe is shown in *Figure 62*. It is possible to distinguish the two different chosen materials. The main body of the horseshoe is made of rubber. On the other hand, for the metal plates the material Titanium Alloy Ti-6Al-4V has been chosen. The properties of the polymer have been taken from Table 2, the Titanium Alloy Ti-6Al-4V properties from Table 1 and both have been introduced in PTC Creo to carry out the simulation.



Figure 62. 3D design of the compliant horseshoe with the nails (own source)

As it has been done with the regular horseshoe, symmetry in the plane $x = 0$ will be applied in the design of the compliant horseshoe too. Selected nails for attach the horseshoe to the hoof are the same which were used in the previously simulation, it means that nails maintain their geometry and material properties.

After assembly the hoof to the horseshoe, a mesh has been created to obtain more accuracy in the results. In *Figure 63*, it can be seen the Maximum Element Size of the mesh is 7.5 mm, as was made in the creation of the others meshes; nevertheless, to increase the accuracy in the nails, a mesh of 2 mm Maximum Element Size has been created.

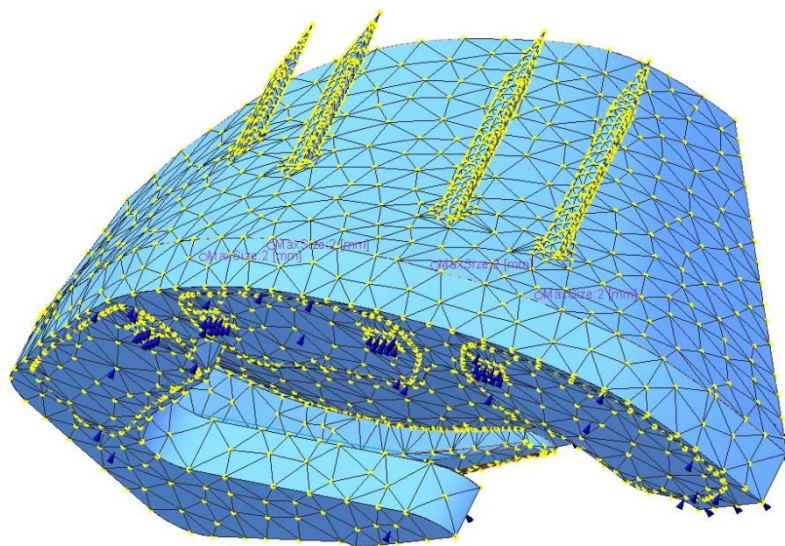


Figure 63. Mesh set for the simulation (own source)

The boundary conditions which have been imposed can be seen in *Figure 64*. In the symmetry plane ($x = 0$), the assembly has been constrained in x- direction. On the other hand, the parts which are in contact with the ground have been constrained in z- direction. And one more time, the edge of the dorsal part that is coincident with the y-axis has been constrained in y- direction.

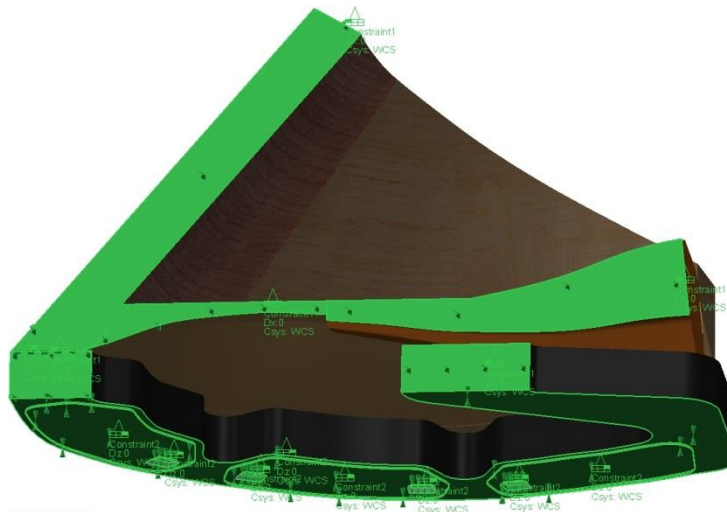


Figure 64. Boundary conditions established in the 3D model (own source)

The applied loads are the same that were applied in the hoof model. These loads have not been changed during the whole study to compare the behaviour of the different horseshoes under the same load conditions.

4.6. Results

In this section two different simulations have been done. In one of them, the friction between the hoof and the horseshoe has been taken into account. On the other hand, the analysis of the assembly has carry out without consider the friction between them. The obtained results will be shown and explained.

4.6.1. Friction between the hoof and the horseshoe

As can be seen in *Figure 65*, the displacements in all directions have been represented in a fringe diagram of the deformed assembly. The value of the deformation scale is 7.5%. A transparent overlay of an unloaded model is added to compare the displacement caused by the forces applies on the hoof.

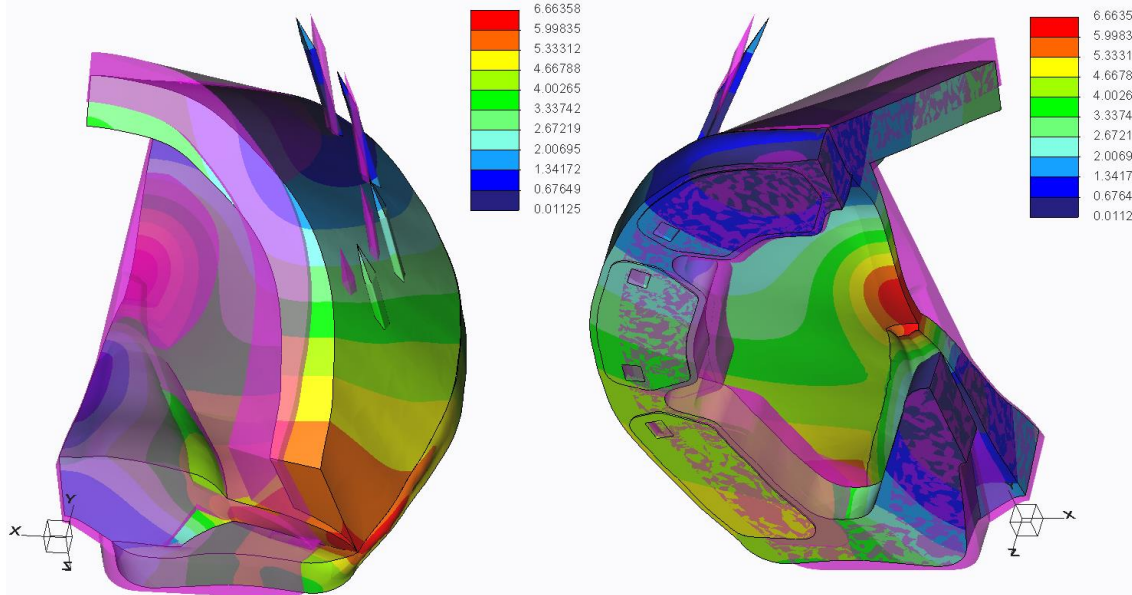


Figure 65. Fringe diagram of the displacements of the design in all directions (own source)

By removing the hoof from the fringe diagram, a better view of the displacement suffered by the compliant horseshoe and the nails in all directions is obtained. In *Figure 66*, it can be observed that the maximum displacement is found in the rear part of the horseshoe. This deformation shows how the hoof expansion in x-direction is able to displace the horseshoe allowing its natural displacement as far as possible. This is due to the great flexibility of the material, which will come back to its natural shape when the hoof will be taken off the ground. The deformation which the horseshoe suffers in z-direction makes the shoe to be able to absorb the impact of the footstep.

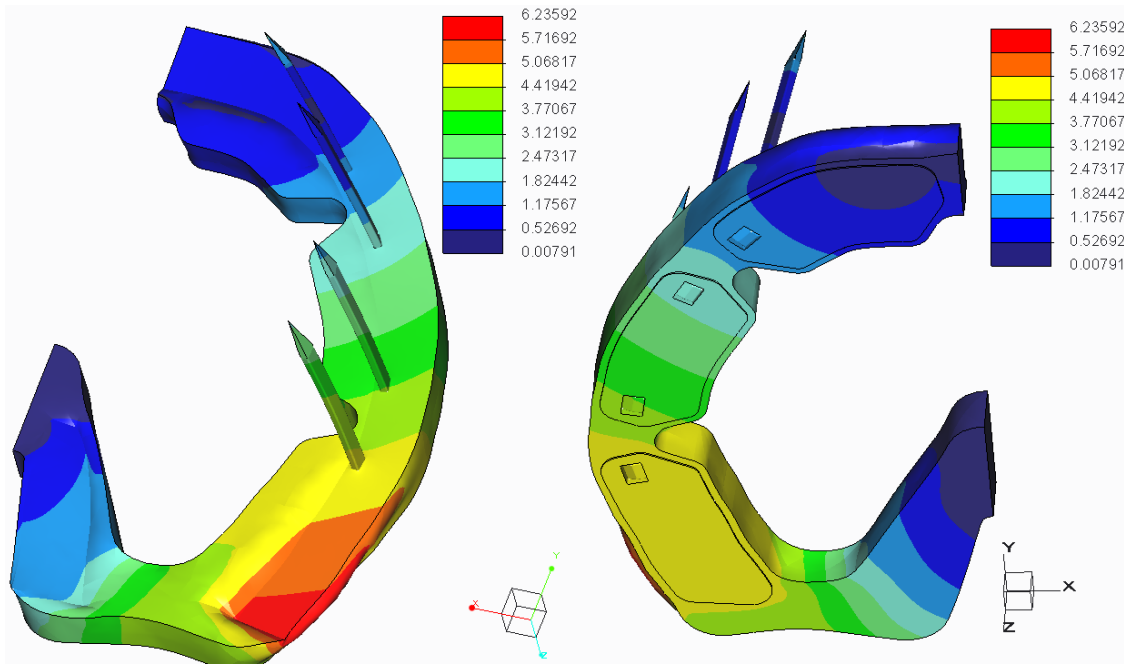


Figure 66. Fringe diagram of the displacements of the horseshoe and nails in all directions (own source)

The outer bottom curve of the hoof has been selected to show the displacements in the x- direction. As can be seen in the graph in *Figure 67*, the displacement of the hoof has been compared with the displacement of the outer upper curve of the horseshoe. The maximum displacement of the hoof is equal to 5.66 mm and the maximum displacement of the horseshoe is also 5.66 mm. The reason of that these obtained values have been equal is because the simulation has been carried out by setting infinite friction.

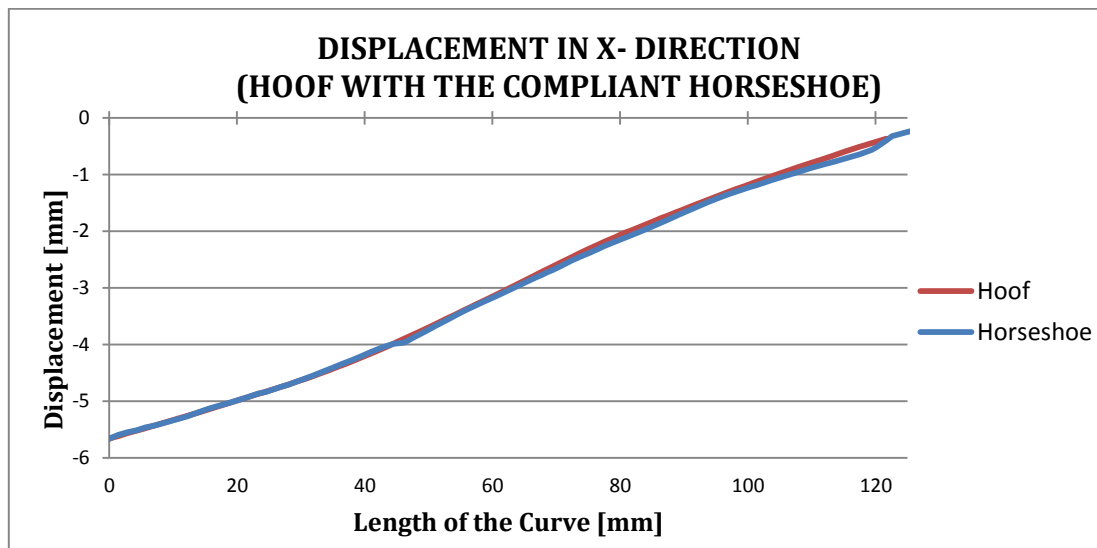


Figure 67. Horseshoe displacement compared with the hoof displacement in the x- direction (own source)

In *Figure 68* has been represented a graph with the displacement in the z- direction of the outer upper curve of the horseshoe. This representation has been chosen as a parameter to quantify the impact absorption capacity of the compliant horseshoe. As can be seen in the graph, the maximum compression of the horseshoe is equal to 1.63 mm, so this horseshoe is able to absorb part of the shock.

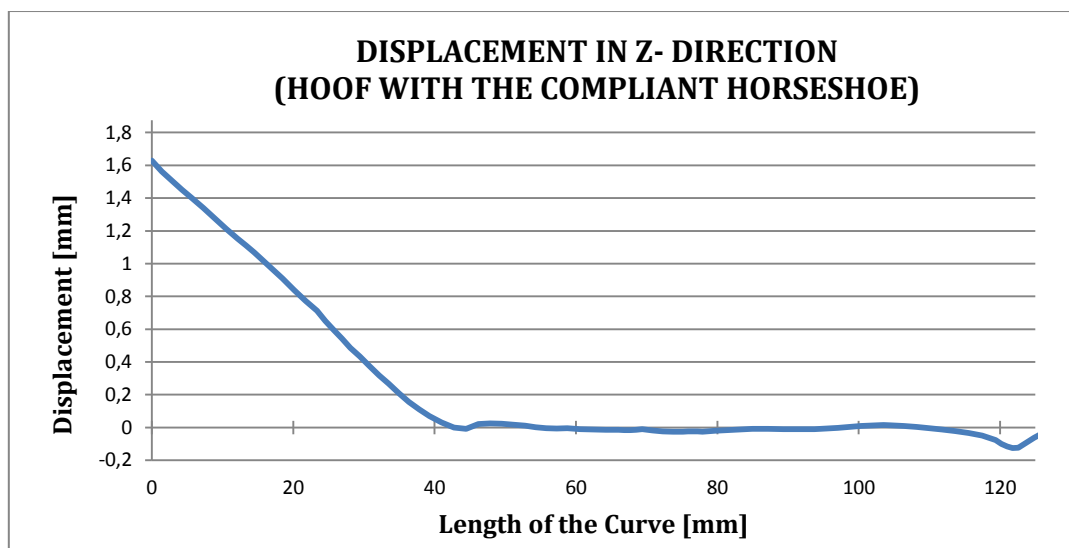


Figure 68. Horseshoe displacement in the z- direction (own source)

Figure 69 shows a fringe diagram of the Von Mises stress in the hoof. As can be seen in the right picture of the figure, the maximum stress is located in the back nail hole and its value is about 290 MPa.

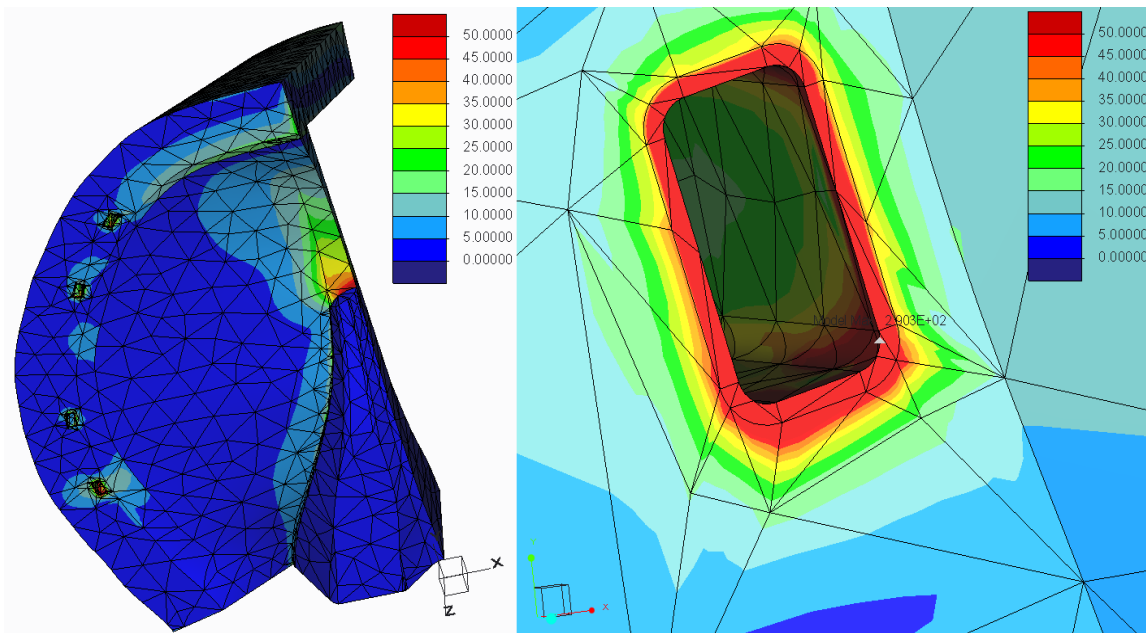


Figure 69. Fringe diagram of the Von Mises stress in the hoof (own source)

In *Figure 70*, the fringe diagram of the Von Mises stress in the polymer part of the horseshoe is shown. As can be seen, the maximum stress obtained is about 3.5 MPa and this stress concentration is located in the cutting plane of the hoof. The peak of stress could be solved by modelling the complete hoof.

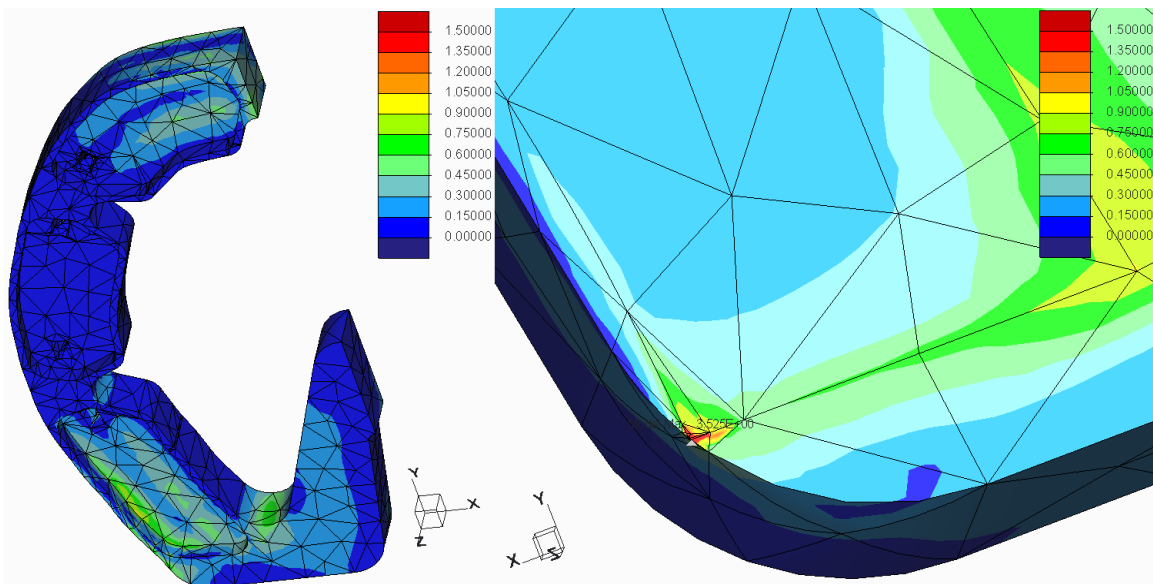


Figure 70. Fringe diagram of the Von Mises stress in the polymer part (own source)

The Von Mises stress in the metal plates is represented in *Figure 71*, as happened before with the regular horseshoe, the software has not allowed to round the edges at the same time that the interfaces have been set. So, this has caused a stress concentration in the edge which is in contact with the nail. The maximum stress is located in the nail hole of the rear plate, being its value equal to 1246 MPa.

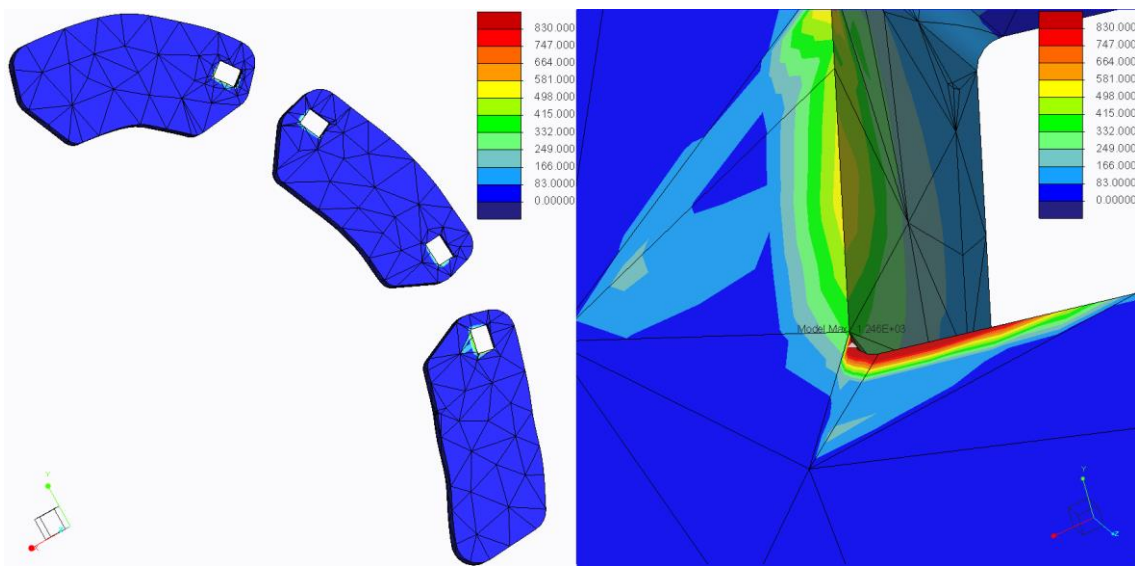


Figure 71. Fringe diagram of the Von Mises stress in the metal plates (own source)

Figure 72 shows a fringe diagram of the Von Mises stress in the nails. As can be seen in the right picture of the figure, the maximum stress is about 1117 MPa and it is located at the bottom of one nail.

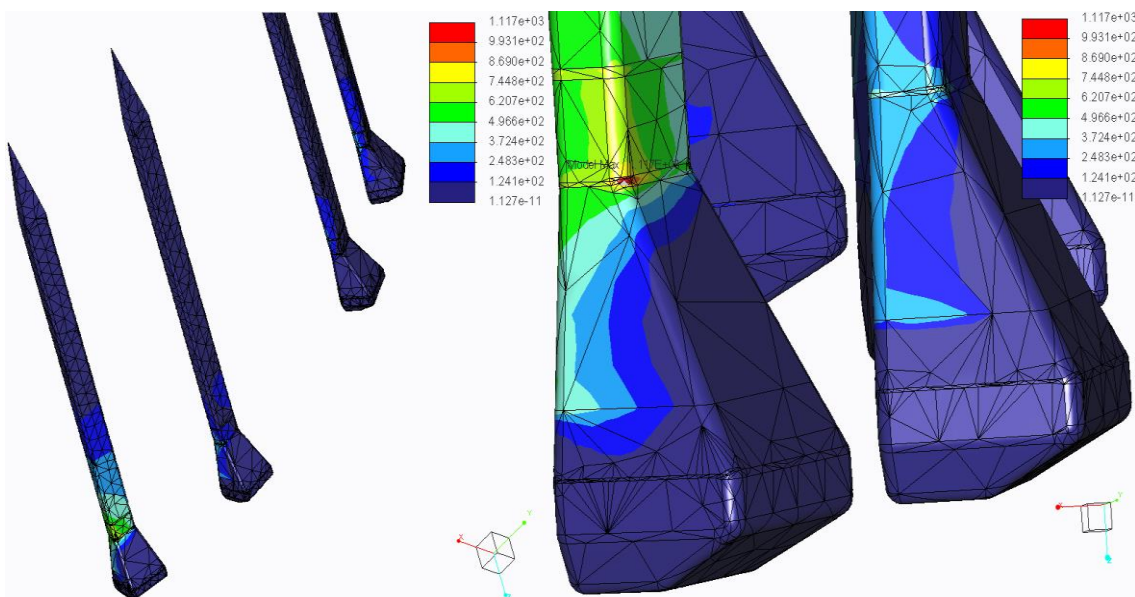


Figure 72. Fringe diagram of the Von Mises stress in the nails (own source)

4.6.2. No friction between the hoof and the horseshoe

As can be seen in *Figure 73*, the displacements in all directions have been represented in a fringe diagram with the deformed assembly. These diagrams have been compared with a transparent overlay where there are not any applied loads.

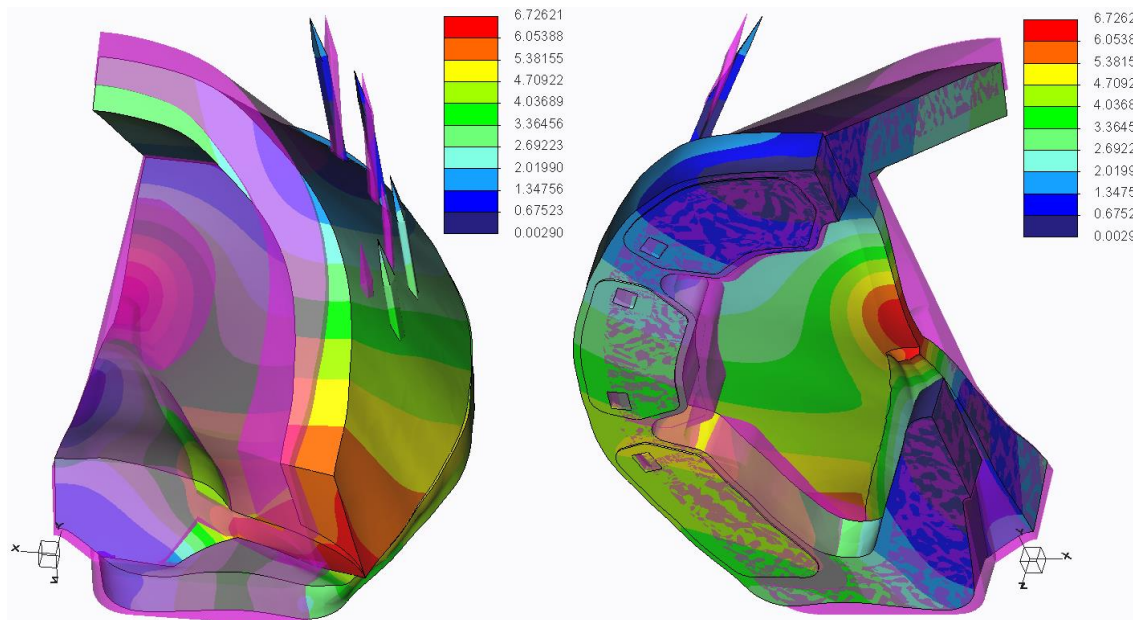


Figure 73. Fringe diagram of the displacements of the design in all directions (own source)

The displacements in all directions are represented in a fringe diagram with the deformed model of the horseshoe with the nails. This diagram is shown in *Figure 74*.

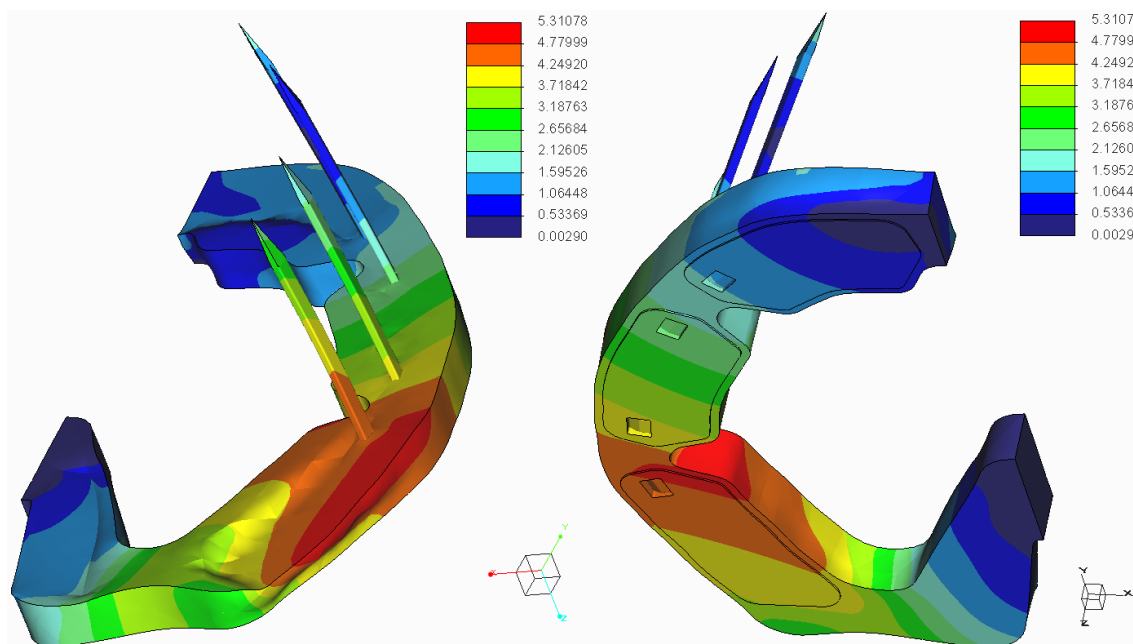


Figure 74. Fringe diagram of the displacements of the horseshoe and nails in all directions (own source)

The outer bottom curve of the hoof has been selected again to show the displacements in the x- direction. As can be seen in the graph in *Figure 75*, the displacement of the hoof has been compared with the displacement of the outer upper curve of the horseshoe. The maximum displacement of the hoof is equal to 5.79 mm and the maximum displacement of the horseshoe is equal to 5.03 mm. The difference between these values is due to the simulation has been done by setting a connection between the horseshoe and the hoof without friction. So, as is logical, the displacement of the hoof is larger than the displacement of the horseshoe.

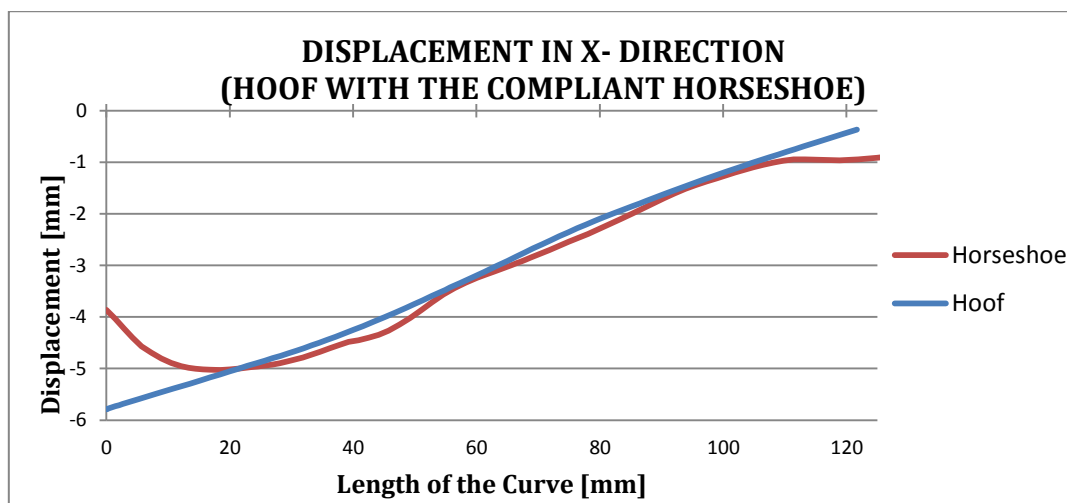


Figure 75. Horseshoe displacement compared with the hoof displacement in the x- direction (own source)

In Figure 76 has been represented a graph with the displacement in the z- direction of the outer upper curve of the horseshoe. As described above, this representation has been chosen as a parameter to quantify the impact absorption capacity of the compliant horseshoe. As can be seen in the graph, the maximum compression of the horseshoe is equal to 1.7 mm, so this horseshoe is able to absorb impacts.

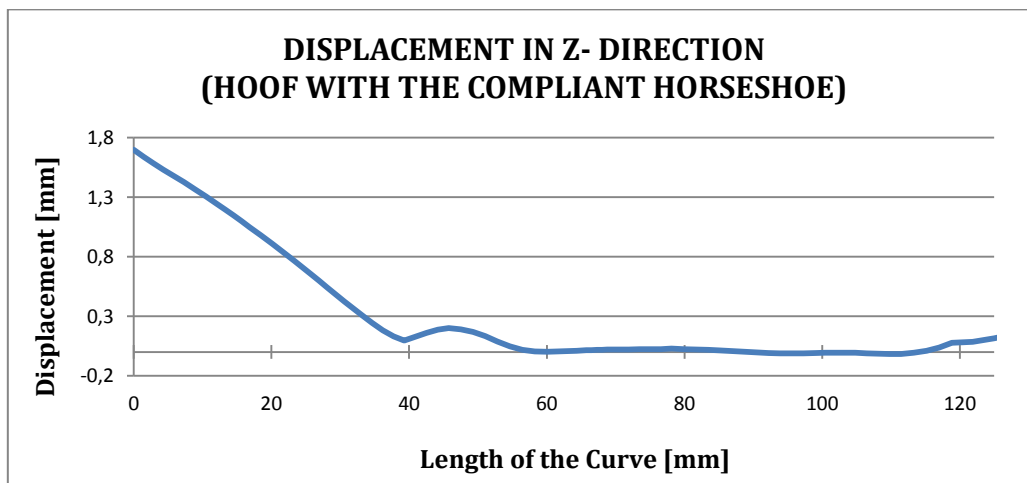


Figure 76. Horseshoe displacement in the z- direction (own source)

Figure 77 shows the fringe diagram of the Von Mises stress in the hoof. As can be seen in the right picture of the figure, the maximum stress is about 203 MPa and it is located in one nail hole.

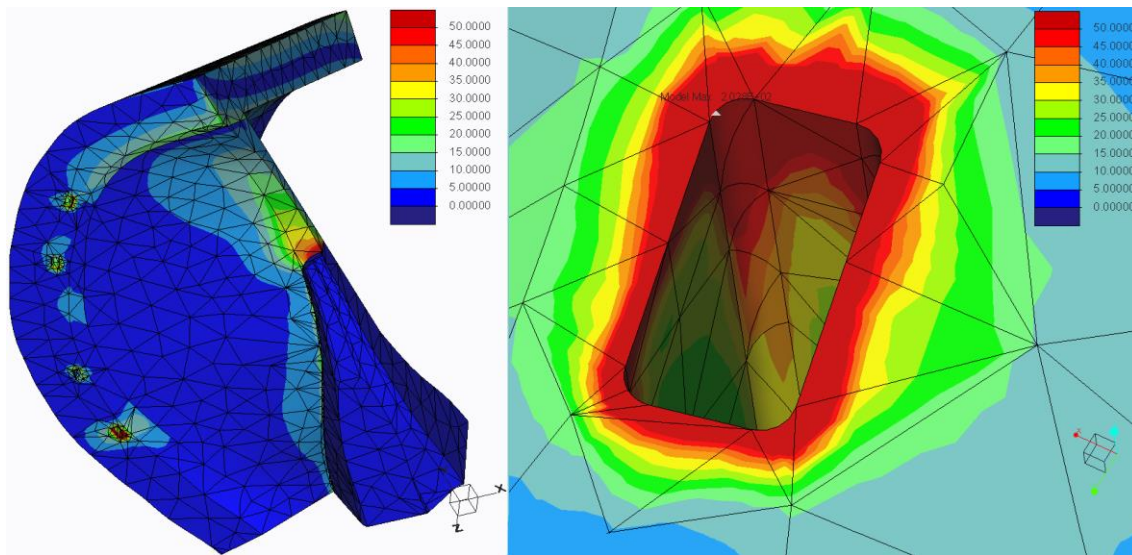


Figure 77. Fringe diagram of the Von Mises stress in the hoof (own source)

Figure 78 shows a fringe diagram of the Von Mises stress in the polymer part of the horseshoe. As can be seen in the right picture of the figure, the maximum stress is about 3 MPa. This stress concentration is also located in the cutting plane of the hoof

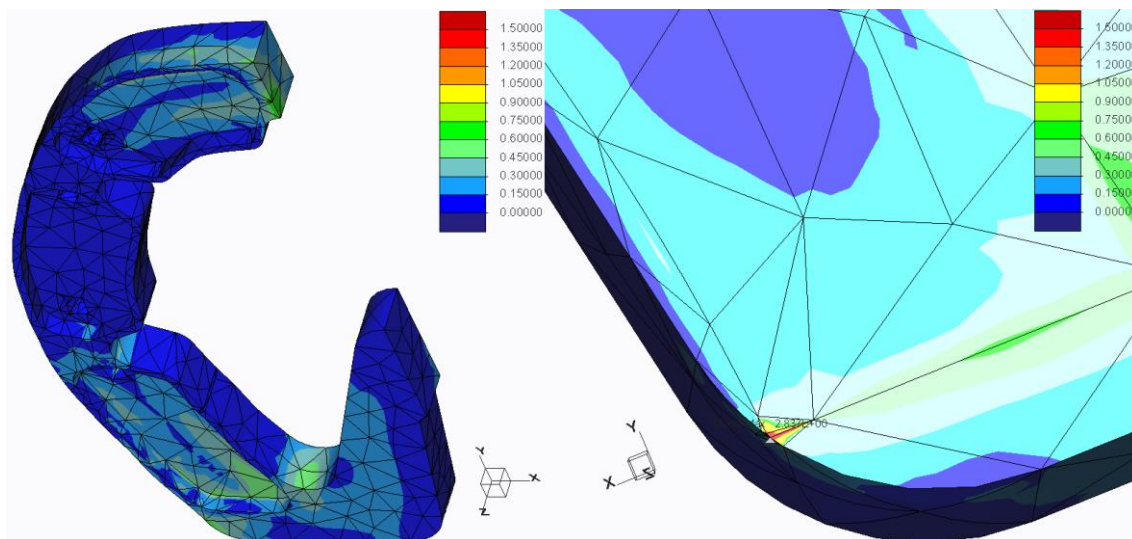


Figure 78. Fringe diagram of the Von Mises stress in the polymer part (own source)

Figure 79 shows the fringe diagram of the Von Mises stress in the metal plates. The maximum stress obtained in this simulation is located in the back nail hole and is equal to 1414 MPa.

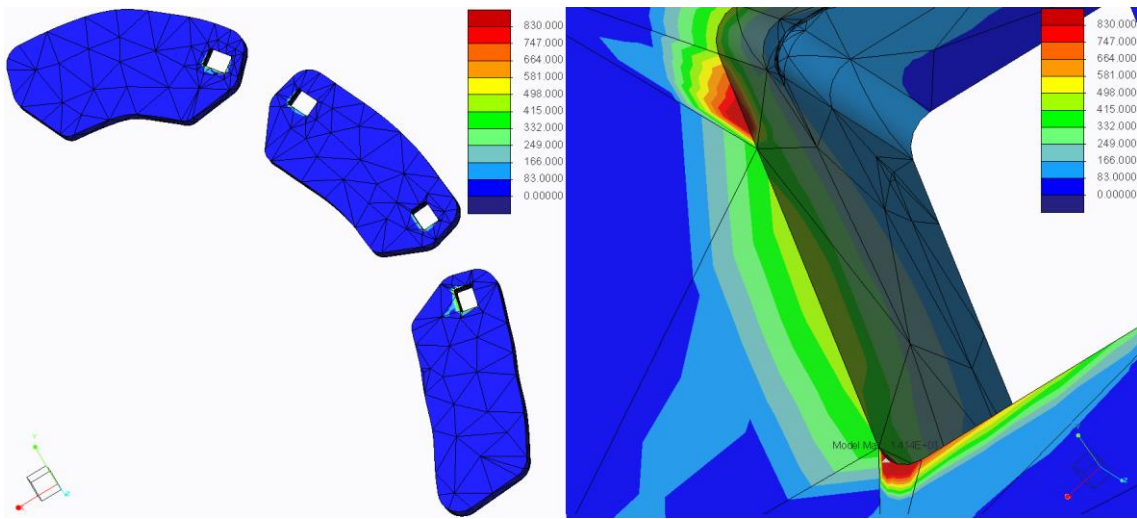


Figure 79. Fringe diagram of the Von Mises stress in the metal plates (own source)

Figure 80 shows a fringe diagram of the Von Mises stress in the nails. As can be seen in the right picture of the figure, the maximum stress is about 1229 MPa and it is located at the bottom of one nail.

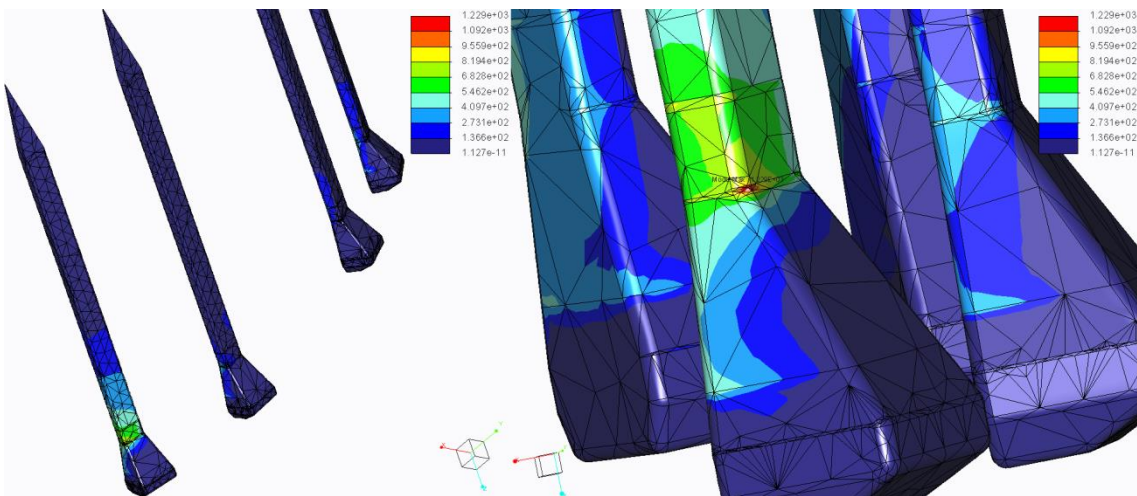


Figure 80. Fringe diagram of the Von Mises stress in the nails (own source)

4.6.3. Attachment with “perfect glue”

As can be seen in *Figure 81*, the displacements in all directions have been represented in a fringe diagram with the deformed assembly. These diagrams have been compared with a transparent overlay where there are not any applied loads.

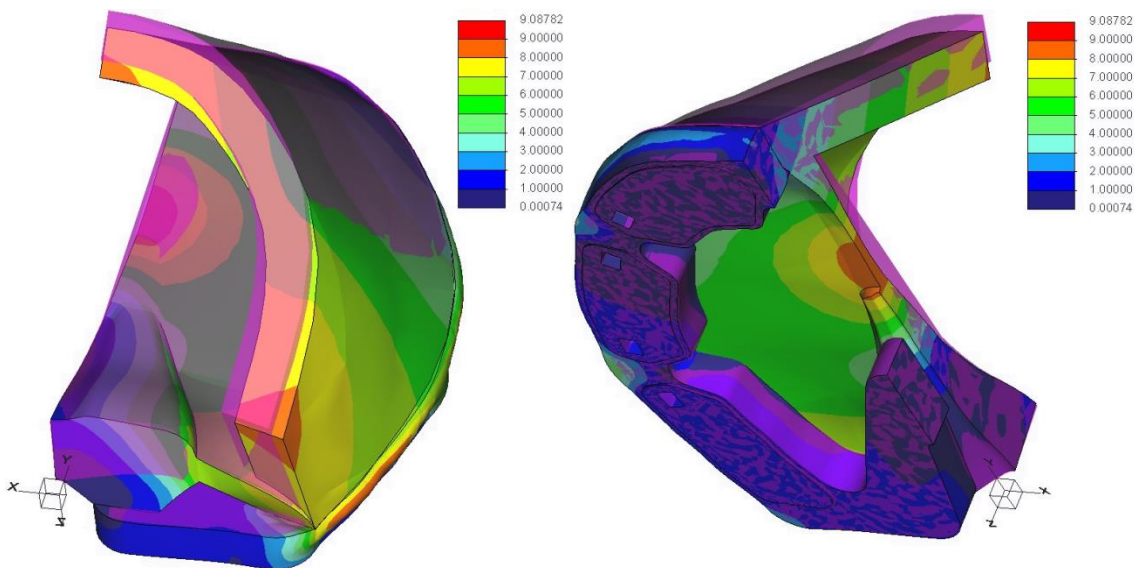


Figure 81. Fringe diagram of the displacements of the glued horseshoe in all directions (own source)

The displacements in all directions are represented in a fringe diagram with the deformed model of the horseshoe attached with adhesive. This diagram is shown in *Figure 82*.

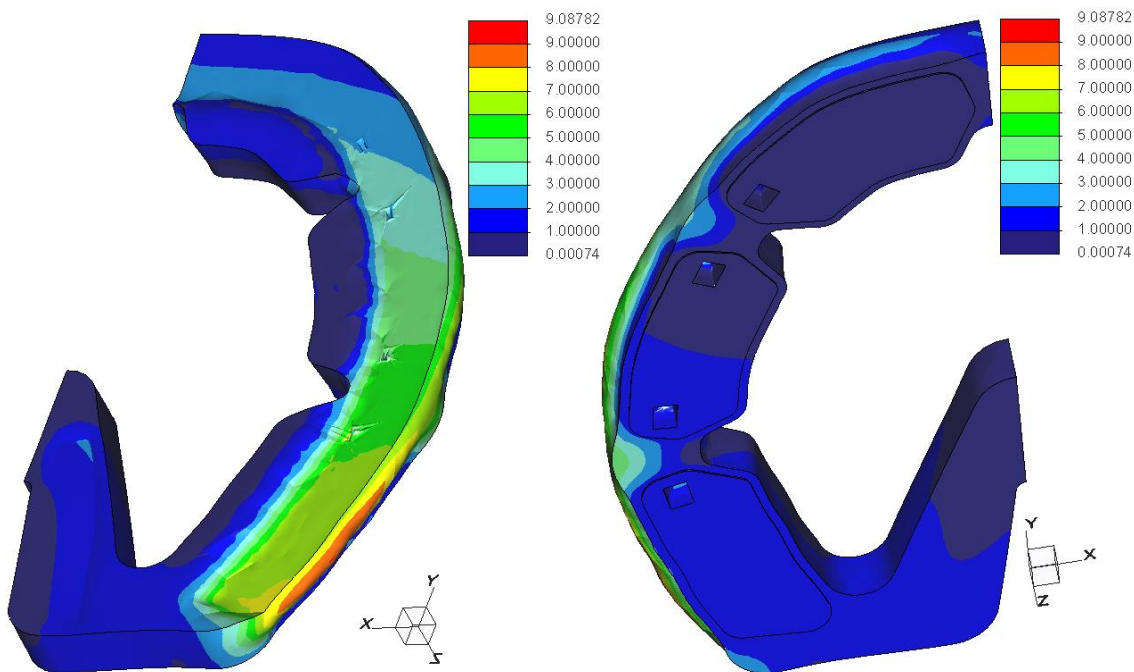


Figure 82. Fringe diagram of the displacements of the horseshoe in all directions (own source)

The outer bottom curve of the hoof has been selected to show the displacements in the x-direction. As can be seen in the graph in *Figure 83*, the displacement of the hoof has been compared with the displacement of the outer upper curve of the horseshoe. The maximum displacement of the hoof is equal to 4.82 mm and the maximum displacement of the horseshoe is also 4.82 mm. The obtained values are equal because the simulation

has been carried out by setting infinite friction, so the hoof curve taken to obtain the graph is the same.

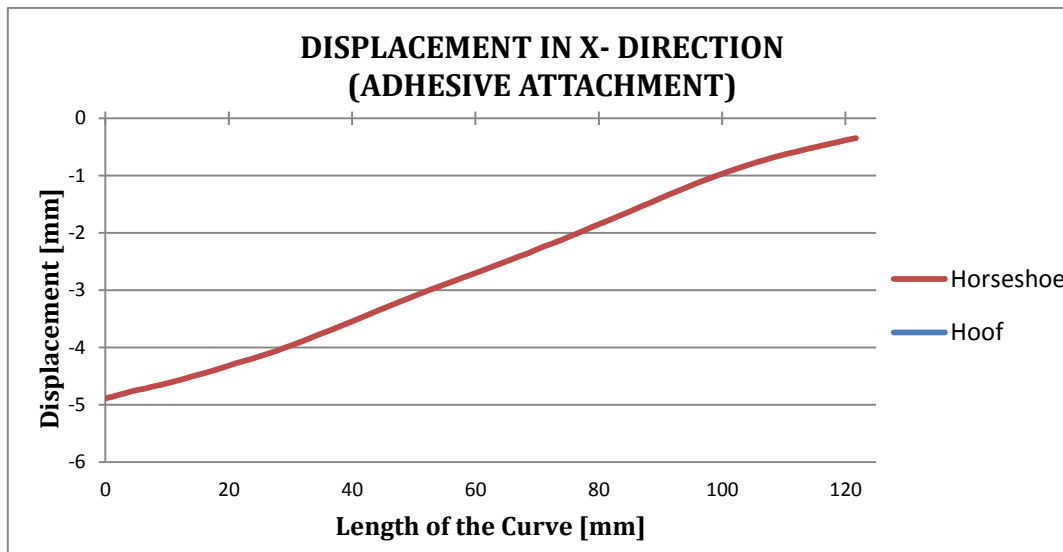


Figure 83. Horseshoe displacement compared with the hoof displacement in the x- direction (own source)

In *Figure 84* has been represented a graph with the displacement in the z- direction of the outer upper curve of the horseshoe. This representation has been chosen as a parameter to quantify the impact absorption capacity of a regular horseshoe. As can be seen in the graph, the maximum compression of the horseshoe is equal to 5.47 mm, so this horseshoe is able to absorb part of the shock.

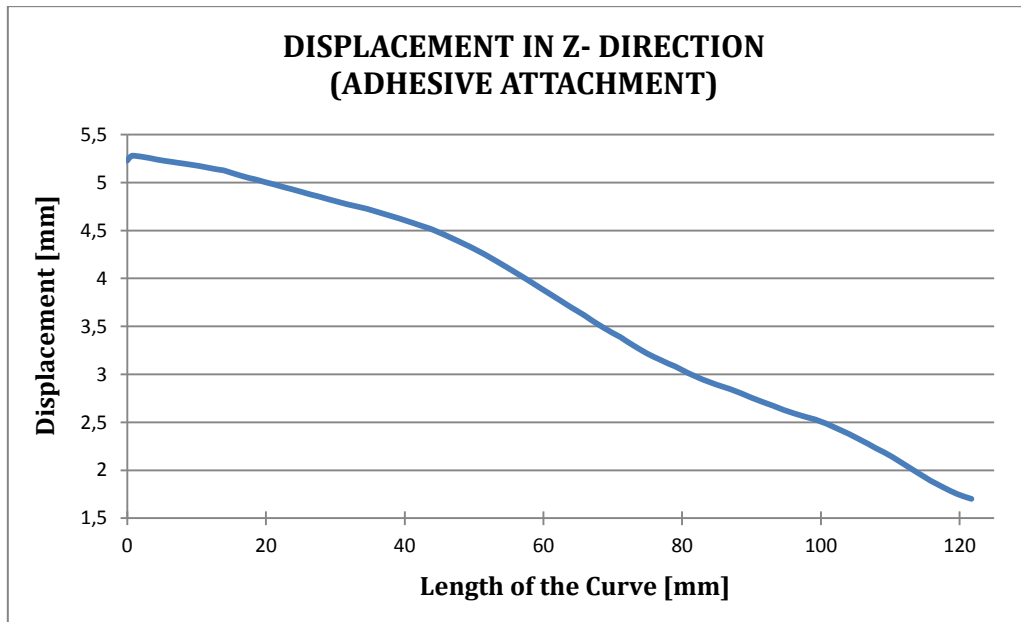


Figure 84. Horseshoe displacement in the z- direction (own source)

Figure 85 shows the fringe diagram of the Von Mises stress in the hoof. As can be seen the most of the stress in the hoof is lower to 25 MPa, but there are some stress

concentrations in the intersection of some different attachment of different parts of the hoof, as can be seen there is an abnormal stress concentration in the join of the frog and the sole and another in the join of the sole and the end of the horn wall. These stress concentrations reach a maximum value of 102 MPa, which is, however, lower than the stresses obtained when the horseshoe is attached by nails.

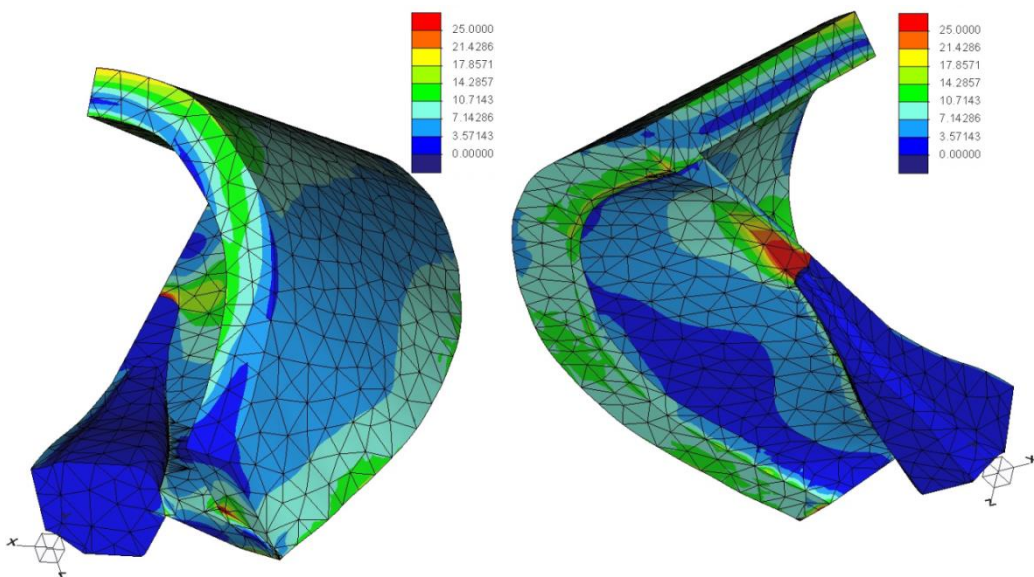


Figure 85. Fringe diagram of the Von Mises stress in the hoof (own source)

Figure 86 shows the fringe diagram of the Von Mises stress in the polymer part of the horseshoe. As can be seen the stress concentration is located in the rear part of the hoof wall which is the part where the maximum displacement of the hoof is found. The stress along the polymer part is lower than 4 MPa.

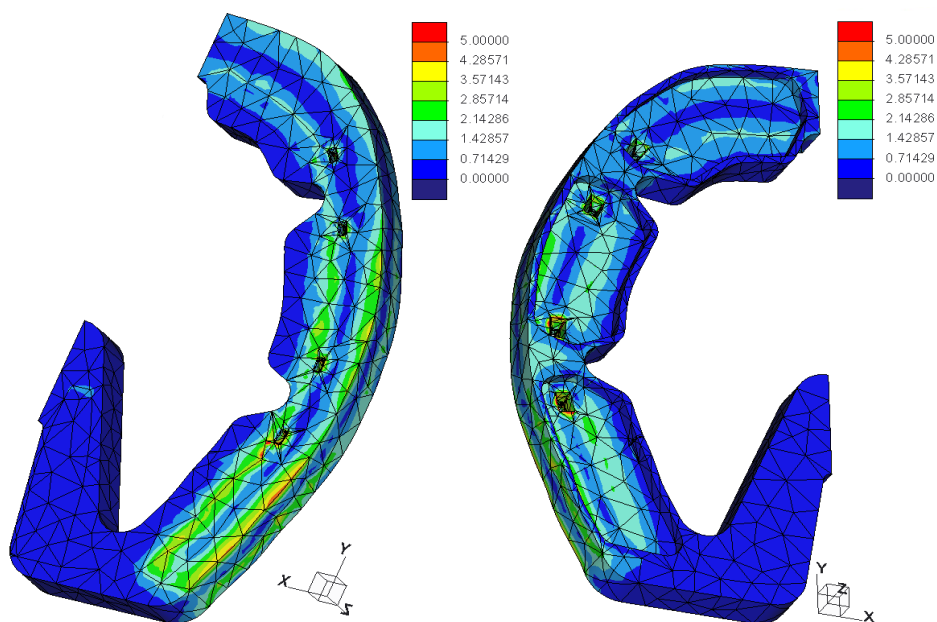


Figure 86. Fringe diagram of the Von Mises stress in the polymer part (own source)

The Von Mises stress in the metal plates is represented in *Figure 87*, as can be seen the stress in the metal plates are quite lower than the stress obtained by nail attachment. The maximum stress is obtained in the outer edge of the plates.

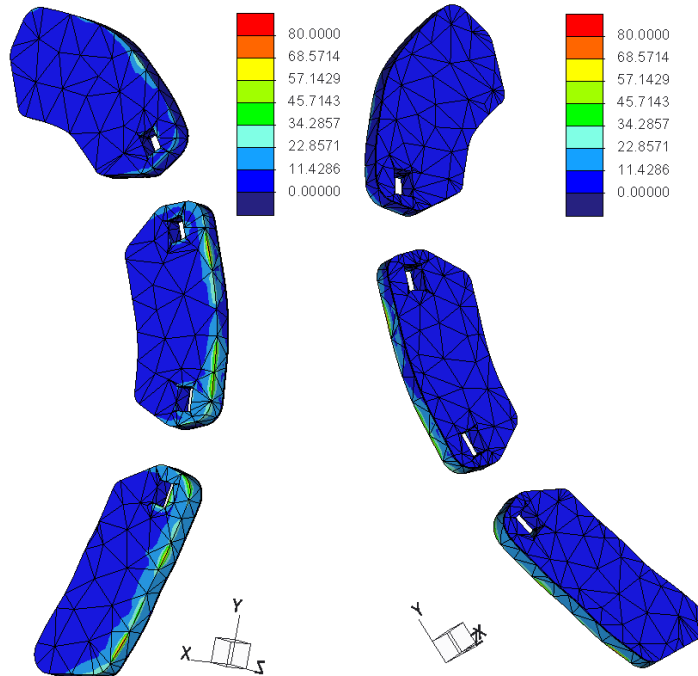


Figure 87. Fringe diagram of the Von Mises stress in the metal plates (own source)

5.CONCLUSIONS AND DISCUSSIONS

5.1. Displacements

Comparing the different displacement graphs obtained in the simulations above, it is possible to come to several conclusions. On one hand, all the hoof displacements in the x- direction have been compared and represented in the graph in *Figure 88*.

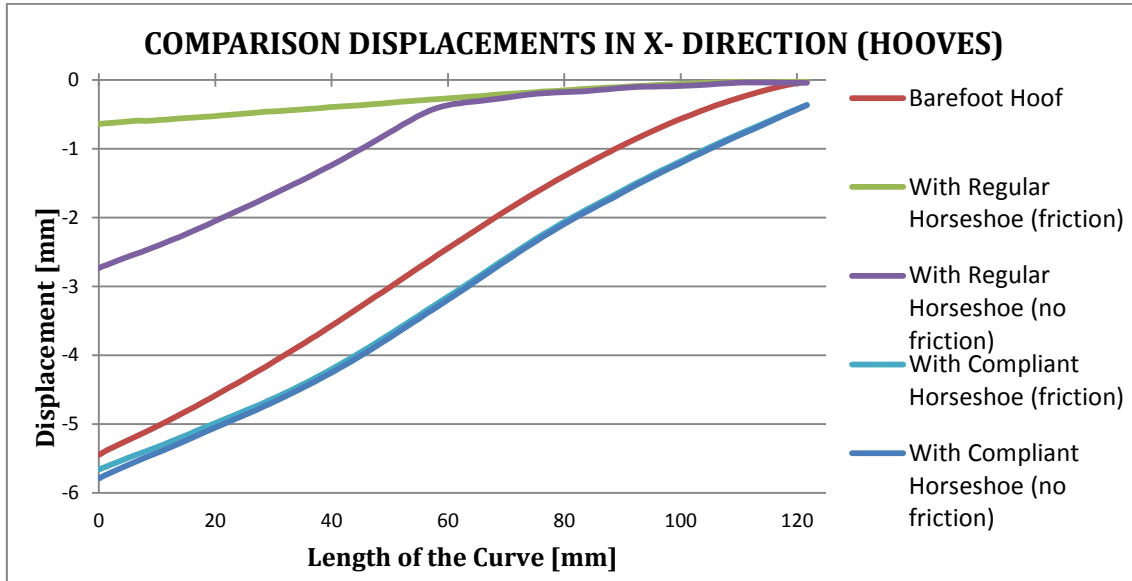


Figure 88. Comparison of the hooves displacements in x- direction (own source)

The displacement of the barefoot hoof, which means the hoof without any horseshoe, has been represented with a red line in the graph. As is logical, the lowest displacement obtained has been in the simulation of the regular horseshoe attached to the hoof due to the stiffness of the steel. It is interesting to see that the displacements obtained in the simulation carried out with the compliant horseshoe are bigger than the ones obtained in the analysis of the barefoot hoof.

The explanation of these results is that the rubber used in the design of the compliant horseshoe is deformed along all directions. So, the hoof continues its expansion along the x- direction while the polymer is deforming along the z- direction. Thereby, the hoof follows a diagonal movement between the x- and z- directions. Otherwise, when the hoof is simulated without any horseshoe the displacement along the z- direction is constrained due to the contact with the ground, so its displacement is lower.

On the other hand, all the horseshoe displacements in the x- direction have been compared and represented in the graph in *Figure 89*.

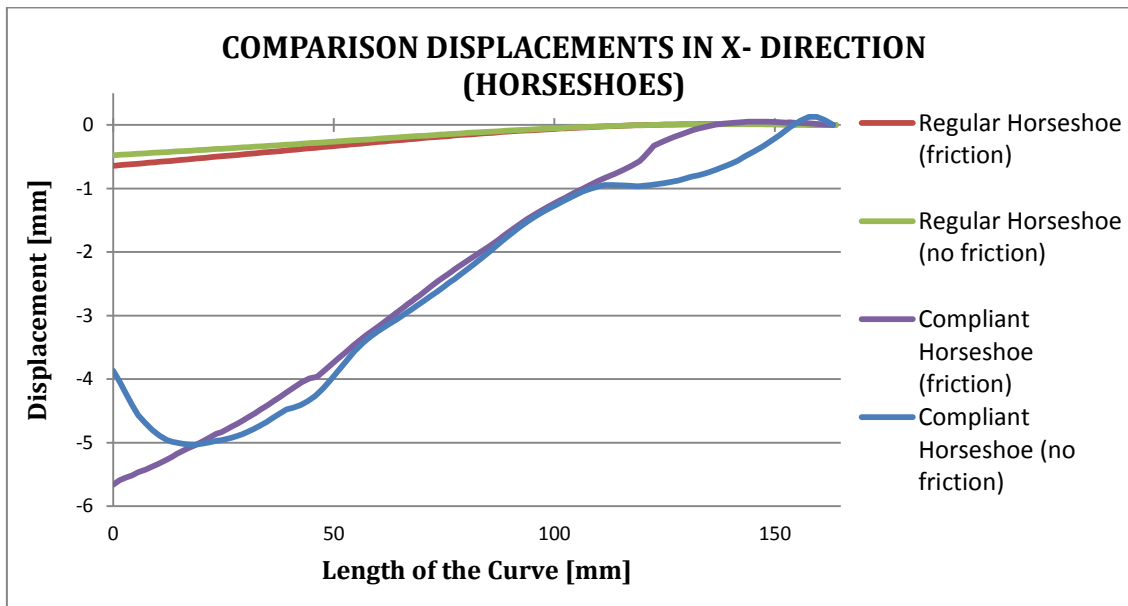


Figure 89. Comparison of the horseshoes displacements in x- direction (own source)

As was expected, the displacements obtained with the compliant horseshoe are bigger than the ones obtained with the regular horseshoe. It has to be stressed that the real results will be between the curve of the simulation performed without friction and the curve of the simulation carried out with friction.

Moreover, all the horseshoe displacements in z- direction have been compared and represented in the graph in *Figure 90*. This representation has been done with the aim of obtaining a parameter to quantify the horseshoe capacity of absorbing impacts.

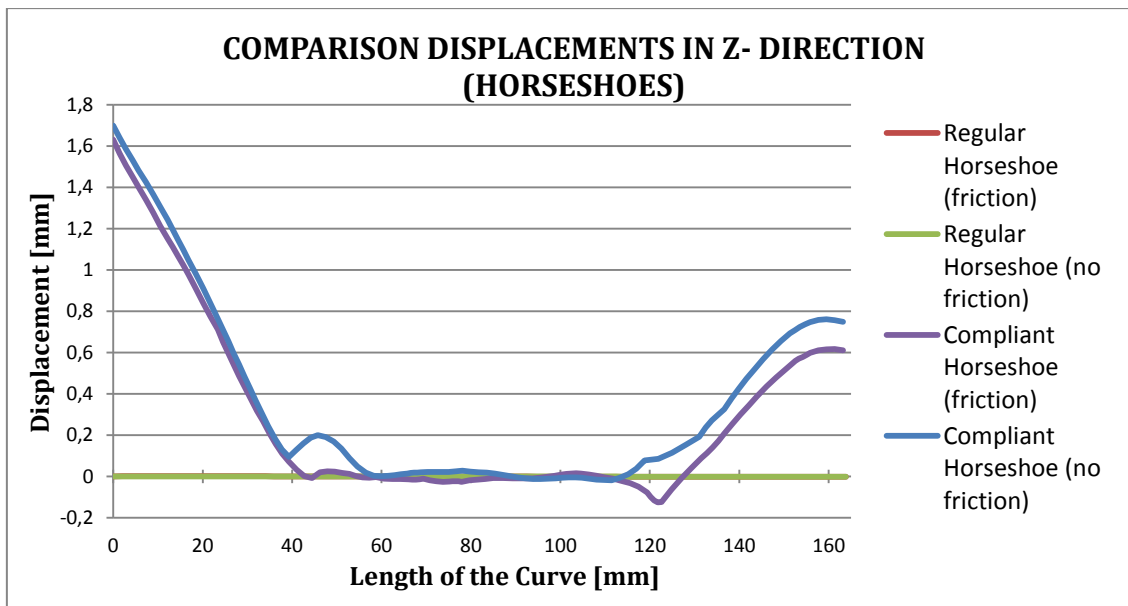


Figure 90. Comparison of the horseshoes displacements in z- direction (own source)

In this way, as can be seen in the figure above, the compliant horseshoe has a very high capacity of absorbing impacts in comparison with the regular horseshoe, which has not almost any deformation in the z- direction.

5.2. Stresses

Attending to stresses, it should be noted that some peaks of stresses have been obtained in the nail holes when the simulation has been performed without the establishment of friction between the hoof and horseshoe surfaces. This is due to, all the forces applied on the horse hoof are transmitted to the horseshoe by means of the nails, and the nails transmit those forces to the holes where they are placed. It is logical that the high stresses are located in the corners of the holes since that the nail holes have not been rounded due to the problems obtained with the software when the different contact interfaces have been set.

The software is able to round the nails; however, the real problem is when the horseshoe edges are rounded. The rounded edges of the assembly horseshoe-nail cannot be simulated in the software because at time of create the mesh the software failed, doing impossible the analysis. For this reason, it is possible to find some high stress concentrations in places not expected, but in the most cases they are located in the right place, as for example, in the rear nail hole. This hole is the one which supports more load due to it is the closer to the part of the hoof wall which moves sideways.

Some complications have been found during the modelled of the horse hoof, but one of the most important issues was the modelling and assembly of the different hoof parts which were impossible to connect due to its complicate geometry. For this reason, the hoof was modelled as a piece and later each part of it was cut taking to account some limitations of the software. All this process was necessary in order to assign to each part different material properties.

The results obtained in the simulation of the barefoot hoof did not reach the value expected but the results are acceptable.

The maximum stresses of the hooves obtained in the different simulations are compared in *Table 3*.

		Max. Stress [MPa]
Friction	Regular Horseshoe	108
	Compliant Horseshoe	290
No Friction	Regular Horseshoe	263
	Compliant Horseshoe	203

Table 3. Comparison of hoof stresses (own source)

The maximum stresses of the horseshoes obtained in the different simulations are compared in *Table 4*.

	Max. Stress [MPa]	Steel Alloy 4340 (annealed 810°C)		Titanium Alloy Ti- 6Al-4V (annealed)		Rubber	
		σ_y [MPa] = 472	σ_u [MPa] = 745	σ_y [MPa] = 830	σ_u [MPa] = 900	σ_y [MPa] = 7	σ_u [MPa] = 20
Friction	Regular Horseshoe	1417	X	X	--	--	--
	Compliant (metal)	1246	--	--	X	X	--
	Compliant (polymer)	3.5	--	--	--	--	✓
No Friction	Regular Horseshoe	5825	X	X	--	--	--
	Compliant (metal)	1414	--	--	X	X	--
	Compliant (polymer)	3	--	--	--	--	✓

Table 4. Comparison of horseshoe stresses (own source)

The maximum stresses of the nails obtained in the different simulations are compared in *Table 5*.

	Max. Stress [MPa]	Steel Alloy 4340 (annealed 810°C)		Steel Alloy 4340 (oil-quenched and tempered 315°C)	
		σ_y [MPa] = 472	σ_u [MPa] = 745	σ_y [MPa] = 1620	σ_u [MPa] = 1760
Friction	Regular Horseshoe	1375	X	X	--
	Compliant Horseshoe	1117	--	--	✓
No Friction	Regular Horseshoe	5774	X	X	--
	Compliant Horseshoe	1229	--	--	✓

Table 5. Comparison of nail stresses (own source)

5.3. Weights

In the design of the horseshoe, the weight of the whole shoe has been reduced. *Figure 91* shows the total volume of the sample horseshoe given by the software PTC Creo.

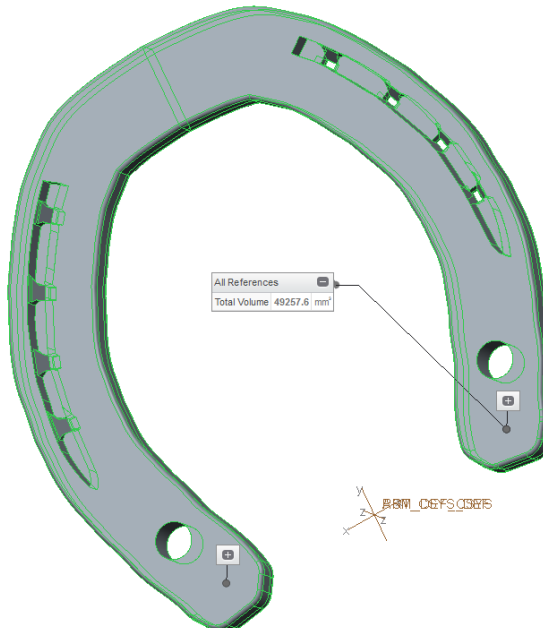


Figure 91. Volume of the regular horseshoe (own source)

The volume is around 49.26 cm^3 , so knowing that the steel density is 7.85 g/cm^3 the mass of the metal horseshoe is given by *Equation 22*:

$$m = \rho \cdot V = 386.7 \text{ [g]} \quad (22)$$

On the other hand, *Figure 92* shows the volume of the polymer body and the volume of the metal parts.



Figure 92. Volume of the compliant horseshoe (own source)

The volume of the polymer body is around 56.10 cm^3 and the volume of the metal parts is around 14.54 cm^3 . Knowing that the rubber density is 1.13 g/cm^3 and the density of the titanium is 4.43 g/cm^3 is possible to calculate the mass of the whole horseshoe by the *Equations 23, 24 and 25*:

$$m_{rub} = \rho_{rub} \cdot V_{rub} = 63.39 \text{ [g]} \quad (23)$$

$$m_{Ti} = \rho_{Ti} \cdot V_{Ti} = 64.41 \text{ [g]} \quad (24)$$

$$m_{total} = m_{rub} + m_{Ti} = 127.8 \text{ [g]} \quad (25)$$

Comparing the weight of both horseshoes, it is reached the conclusion that in the design of this new horseshoe the weight has been reduced one third in comparison with the metal horseshoe.

5.4. Costs

Knowing the mass of the materials used to manufacture the horseshoe, a comparison of the cost of the needed material can be done.

On the one hand, the cost of the material required to manufacture one steel horseshoe, as the regular horseshoe analysed, is given by *Equations 26*:

$$m_{steel} \cdot 10^{-3}[\text{kg}] \cdot 3.6 \left[\frac{\text{US\$}}{\text{kg}} \right] = 1.39 \text{ [US\$]} \quad (26)$$

On the other hand, the cost of the material required to manufacture the horseshoe designed during this project is given by *Equations 27 and 28*:

$$m_{rub} \cdot 10^{-3}[\text{kg}] \cdot 2 \left[\frac{\text{US\$}}{\text{kg}} \right] = 0.13 \text{ [US\$]} \quad (27)$$

$$m_{Ti} \cdot 10^{-3}[\text{kg}] \cdot 110 \left[\frac{\text{US\$}}{\text{kg}} \right] = 7.08 \text{ [US\$]} \quad (28)$$

So the price of the required material for the compliant horseshoe is 7.21 US\$, this is an estimation and the values has been taken according to Callister & Rethwisch (2011). These values can vary due the constantly change in the price of the raw materials. However, although the material price has been increased, the flexibility, the lightweigth, the shock absorption have been improved.

6. FUTURE RESEARCH

During this project some areas, which are important to be investigated, have been found. Several researches are suggested to be aim of future investigations. Regarding the interaction nail-hoof, carry out a thorough study is recommended to obtain a better knowledge about the behaviour of this interaction. It is important to study the friction between the horn wall and the nails such as the relative displacement between them. A non-linear analysis should be done in order to analyse the stress concentrations to know what occurs when the yield stress is overpass. It is recommended to perform a fatigue study of the designed horseshoe to determinate its fatigue life. It is necessary an improvement of the friction analysis, in which the friction between the hoof, the nails, the horseshoe and the ground can be set and analysed. It is suggested to analyse the different adhesive attachments, i.e. analyse the behaviour of the different glues under the load conditions of the hoof. A study about the manufacturing process is also recommended. Last but not least, it is highly recommended an improvement of the design of the 3D model of the horse hoof.

APPENDIX A

STEEL ALLOY 4340
Modulus of Elasticity → $E = 207 \text{ [GPa]}$
Poisson's Ratio → $\nu = 0.30$
Density → $\rho = 7.85 \text{ [g/cm}^3\text{]}$
Maximum displacement in the x- direction (shown in <i>Figure 93</i>) → 0.48 [mm]
Maximum displacement in the z- direction (shown in <i>Figure 94</i>) → $2.78 \cdot 10^{-4} \text{ [mm]}$

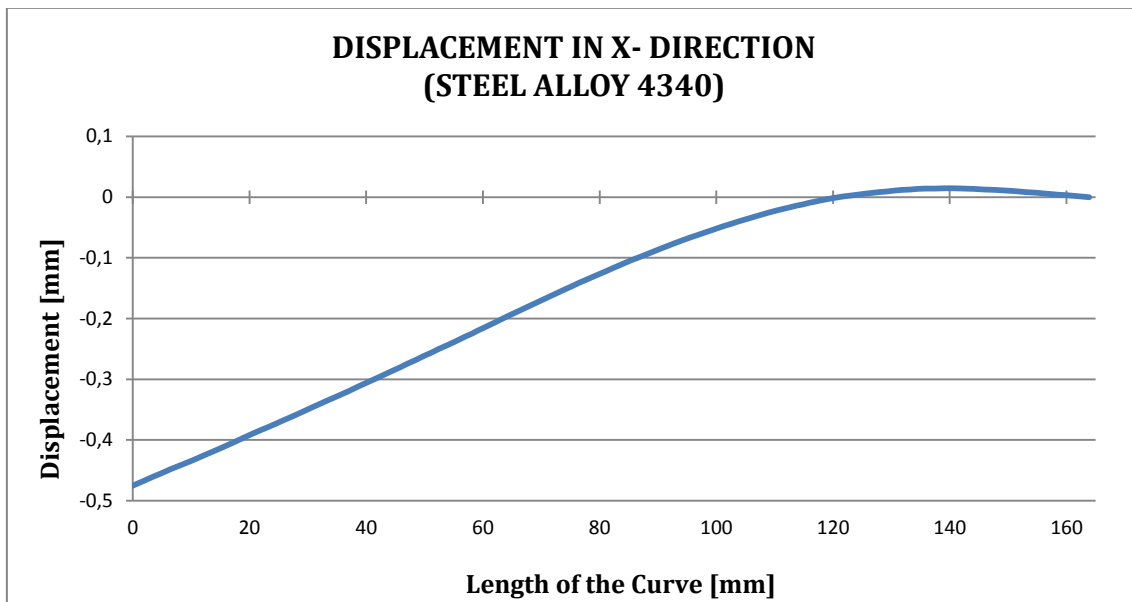


Figure 93. Test performed with steel alloy 4340. Displacement in x- direction (own source)

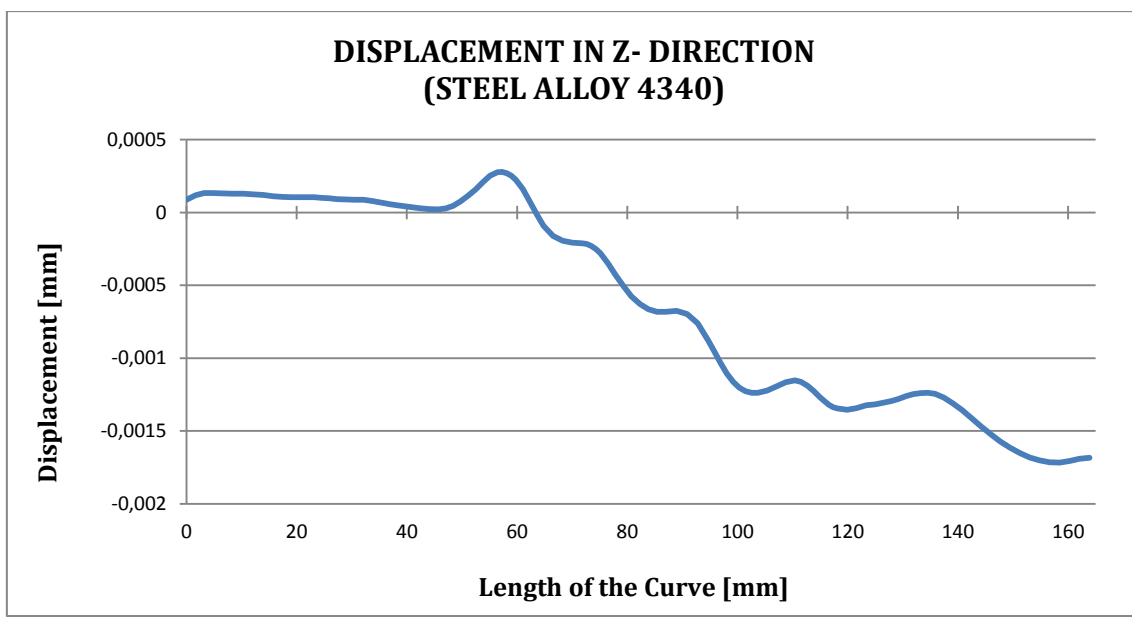


Figure 94. Test performed with steel alloy 4340. Displacement in z- direction (own source)

GRAY IRON G4000
Modulus of Elasticity → $E = 81.5 \text{ [GPa]}$
Poisson's Ratio → $\nu = 0.26$
Density → $\rho = 7.30 \text{ [g/cm}^3\text{]}$
Maximum displacement in the x- direction (shown in <i>Figure 95</i>) → 1.06 [mm]
Maximum displacement in the z- direction (shown in <i>Figure 96</i>) → $7.72 \cdot 10^{-4} \text{ [mm]}$

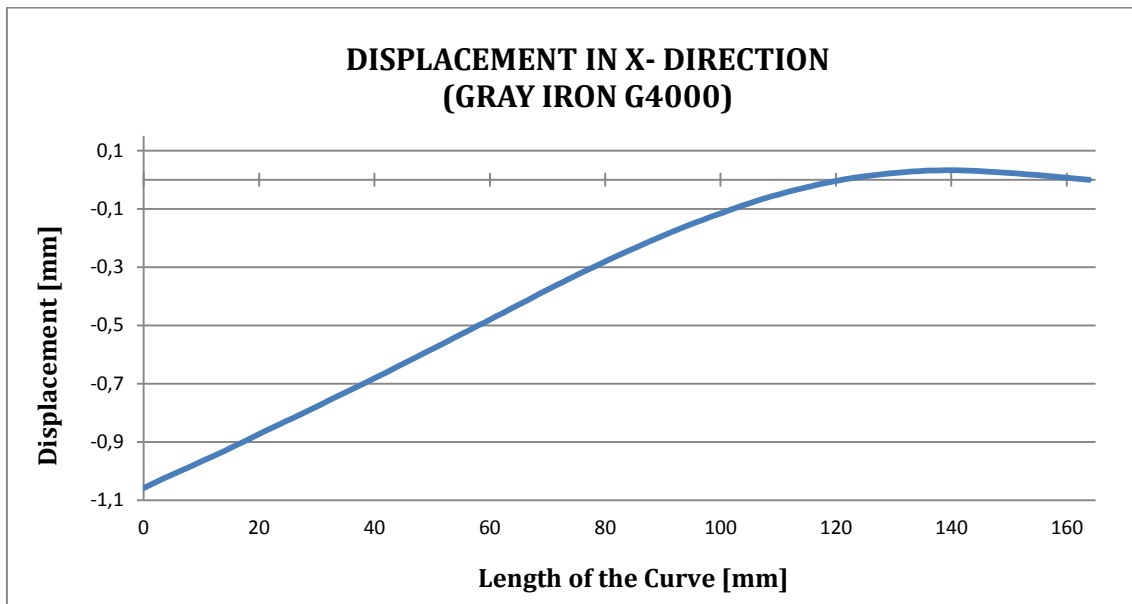


Figure 95. Test performed with gray iron G4000. Displacement in x- direction (own source)

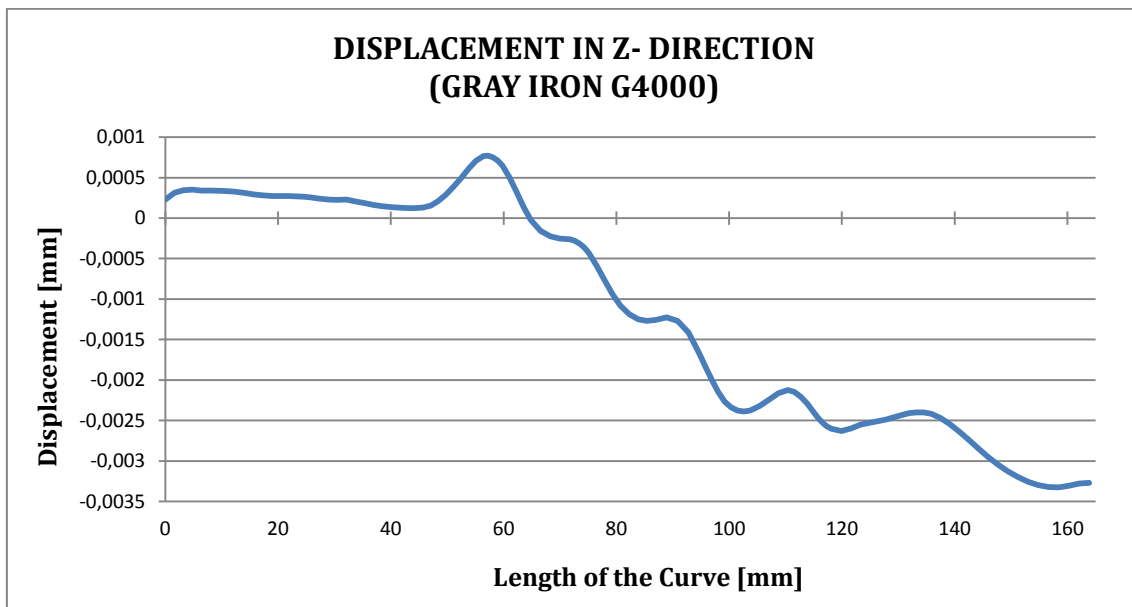


Figure 96. Test performed with gray iron G4000. Displacement in z- direction (own source)

DUCTILE IRON 120-90-02
Modulus of Elasticity → $E = 164$ [GPa]
Poisson's Ratio → $\nu = 0.28$
Density → $\rho = 7.10$ [g/cm^3]
Maximum displacement in the x- direction (shown in <i>Figure 97</i>) → 0.59 [mm]
Maximum displacement in the z- direction (shown in <i>Figure 98</i>) → $3.69 \cdot 10^{-4}$ [mm]

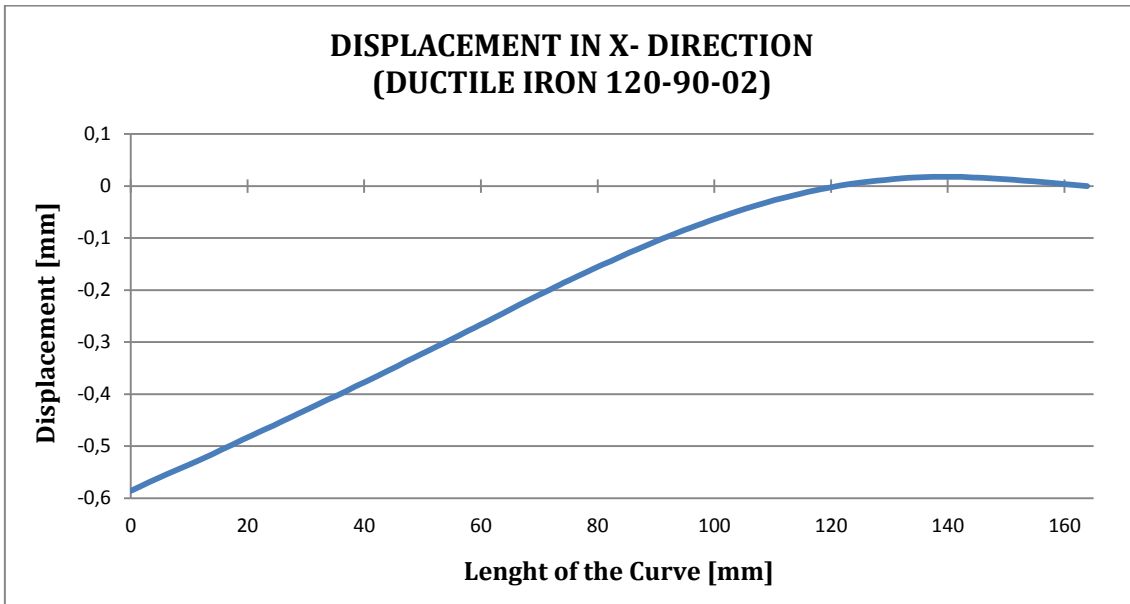


Figure 97. Test performed with ductile iron 120-90-02. Displacement in x- direction (own source)

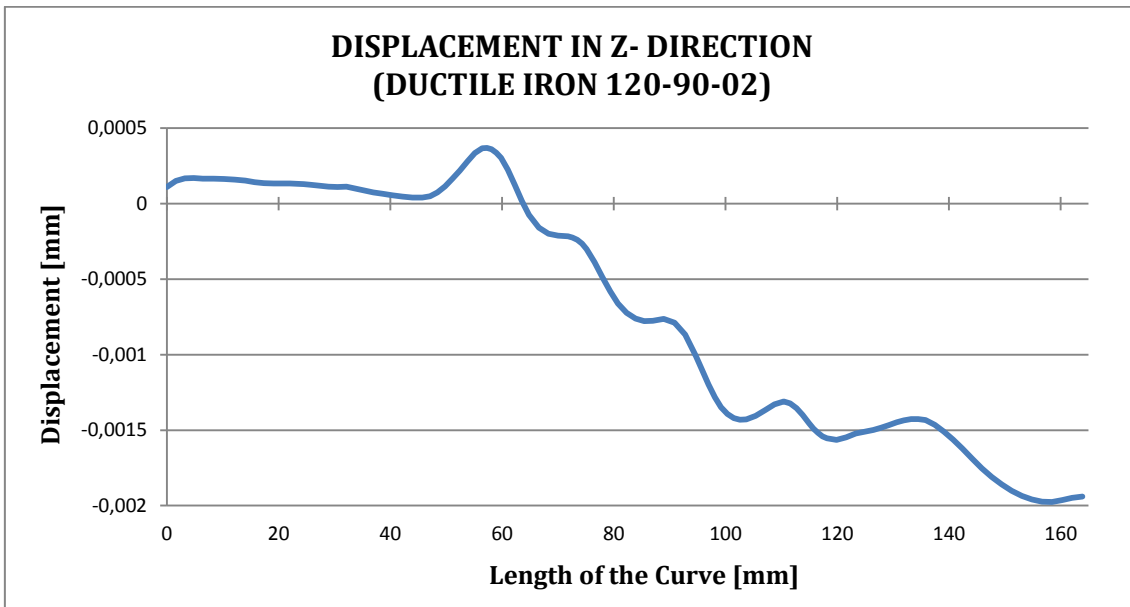


Figure 98. Test performed with ductile iron 120-90-02. Displacement in z- direction (own source)

ALUMINIUM ALLOY 7075
Modulus of Elasticity → $E = 71$ [GPa]
Poisson's Ratio → $\nu = 0.33$
Density → $\rho = 2.80$ [g/cm^3]
Maximum displacement in the x- direction (shown in <i>Figure 99</i>) → 1.18 [mm]
Maximum displacement in the z- direction (shown in <i>Figure 100</i>) → $9.19 \cdot 10^{-4}$ [mm]

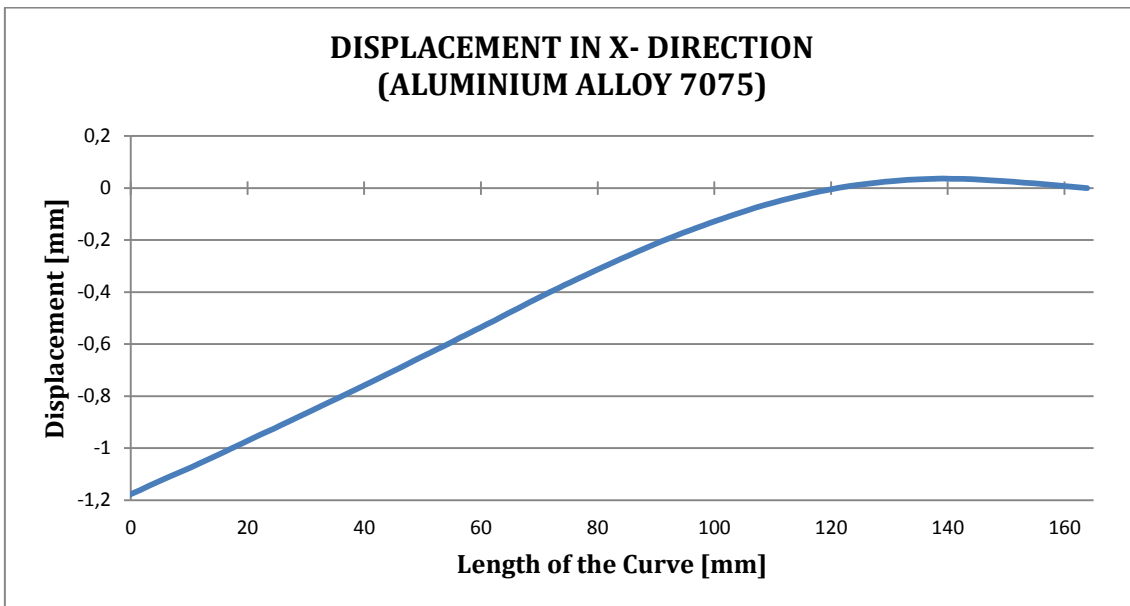


Figure 99. Test performed with aluminium alloy 7075. Displacement in x- direction (own source)

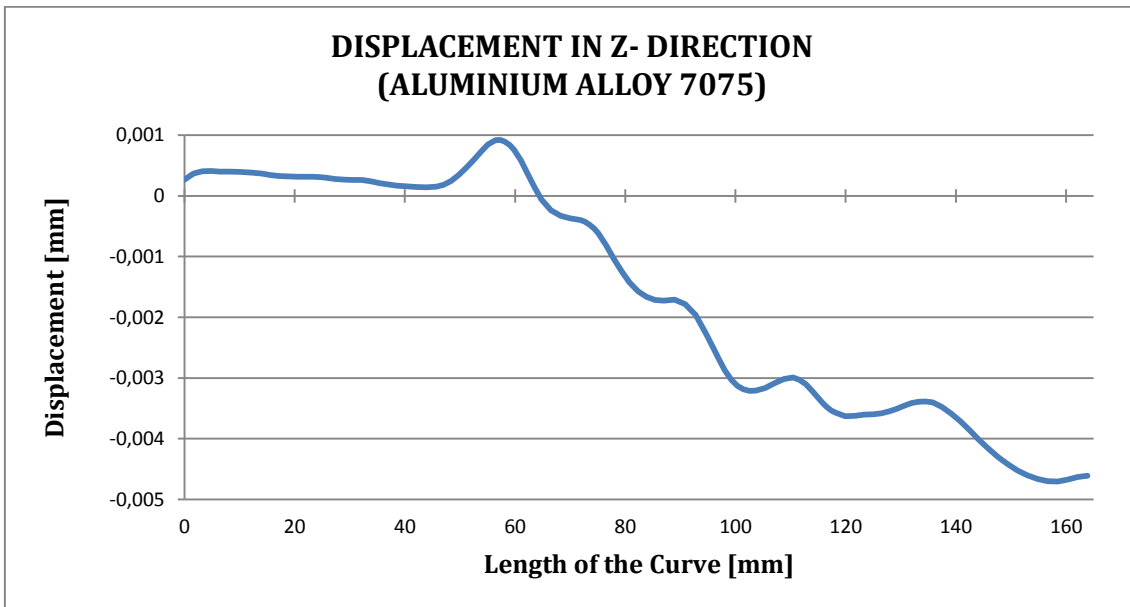


Figure 100. Test performed with aluminium alloy 7075. Displacement in z- direction (own source)

MAGNESIUM ALLOY AZ31B
Modulus of Elasticity → $E = 45 \text{ [GPa]}$
Poisson's Ratio → $\nu = 0.35$
Density → $\rho = 1.77 \text{ [g/cm}^3\text{]}$
Maximum displacement in the x- direction (shown in <i>Figure 101</i>) → 1.64 [mm]
Maximum displacement in the z- direction (shown in <i>Figure 102</i>) → $1.35 \cdot 10^{-3} \text{ [mm]}$

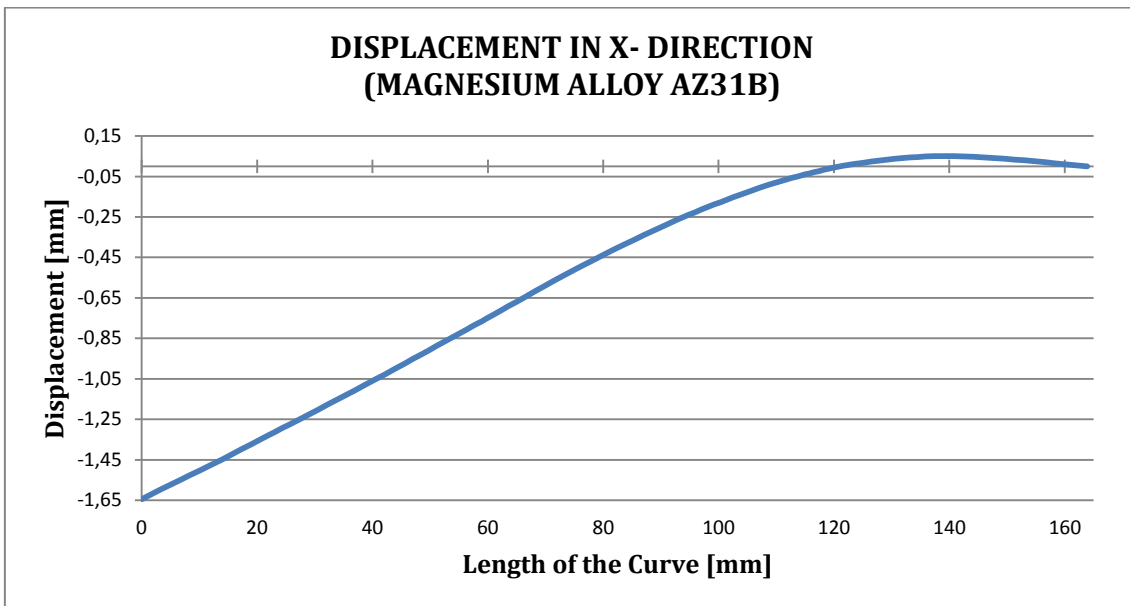


Figure 101. Test performed with magnesium alloy AZ31B. Displacement in x- direction (own source)

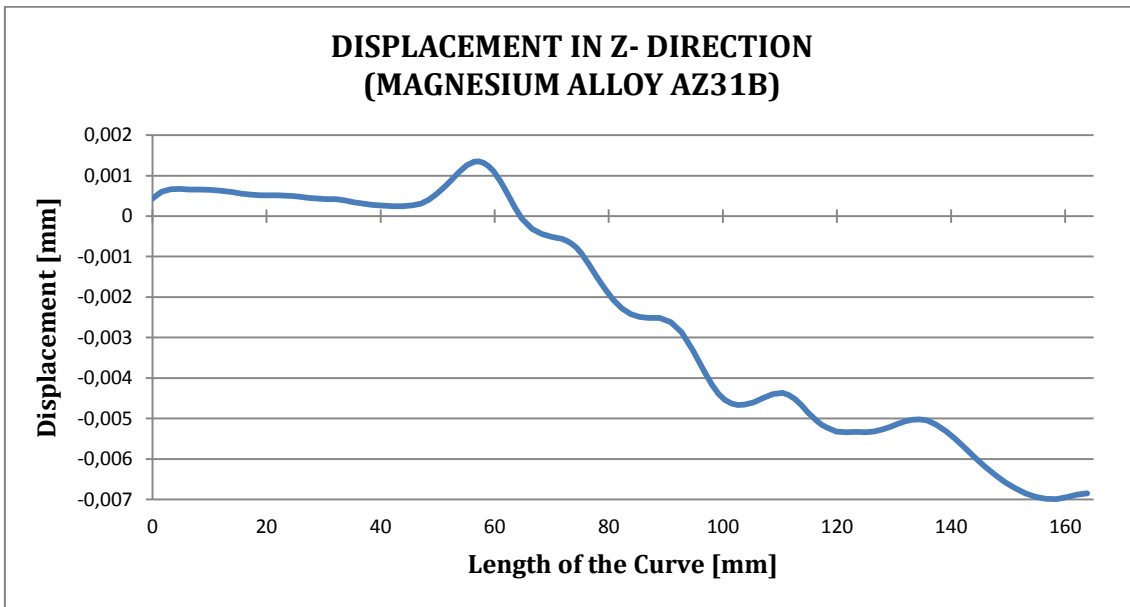


Figure 102. Test performed with magnesium alloy AZ31B. Displacement in z- direction (own source)

TITANIUM ALLOY Ti-6Al-4V
Modulus of Elasticity → $E = 114$ [GPa]
Poisson's Ratio → $\nu = 0.34$
Density → $\rho = 4.43$ [g/cm^3]
Maximum displacement in the x- direction (shown in <i>Figure 103</i>) → 0.8 [mm]
Maximum displacement in the z- direction (shown in <i>Figure 104</i>) → $5.86 \cdot 10^{-4}$ [mm]

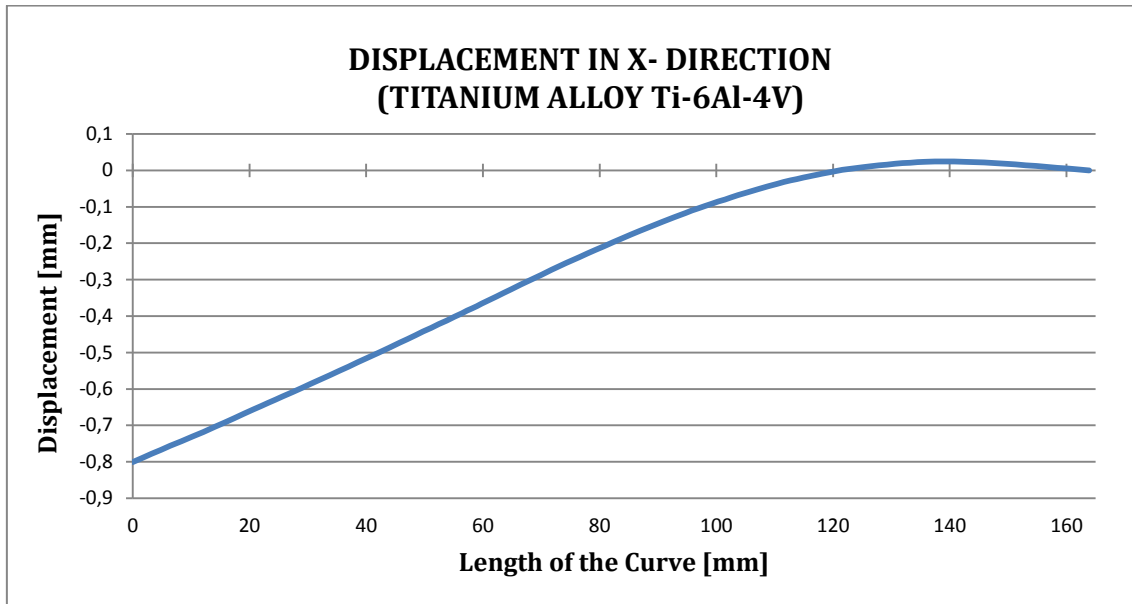


Figure 103. Test performed with titanium alloy Ti-6Al-4V. Displacement in x- direction (own source)

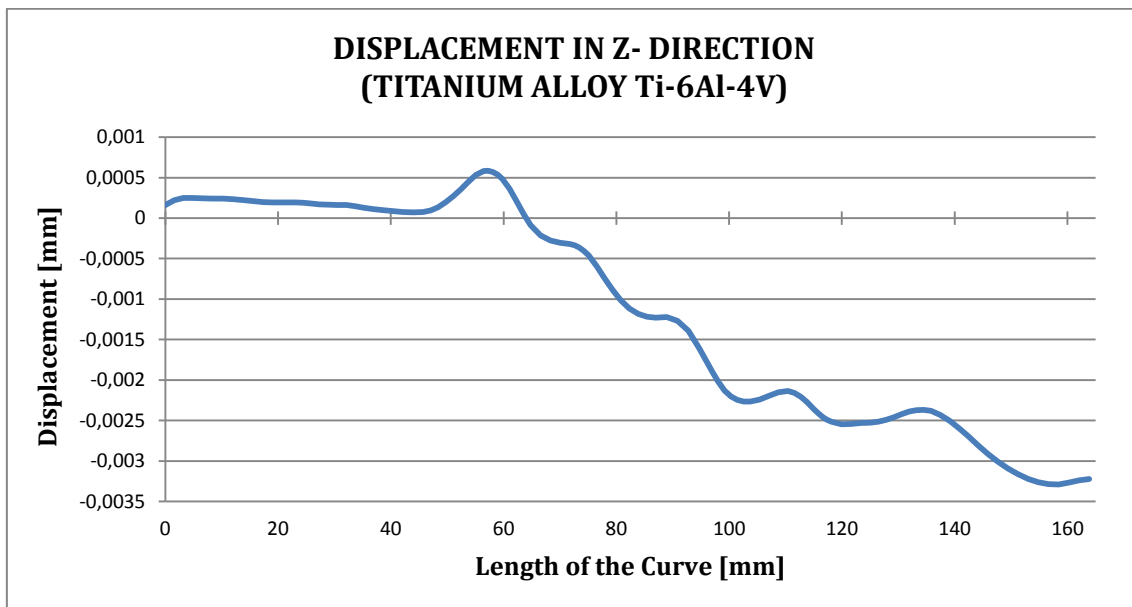


Figure 104. Test performed with titanium alloy Ti-6Al-4V. Displacement in z- direction (own source)

COPPER ALLOY C17200
Modulus of Elasticity → $E = 128$ [GPa]
Poisson's Ratio → $\nu = 0.30$
Density → $\rho = 8.25$ [g/cm^3]
Maximum displacement in the x- direction (shown in <i>Figure 105</i>) → 0.73 [mm]
Maximum displacement in the z- direction (shown in <i>Figure 106</i>) → $5.01 \cdot 10^{-4}$ [mm]

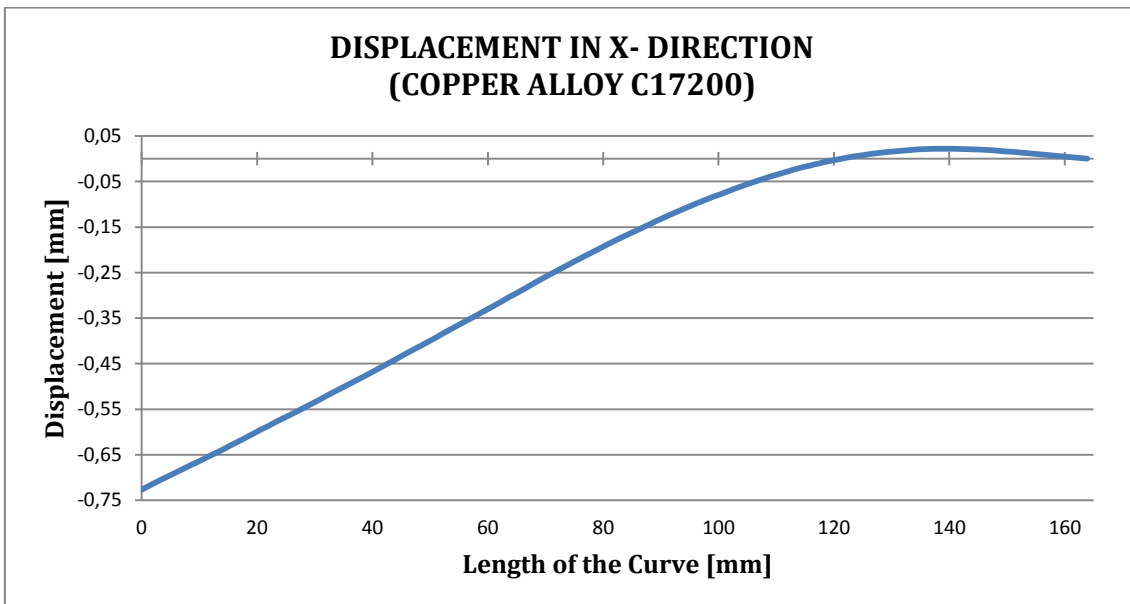


Figure 105. Test performed with cooper alloy C17200. Displacement in x- direction (own source)

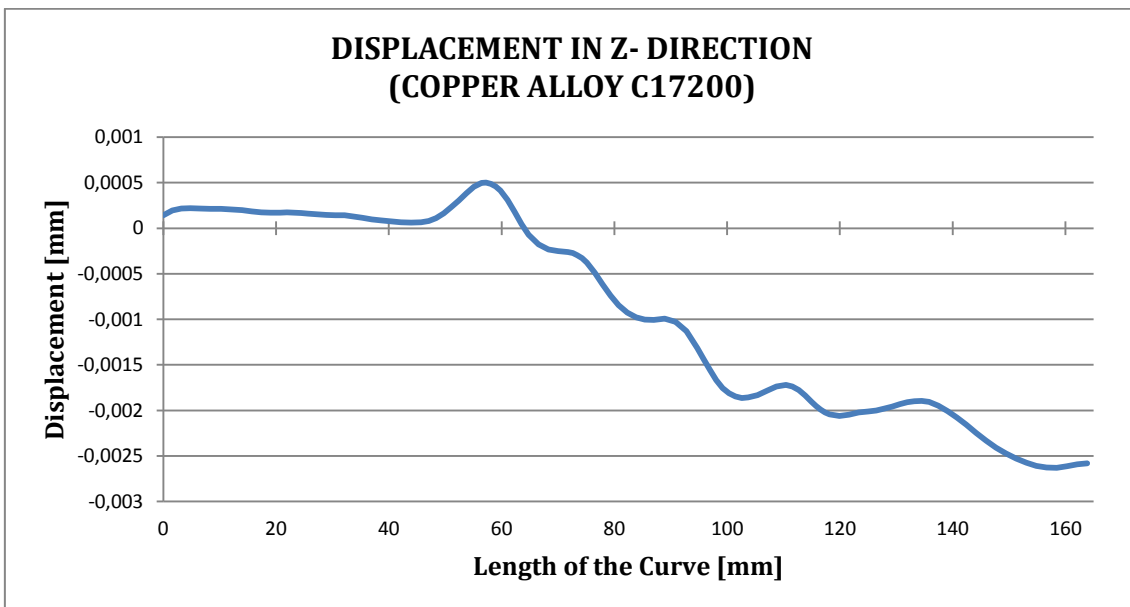


Figure 106. Test performed with cooper alloy C17200. Displacement in z- direction (own source)

POLYETHERETHERKETONE (PEEK)
Modulus of Elasticity → $E = 1100$ [MPa]
Poisson's Ratio → $\nu = 0.40$
Density → $\rho = 1.31$ [g/cm^3]
Maximum displacement in the x- direction (shown in <i>Figure 107</i>) → 5.12 [mm]
Maximum displacement in the z- direction (shown in <i>Figure 108</i>) → $3.39 \cdot 10^{-2}$ [mm]

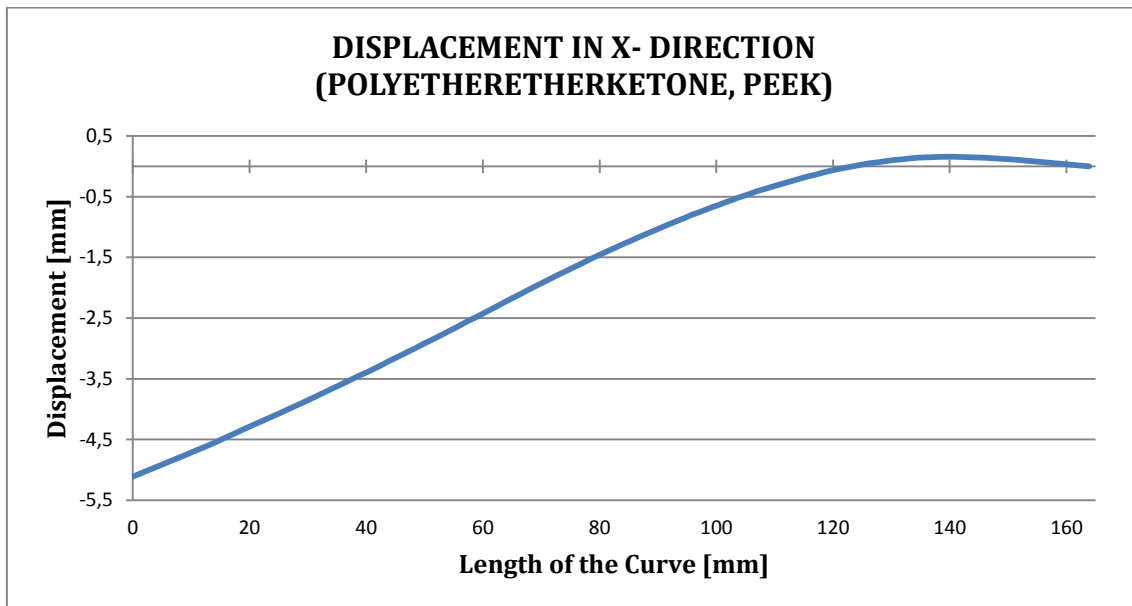


Figure 107. Test performed with PPEK. Displacement in x- direction (own source)

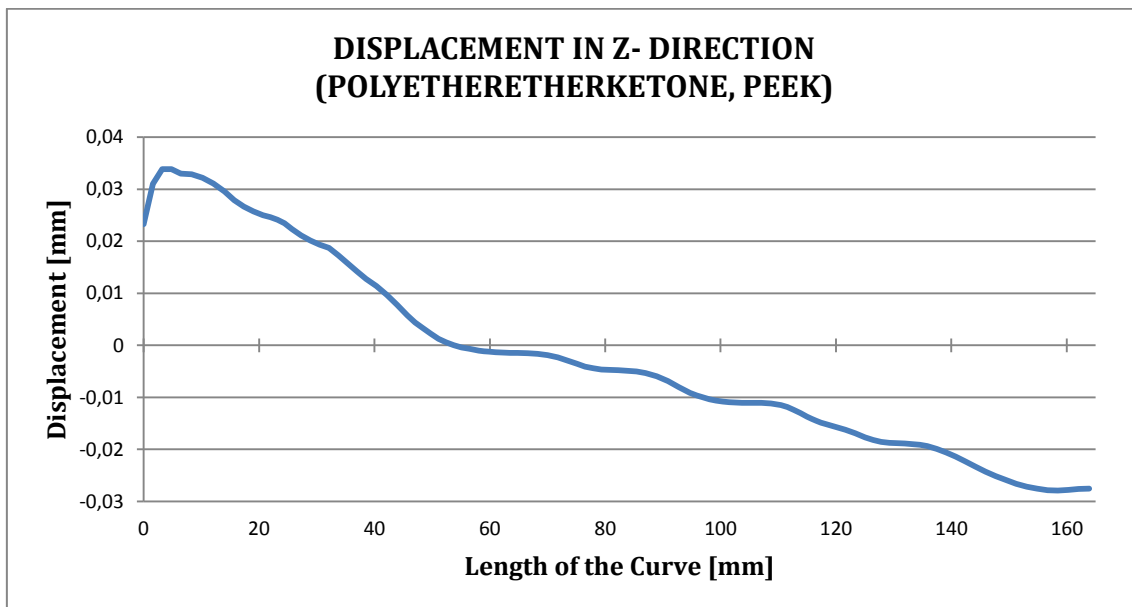


Figure 108. Test performed with PEEK. Displacement in z- direction (own source)

POLYETHYLENE LDPE
Modulus of Elasticity → $E = 227 \text{ [MPa]}$
Poisson's Ratio → $\nu = 0.365$
Density → $\rho = 0.925 \text{ [g/cm}^3\text{]}$
Maximum displacement in the x- direction (shown in <i>Figure 109</i>) → 5.18 [mm]
Maximum displacement in the z- direction (shown in <i>Figure 110</i>) → 0.15 [mm]

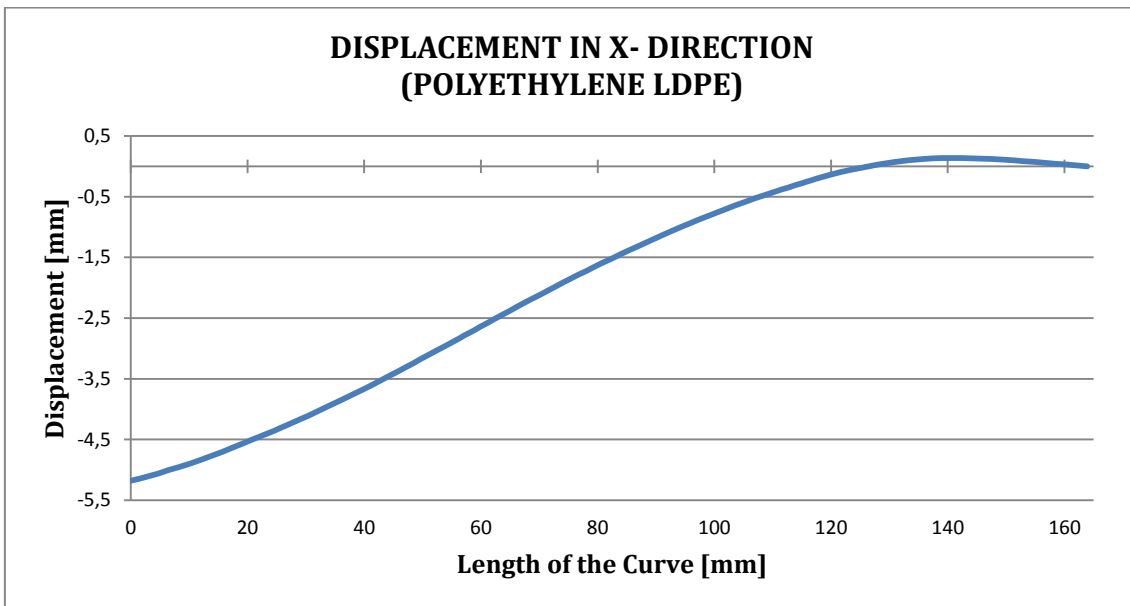


Figure 109. Test performed with LDPE. Displacement in x- direction (own source)

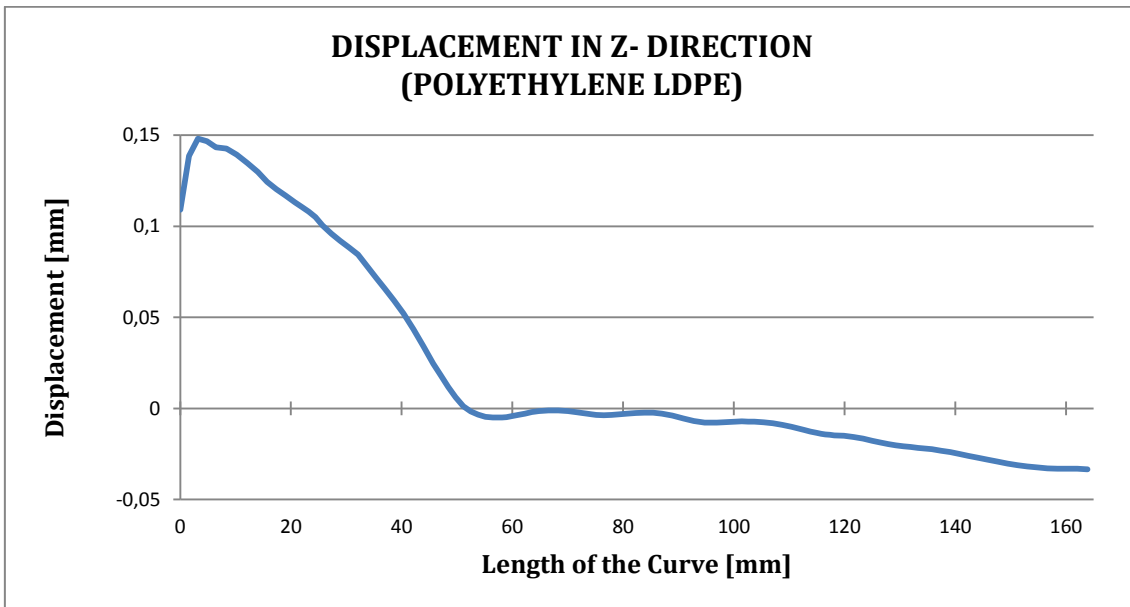


Figure 110. Test performed with LDPE. Displacement in z- direction (own source)

POLYETHYLENE HDPE
Modulus of Elasticity → $E = 1080$ [MPa]
Poisson's Ratio → $\nu = 0.46$
Density → $\rho = 0.959$ [g/cm^3]
Maximum displacement in the x- direction (shown in <i>Figure 111</i>) → 5.09 [mm]
Maximum displacement in the z- direction (shown in <i>Figure 112</i>) → $3.5 \cdot 10^{-2}$ [mm]

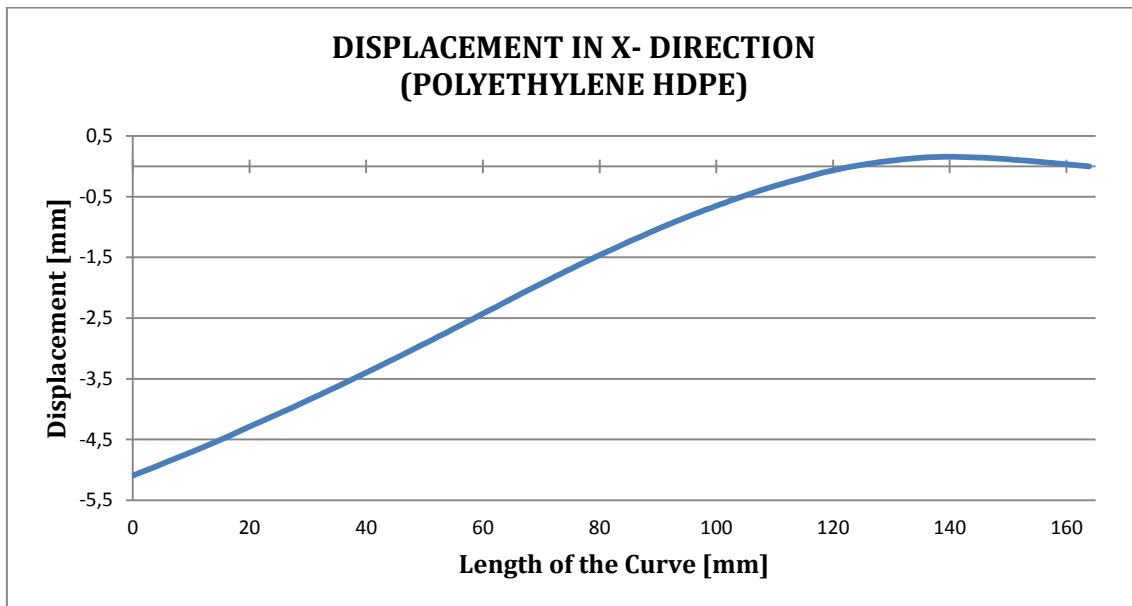


Figure 111. Test performed with HDPE. Displacement in x- direction (own source)

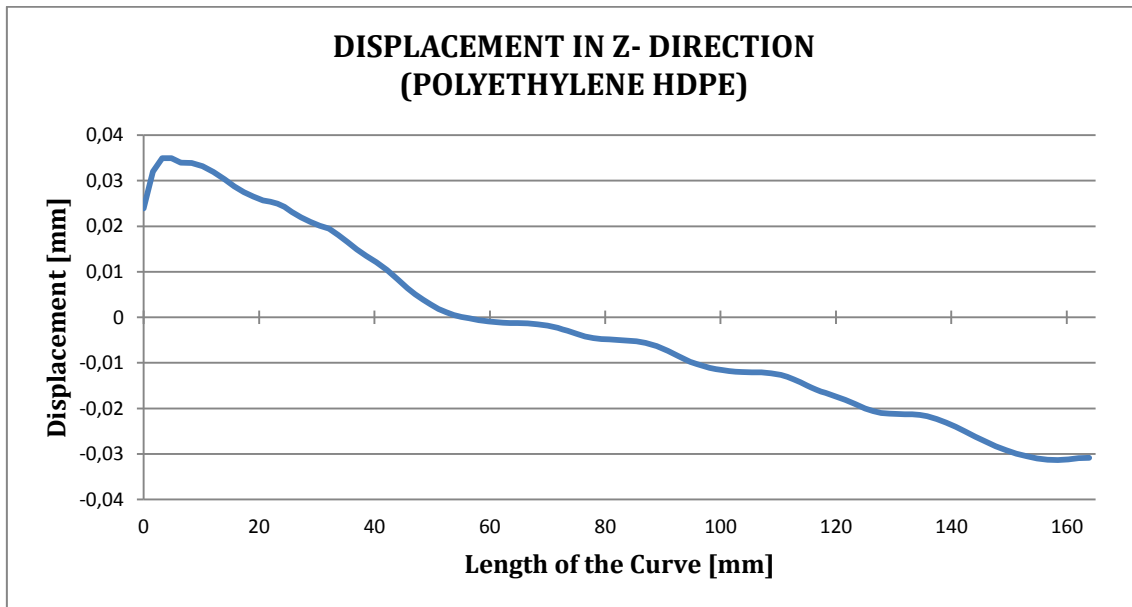


Figure 112. Test performed with HDPE. Displacement in z- direction (own source)

POLYTETRAFLUOROETHYLENE (PTFE)
Modulus of Elasticity → $E = 475$ [MPa]
Poisson's Ratio → $\nu = 0.46$
Density → $\rho = 2.17$ [g/cm^3]
Maximum displacement in the x- direction (shown in <i>Figure 113</i>) → 5.18 [mm]
Maximum displacement in the z- direction (shown in <i>Figure 114</i>) → $7.7 \cdot 10^{-2}$ [mm]

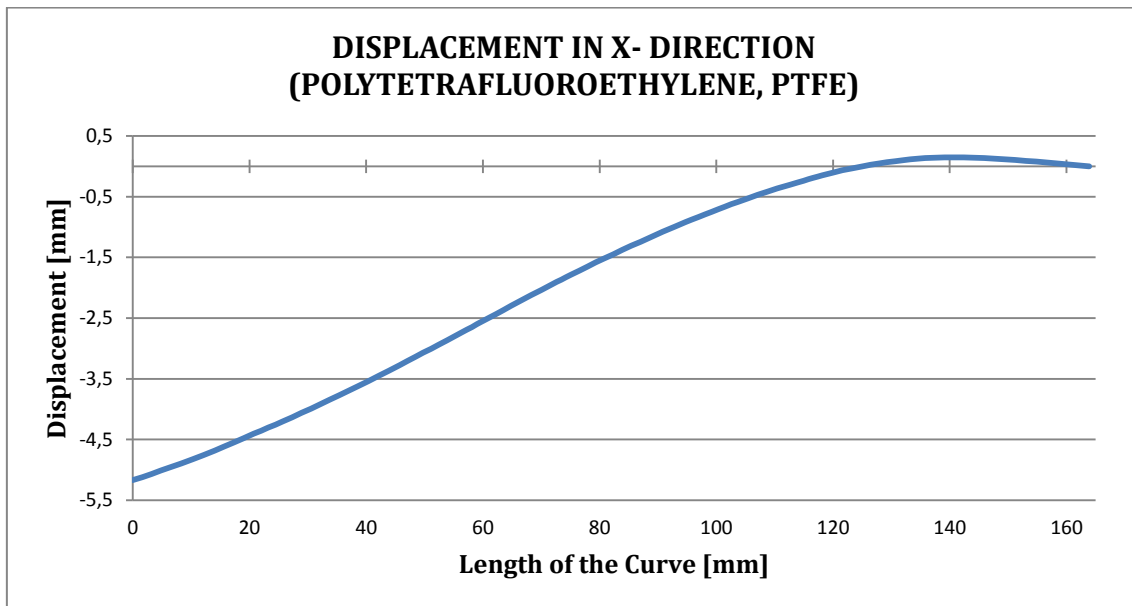


Figure 113. Test performed with PTFE. Displacement in x- direction (own source)

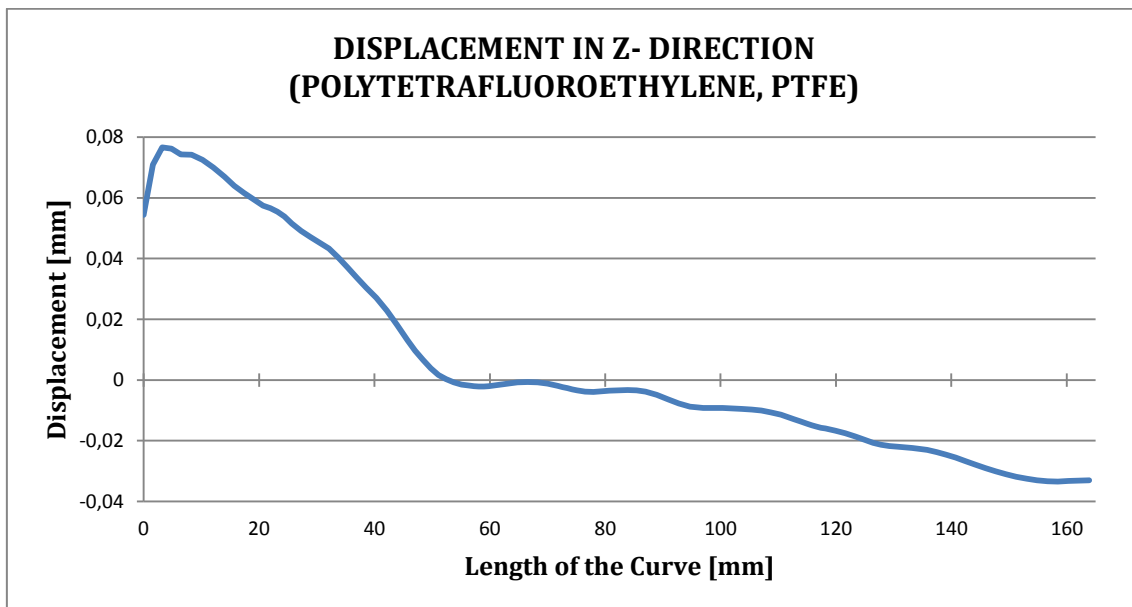


Figure 114. Test performed with PTFE. Displacement in z- direction (own source)

POLYURETHANE THERMOPLASTIC
Modulus of Elasticity → $E = 25 \text{ [MPa]}$
Poisson's Ratio → $\nu = 0.25$
Density → $\rho = 1.12 \text{ [g/cm}^3\text{]}$
Maximum displacement in the x- direction (shown in <i>Figure 115</i>) → 5.04 [mm]
Maximum displacement in the z- direction (shown in <i>Figure 116</i>) → 0.95 [mm]

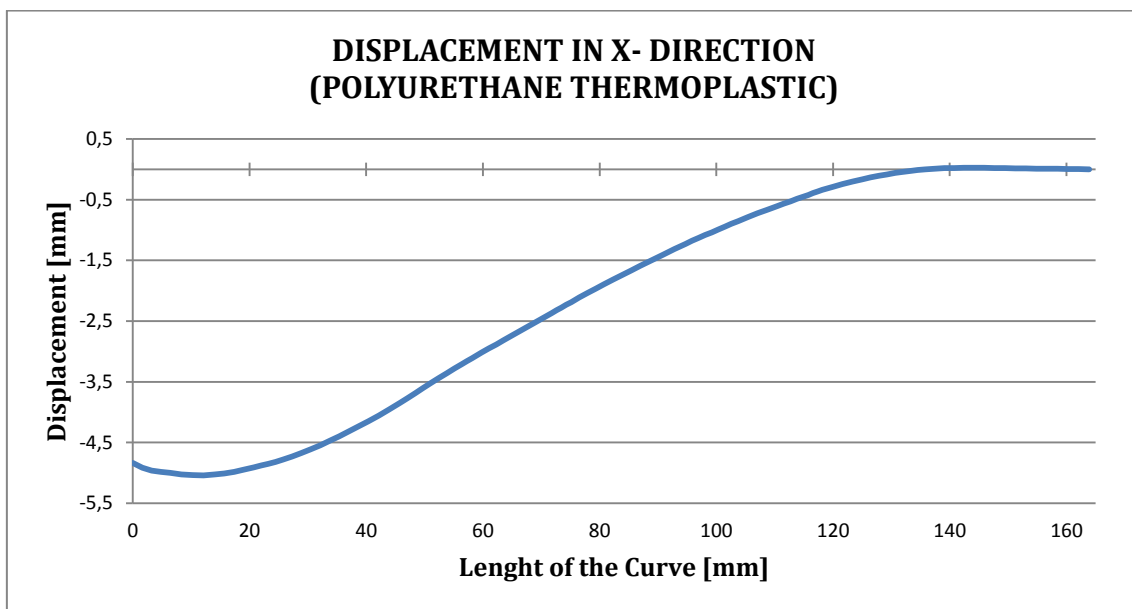


Figure 115. Test performed with polyurethane thermoplastic. Displacement in x- direction (own source)

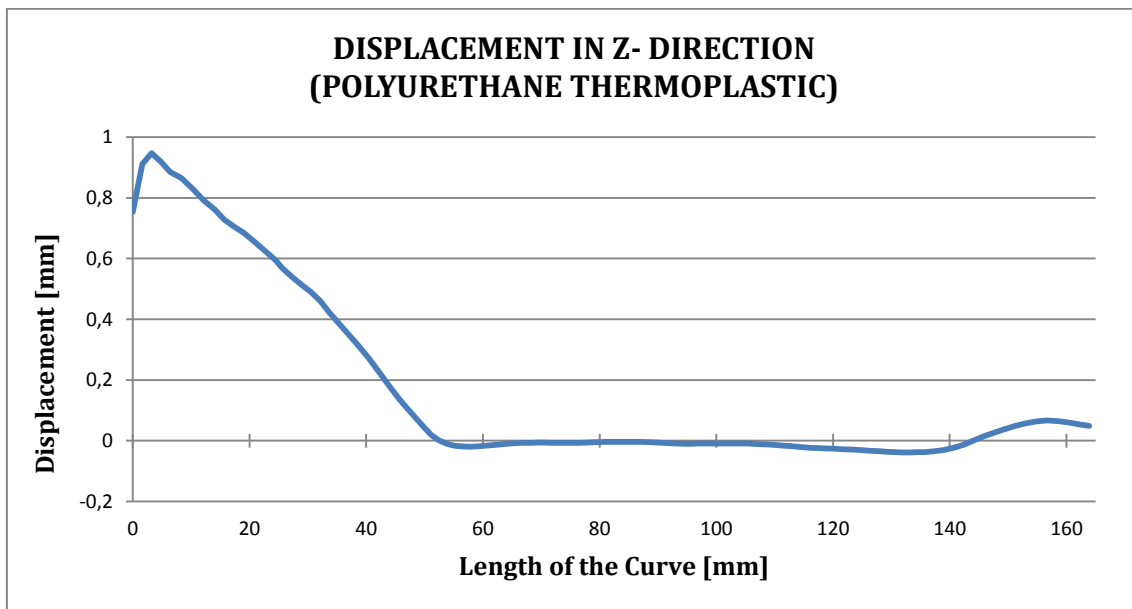


Figure 116. Test performed with polyurethane thermoplastic. Displacement in z- direction (own source)

RUBBER
Modulus of Elasticity $\rightarrow E = 2.35 \text{ [MPa]}$
Poisson's Ratio $\rightarrow \nu = 0.475$
Density $\rightarrow \rho = 1.13 \text{ [g/cm}^3\text{]}$
Maximum displacement in the x- direction (shown in <i>Figure 117</i>) $\rightarrow 5.8 \text{ [mm]}$
Maximum displacement in the z- direction (shown in <i>Figure 118</i>) $\rightarrow 3.11 \text{ [mm]}$

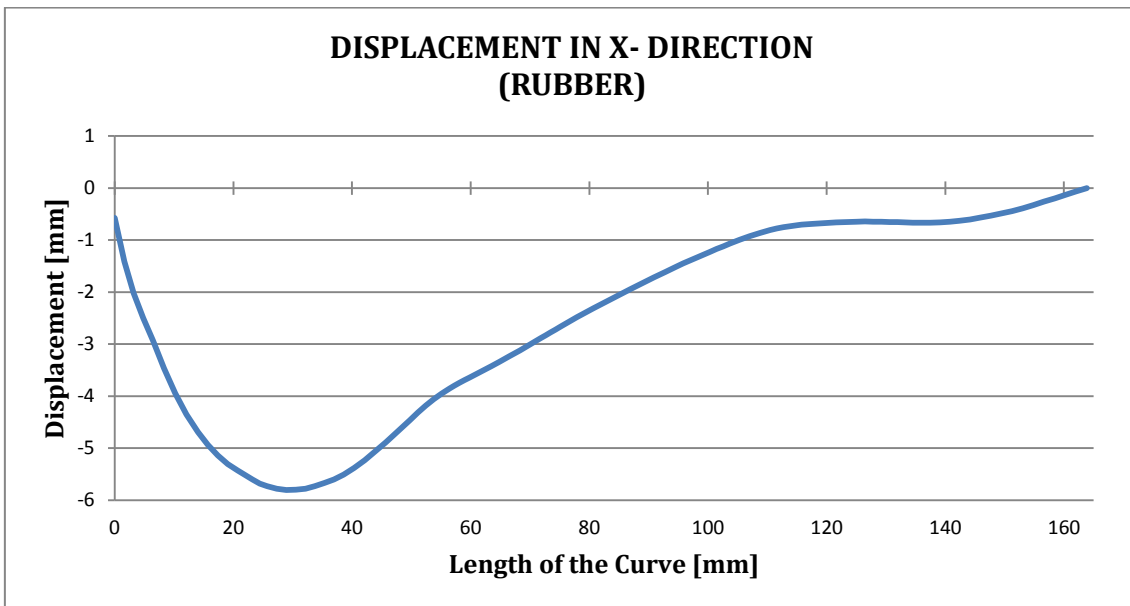


Figure 117. Test performed with rubber. Displacement in x- direction (own source)

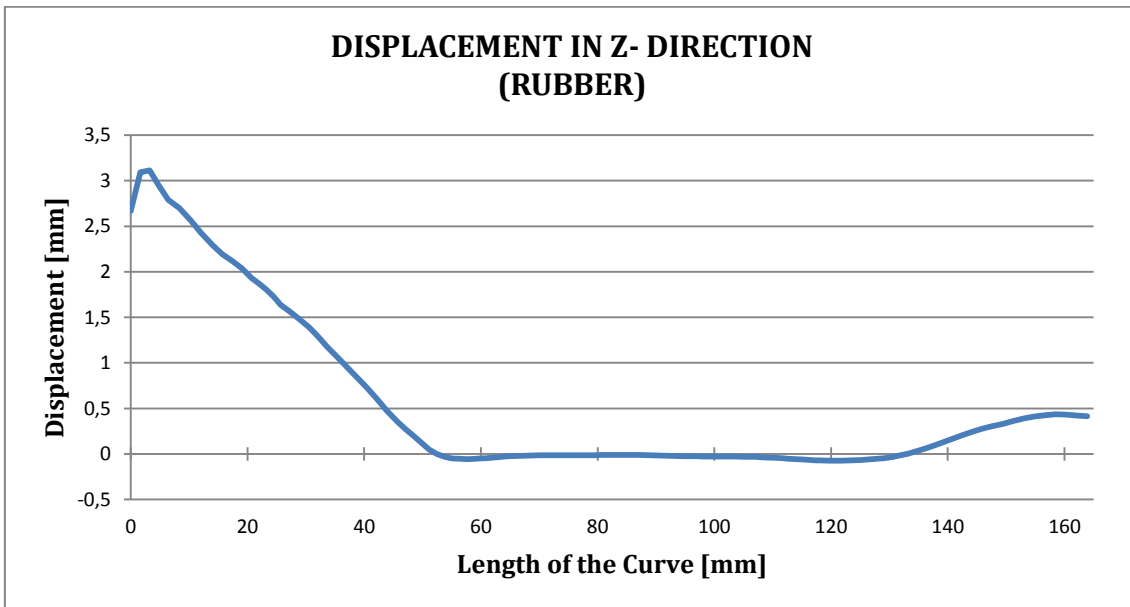


Figure 118. Test performed with rubber. Displacement in z- direction (own source)

ADIPRENE LF-950	
Modulus of Elasticity → $E = 15.2 \text{ [MPa]}$	
Poisson's Ratio → $\nu = 0.46$	
Density → $\rho = 1.2 \text{ [g/cm}^3\text{]}$	
Maximum displacement in the x- direction (shown in <i>Figure 119</i>) → 4.93 [mm]	
Maximum displacement in the z- direction (shown in <i>Figure 120</i>) → 1.39 [mm]	

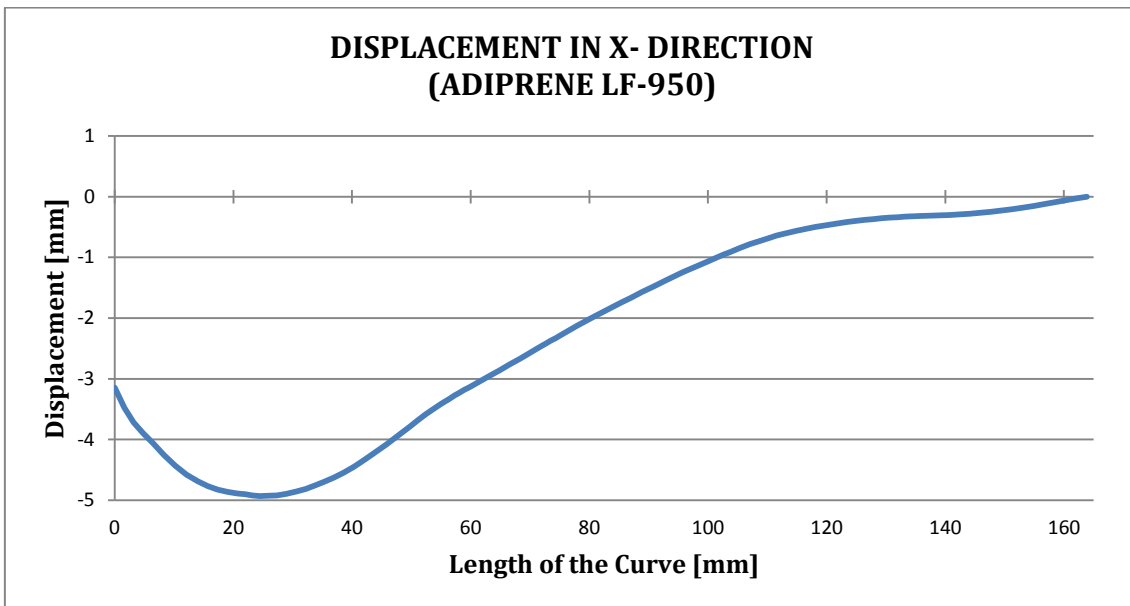


Figure 119. Test performed with adiprene LF-950. Displacement in x- direction (own source)

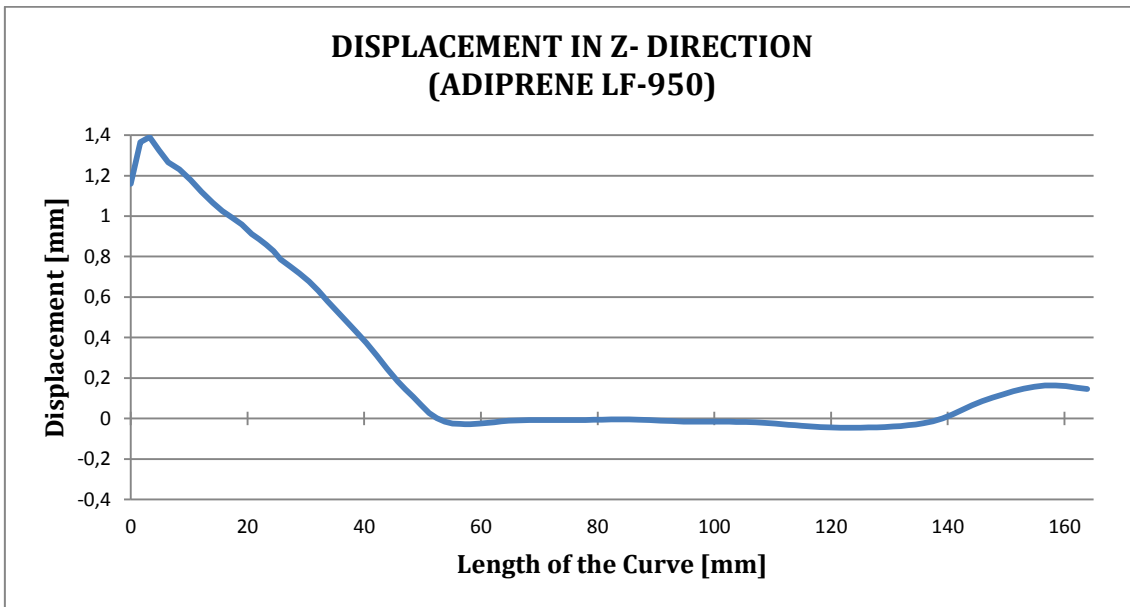
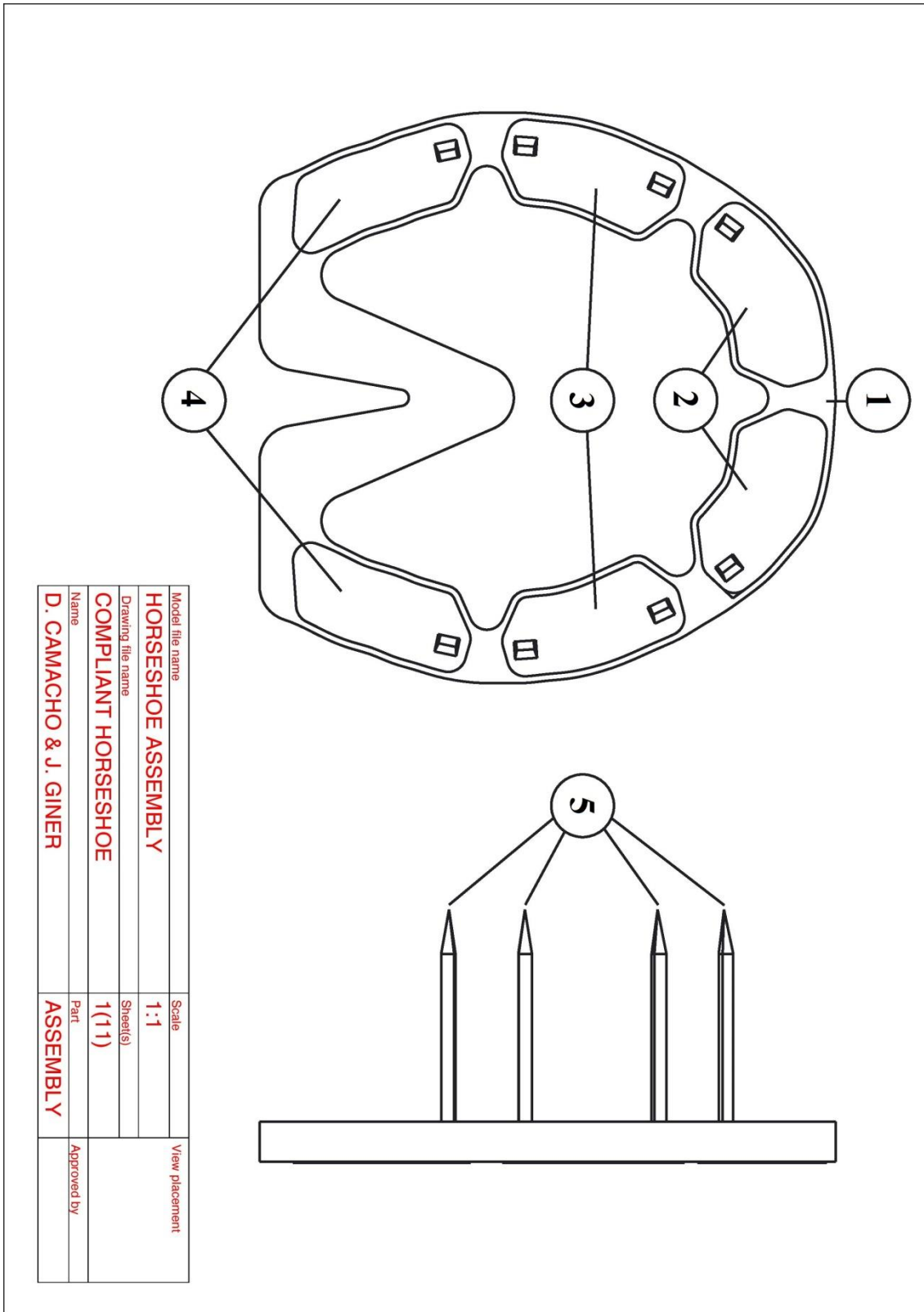
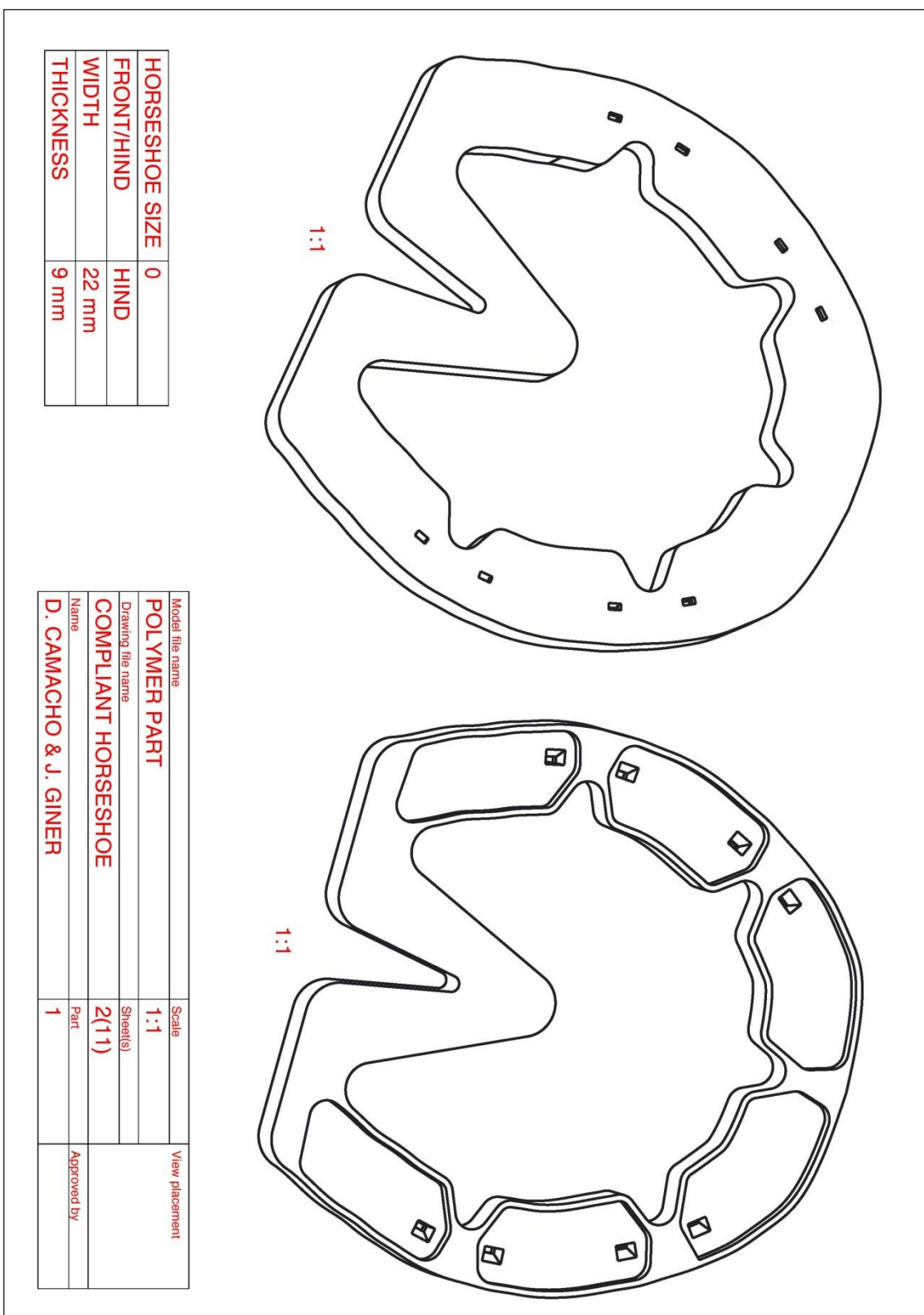
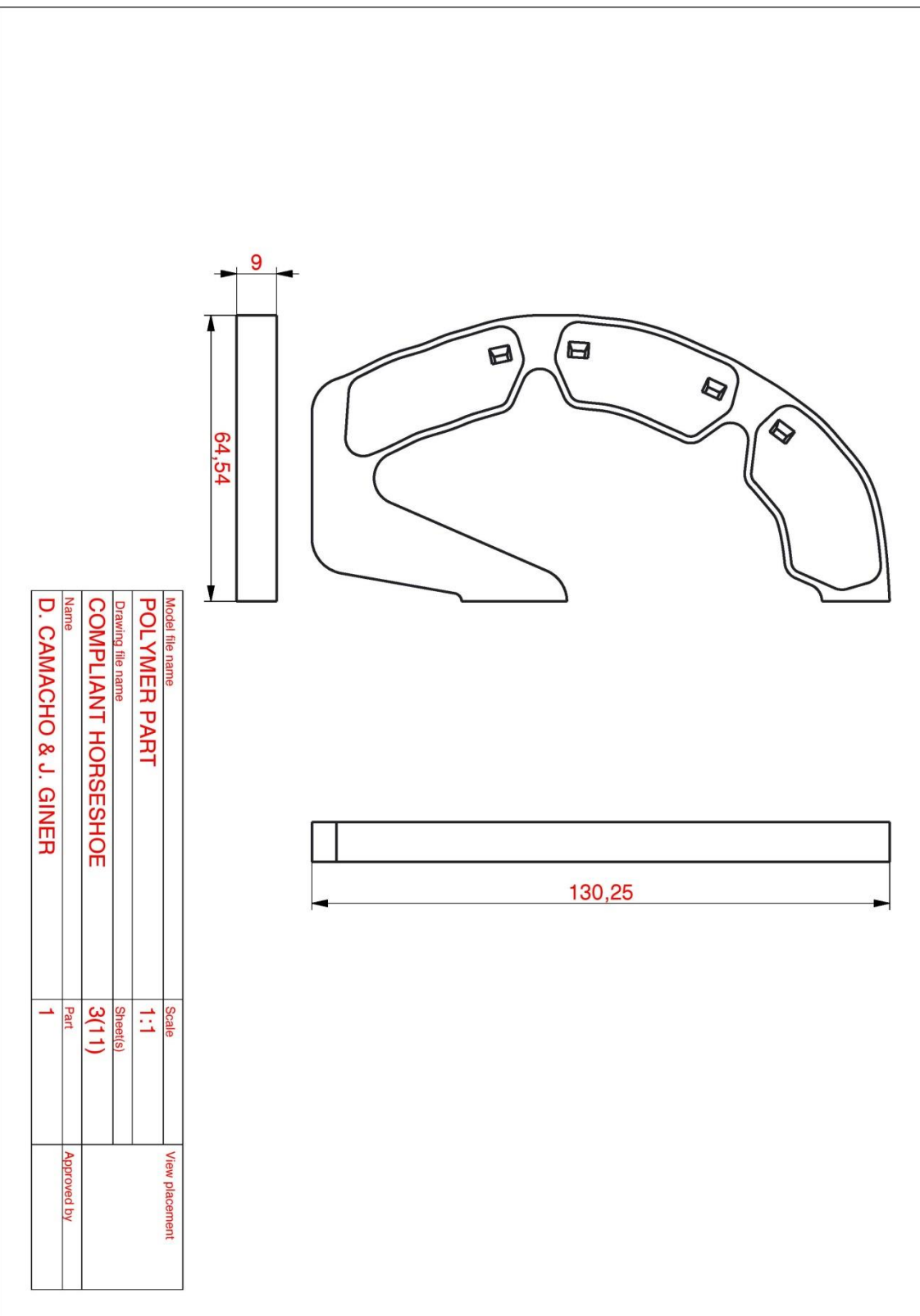


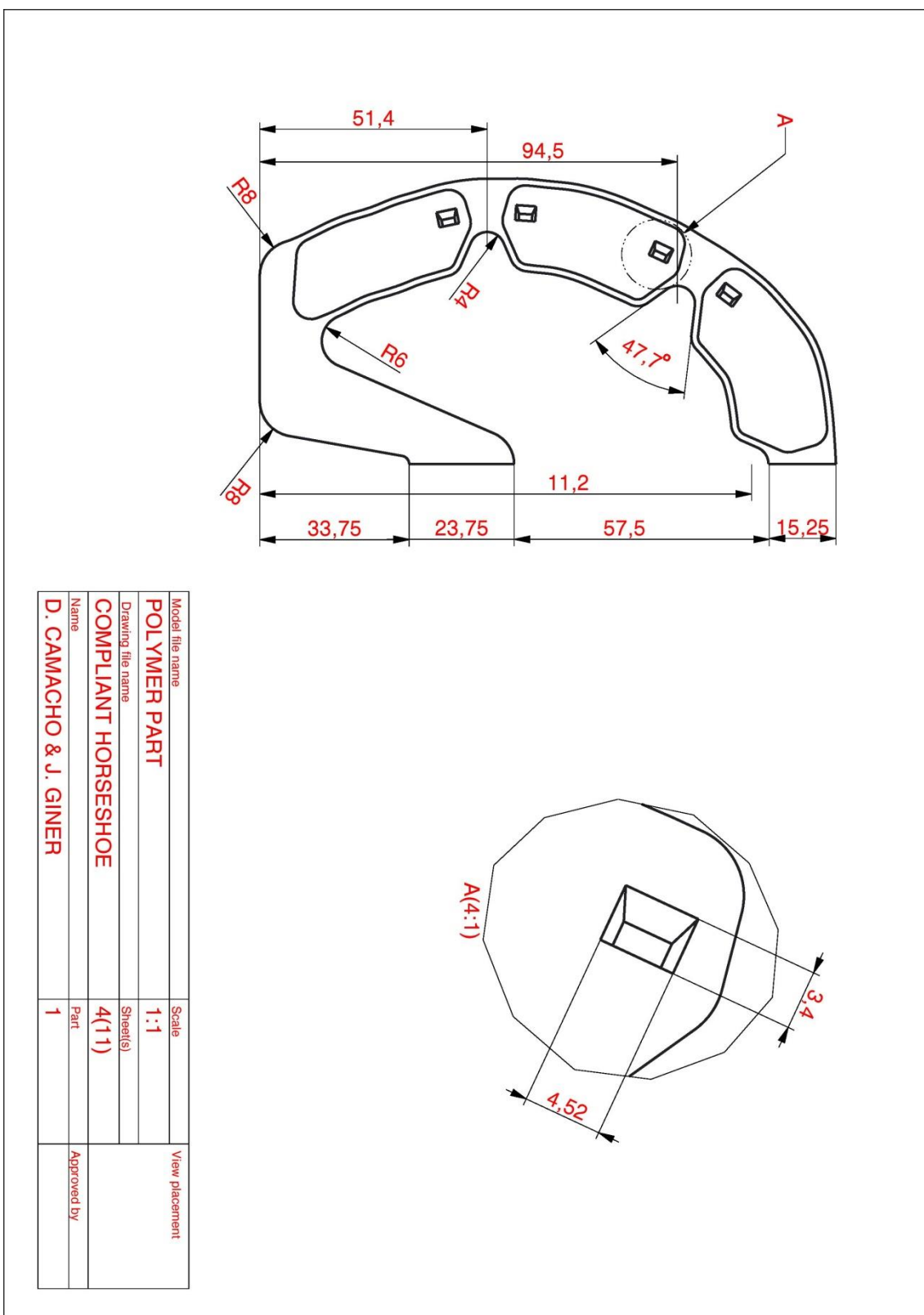
Figure 120. Test performed with adiprene LF-950. Displacement in z- direction (own source)

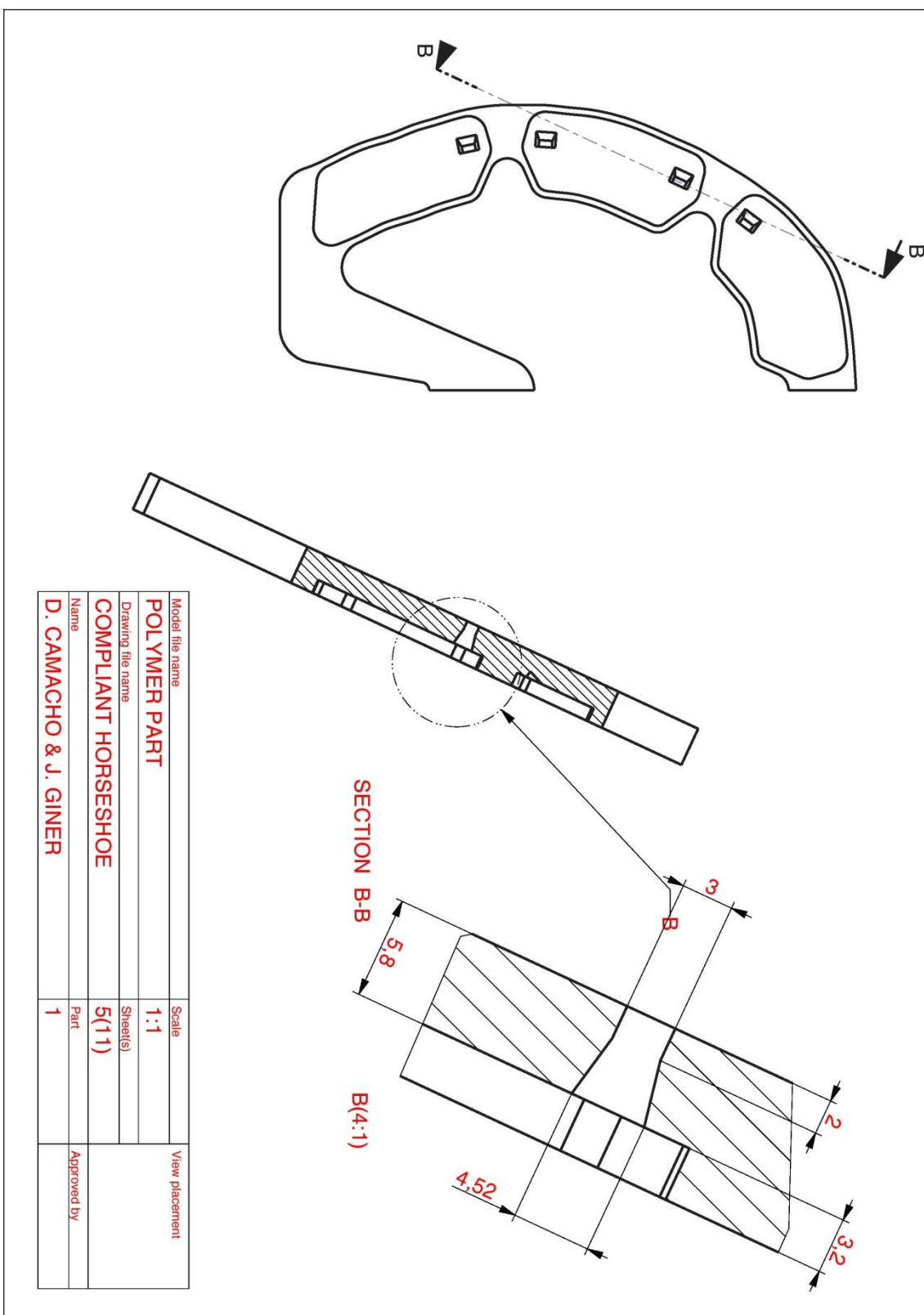
APPENDIX B

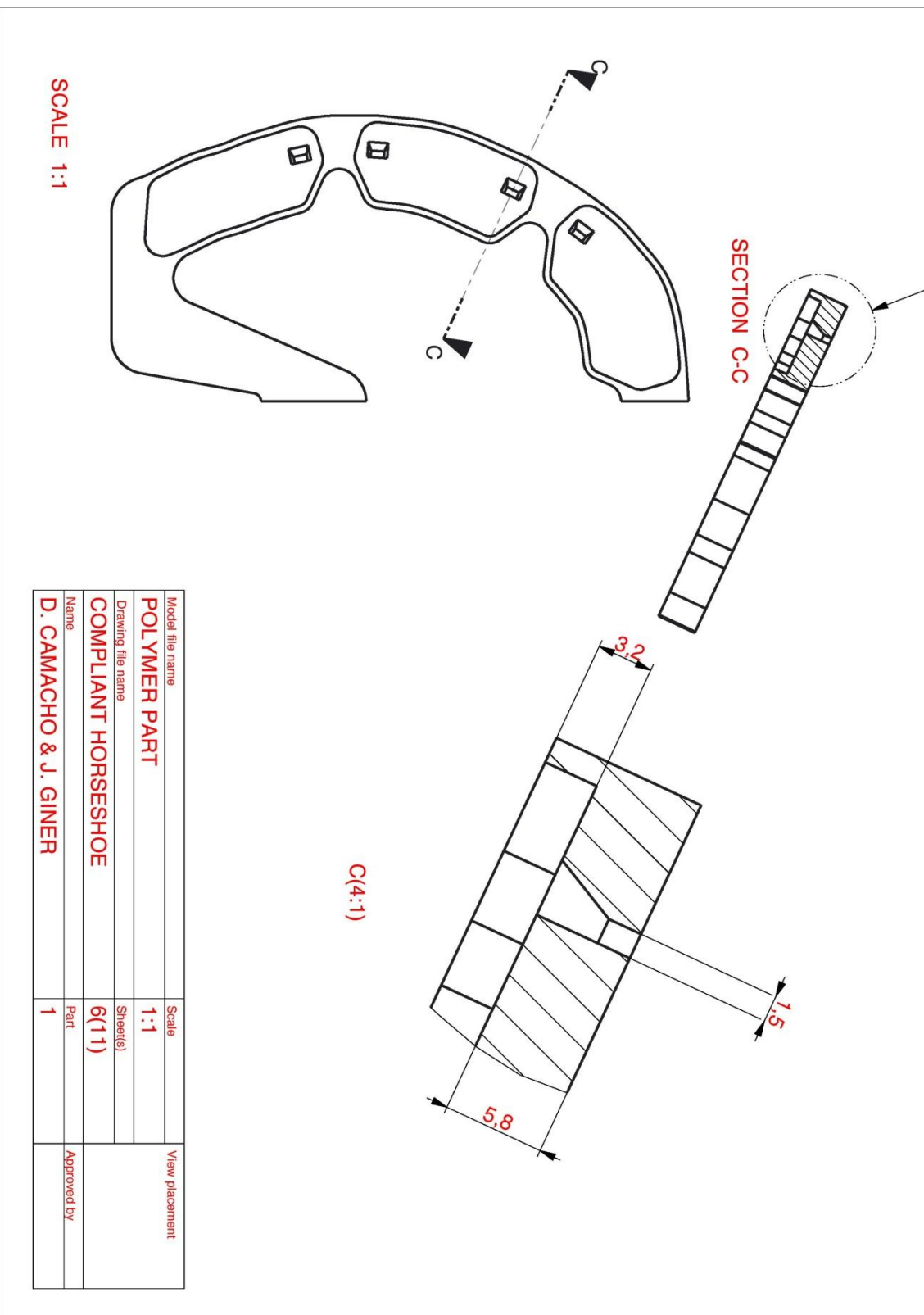


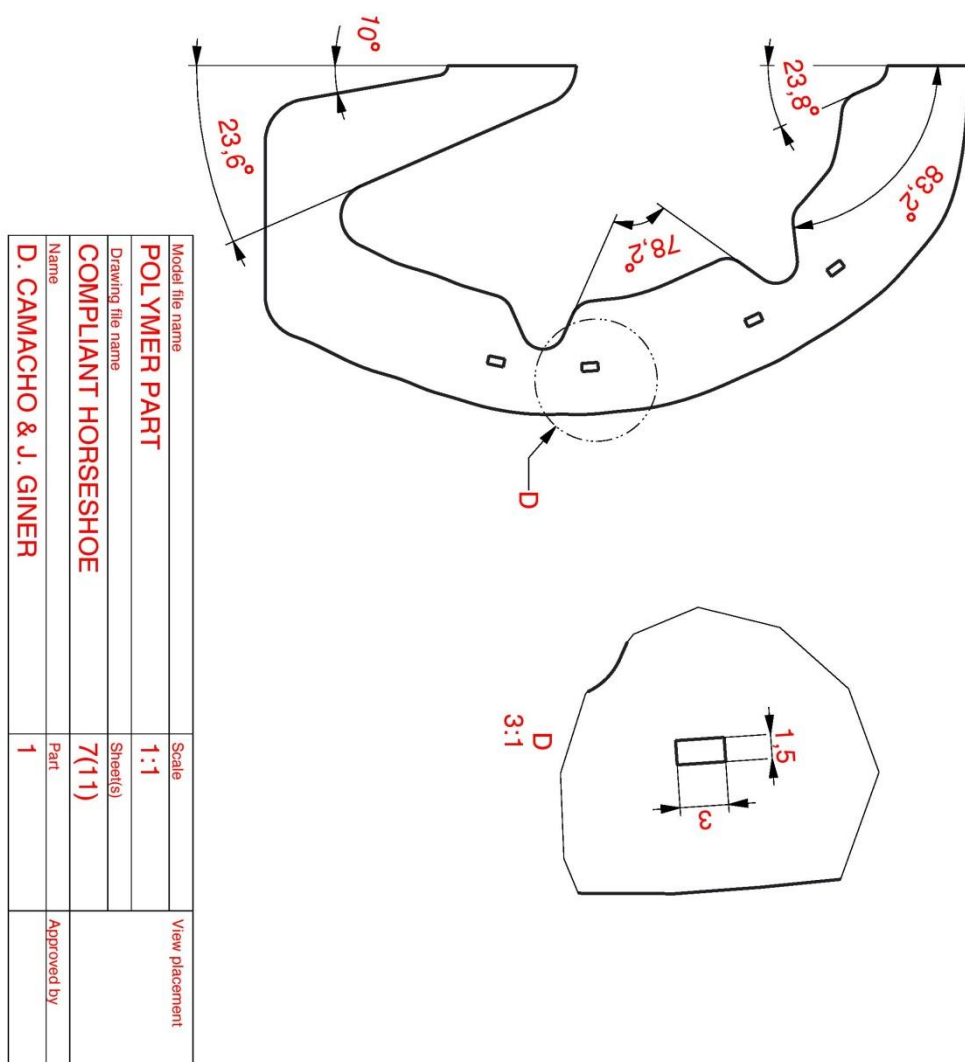


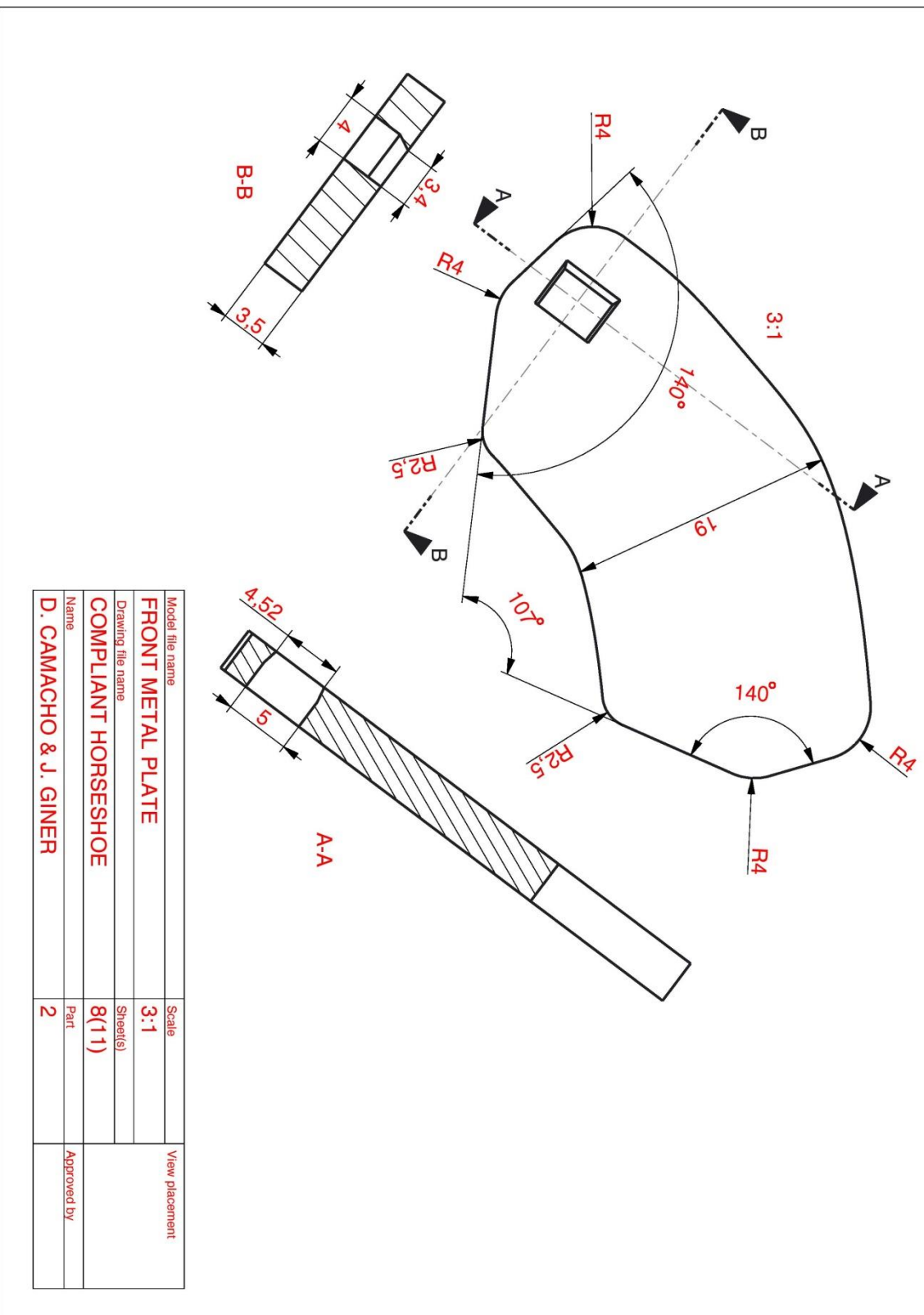


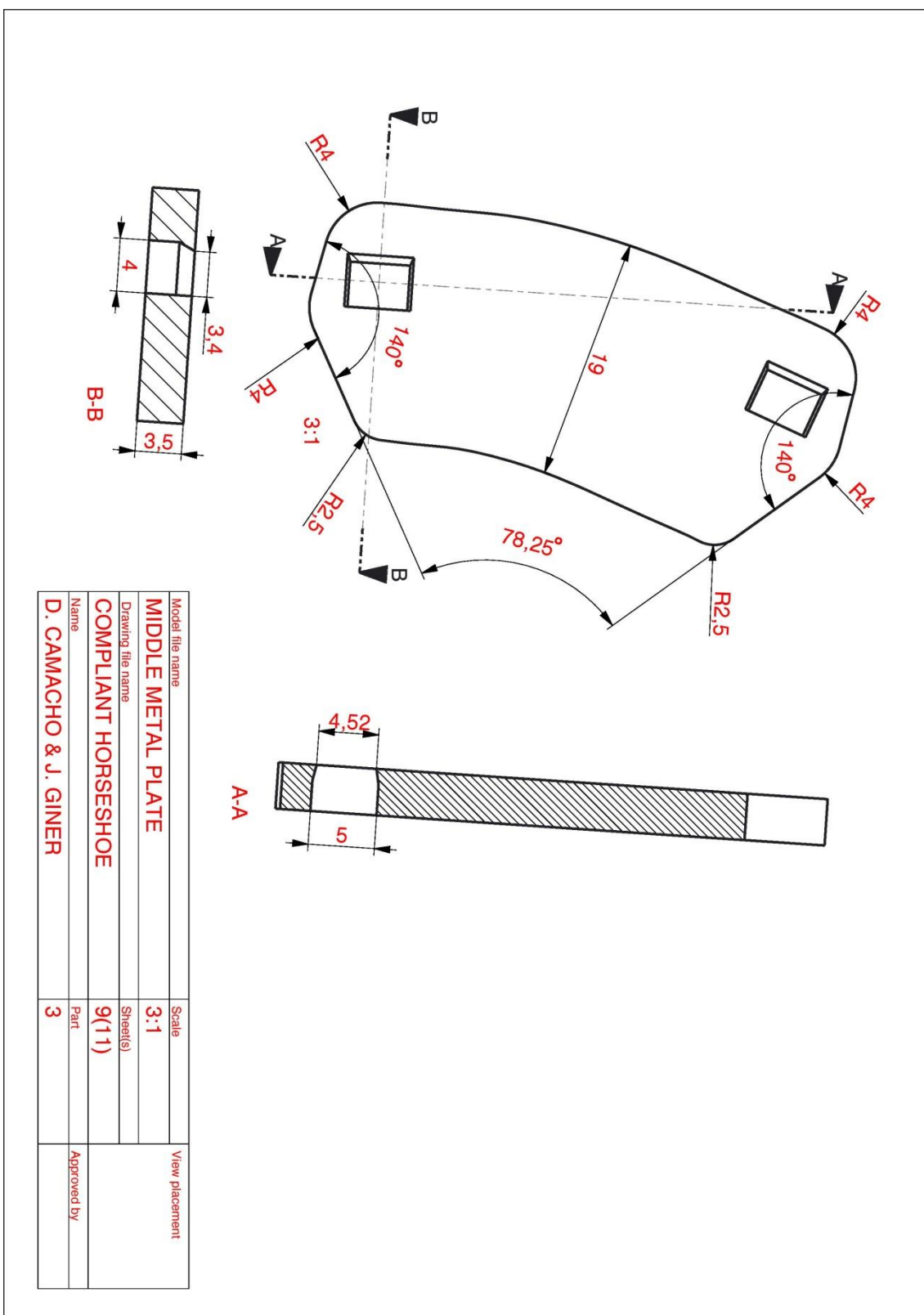


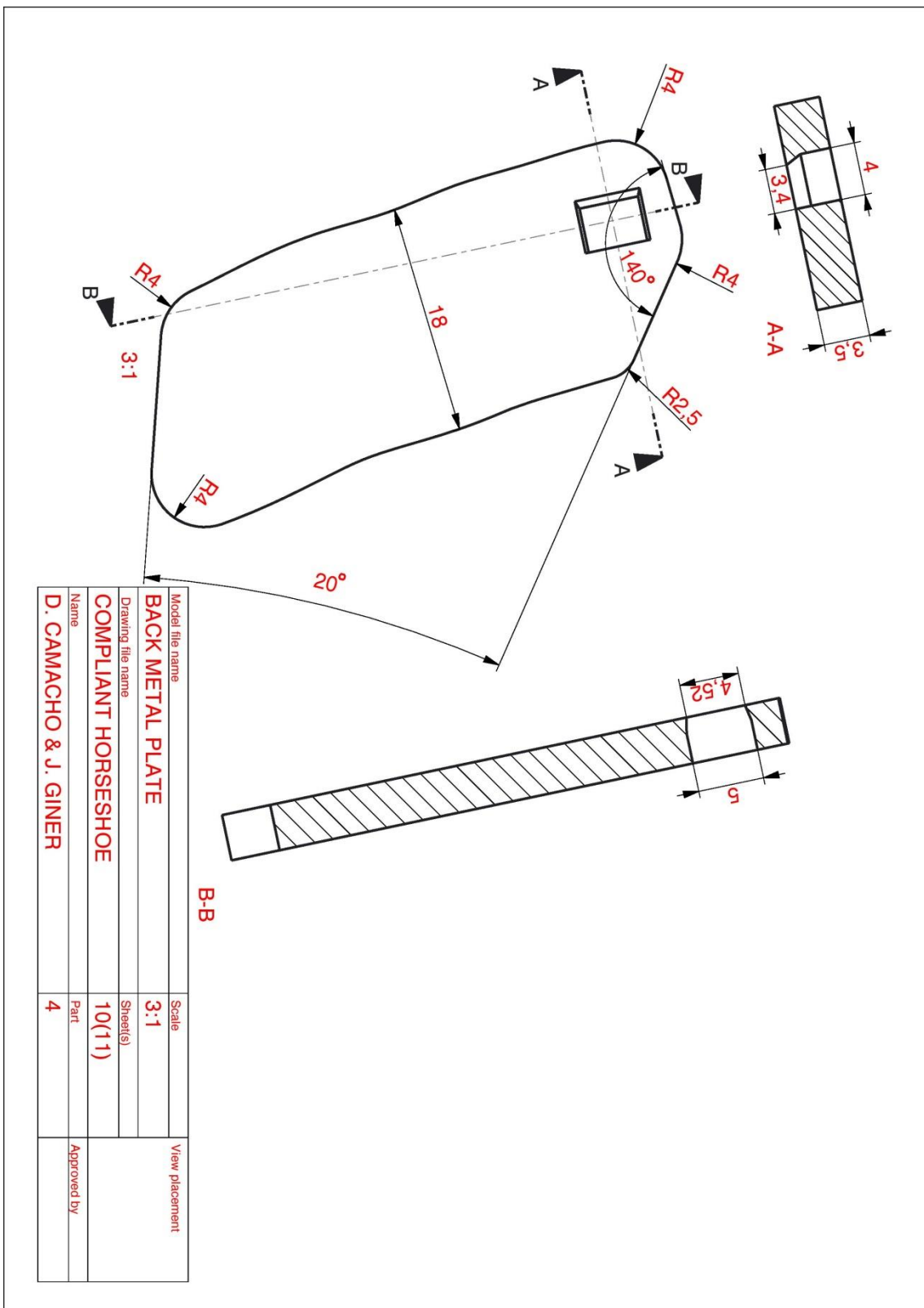


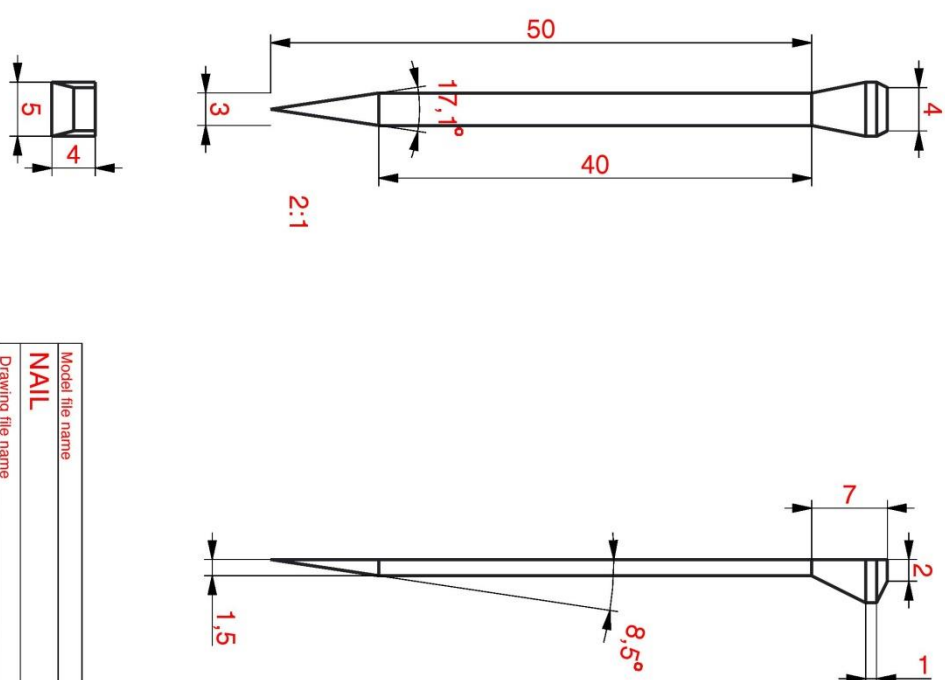












Model file name	Scale	View placement
NAIL	2:1	
Drawing file name		Sheet(s)
COMPLIANT HORSESHOE	11(11)	
Name	Part	Approved by
D. CAMACHO & J. GINER	5	

REFERENCES

- Anon., 1996. *Horseshoes.com*. [Online]
Available at:
http://www.horseshoes.com/websites/georgiafarriersupply/media/mustad_easy_glu.gif
[Accessed 02 05 2014].
- Anon., 1999. *SoundHorse Technologies*. [Online]
Available at: <http://www.soundhorse.com/images/products-quicklist/elite-hind.jpg>
[Accessed 02 05 2014].
- Anon., 2001. *Eki*. [Online]
Available at: <http://www.eki.es/catalogo/ampliadas/5105.jpg>
[Accessed 03 05 2014].
- Anon., 2008. *America's Horse Daily*. [Online]
Available at: <http://americashorsedaily.com/wp-content/uploads/hoofweb.jpg>
[Accessed 02 05 2014].
- Anon., 2009. *Stablemade.com*. [Online]
Available at: <http://www.stablemade.com/hproducts/images/Horses/Hotnail.jpg>
[Accessed 02 05 2014].
- Anon., 2011. *Independent Farrier Supplies*. [Online]
Available at: <http://www.independentfarriersupplies.com.au/products/horseshoe-nails/>
[Accessed 02 05 2014].
- Anon., 2013. *Blue Pegasos*. [Online]
Available at: http://www.bluepegasos.com.au/uploads/transition_glue_on_1134_1_sml.jpg
[Accessed 02 05 2014].
- Barefoot-Hoofcare, 2013. *Barefoot Hoofcare*. [Online]
Available at: <http://barefoothoofcare.net/?p=808>
[Accessed 25 April 2014].
- Butler, D. & Butler, J., 2004. *The Principles of Horseshoeing III*. Crawford: Doug Butler Enterprises.
- Callister, W. & Rethwisch, D., 2011. *Materials Science and Engineering*. 8th ed. s.l.:s.n.
- Colles, C., 2009. *Anatomía del caballo*. Barcelona: Hispano Europea.
- Douglas, J., Mittal, C., Thomason, J. & Jofriet, J., 1996. The modulus of elasticity of equine hoof wall: Implications for the mechanical function of the hoof. *The Journal of Experimental Biology*, pp. 1829-1836.
- EponaShoe, 2010. *EponaShoe*. [Online]
Available at: <http://www.eponashoe.com/index.htm>
[Accessed 25 April 2014].

- Fleming, G., 1869. *Horse-shoes and horse-shoeing: their origins, history, uses and abuses.* London: Chapman and Hall.
- García, M., 2013. *Structural material investigation of horse hoof*, Skövde: Högskolan i Skövde.
- Hinterhofer, C., Stanek, C. & Binder, K., 1998. Elastic modulus of equine hoof horn, tested in wall samples, sole samples and frog samples at varying levels of moisture. *Berliner und Münchener Tierärztliche Wochenschrift* 111, pp. 217-221.
- Hinterhofer, C., Stanek, C. & Haider, H., 2001. Finite element analysis (FEA) as a model to predict effects of farriery on the equine hoof. *Equine Veterinary Journal*, pp. 58-62.
- Hinterhofer, C. et al., 2006. Motion analysis of hoof wall, sole and frog under cyclic load in vitro: Deformation of the equine hoof shod with regular horse shoe, straight bar shoe and bare hoof. *Pferdeheilkunde*, 22(3), pp. 314-319.
- ImprintSport, 2008. *ImprintSport*. [Online]
Available at: <http://www.imprintsport.com/>
[Accessed 25 April 2014].
- Mustad, 1999. *Mustad*. [Online]
Available at: <http://www.mustad.com/en/mshop-product/76/libero?back=undefined>
[Accessed 29 04 2014].
- Nassau, R. V., 2008. *El casco del caballo*. Barcelona: Hispano Europea.
- Parker, S., 2010. *Parker Farrier Service*. [Online]
Available at: <http://www.parkerfarrierservice.com>
[Accessed 5 April 2014].
- Perrin, R., 2010. *The horseshoe nail from a veterinarian's perspective*. [Online]
Available at: http://www.mustadhoofnails.com/p/59/a_veterinarian_s_perspective/
[Accessed 02 05 2014].
- Roepstorff, L., Johnston, C. & Drevemo, S., 1999. The effect of shoeing on kinetics and kinematics during the stance phase. *Equine Veterinary Journal*, 31(S30), pp. 279-285.
- Roepstorff, L., Johnston, C. & Drevemo, S., 2001. In vivo and in vitro heel expansion in relation to shoeing and frog pressure.. *Equine Veterinary Journal*, 33(S33), pp. 54-57.
- Romero, M., Museros, P., Rodrigo, M. & Poy, A., 2002. *Resistencia de Materiales*. 2nd ed. Castellón: Universidad Jaume I.
- SaintJohn, B., 2008. *Horseshoe Museum*. [Online]
Available at: <http://www.horseshoemuseum.com/Ancient/BritishMuseum.htm>
[Accessed 4 March 2014].
- Salo, Z., Thomason, J. & Runciman, R., 2010. Analysis of strain and stress in the equine hoof using finite element analysis: Comparison with minimum principal strains recorded in vivo. *Biosystems Engineering* 107, pp. 262-270.

- Sandgren, B., 2007. *Hästens fysiologi*. Stockholm: Svenska travsportens centralförbund.
- Stachurska, A. et al., 2008. Differentiation between fore and hind hoof dimensions in the horse (*Equus caballus*). *Arch. Tierz., Dummerstorf* 51, pp. 531-540.
- TruShu-Equine, 2013. *TruShu Equine*. [Online]
Available at: <http://trushuequine.com/>
[Accessed 25 April 2014].
- Windt-im-Wald-Farm, 2007. *Windt im Wald Farm*. [Online]
Available at: <http://www.wiwfarm.com/horseshoenails.htm>
[Accessed 02 05 2014].
- Witte, T., Knill, K. & Wilson, A., 2004. Determination of peak vertical ground reaction force from duty factor in the horse (*Equus caballus*). *The Journal of Experimental Biology* 207, pp. 3639-3648.